ALFRED-WEGENER-INSTITUT
HELMHOLTZ-ZENTRUM FÜR POLAR- UND MEERESFORSCHUNG

Universität Potsdam

University of Potsdam
Institute for Earth and Environmental Science

Master Thesis

Impacts of Thermo-erosion on Organic Matter Stocks

Analysis of Total Organic Carbon and Total Nitrogen Distribution in three Thermo-erosional Valleys in the Lena River Delta

submitted by:
Nadja Kuhl

to attain the academic degree
Master of Science (M. Sc.) in Geoecology

First supervisor: Prof. Dr. Hugues Lantuit
Second supervisor: Dr. Anne Morgenstern

1st July 2018

"I wish I could stay in this moment forever.
[...] But then it wouldn't be a moment."

Max Caulfield in “Life is Strange”
Dontnod Entertainment, 2015

ABSTRACT

The ongoing climate change has a huge impact on the Arctic, including its underlaying permafrost soils. Due to increased warming the permafrost thaws and gets degraded, for example by thermo-erosional processes. As a result, the biogeochemical cycling increases because of the redistribution of organic carbon (OC) and nitrogen.

This study examines the spatial distribution of OC and its availability within three thermo-erosional valleys in the Yedoma-underlain Lena River Delta that were formed by thermo-erosional processes. Therefore, permafrost soil samples were investigated on their total organic carbon (TOC) content, total nitrogen (TN) content and soil organic carbon (SOC) storage as well as the total organic carbon to total nitrogen (C/N) ratio. The resulting datasets were divided into different categories (transects, geomorphological unit and depth) and tested on their statistical difference to estimate the impact of thermo-erosional processes on the spatial distribution of the investigated geochemical parameters.

The mean SOC storages of the three thermo-erosional valleys for 0-100 cm ranged between 19.7 ± 13.9 kg · m^{-2} and 27.0 ± 15.3 kg · m^{-2}, the average TN content between 0.3 ± 0.1 wt% and 0.4 ± 0.2 wt%. The average C/N-ratio was ranging between 15.3 ± 3.4 and 17.2 ± 2.6. All parameters showed great differences in spatial distribution within the valleys. In most cases, the highest values of the parameters occurred in areas of the valleys with lower erosion rates (in the upstream transect and on the upland), whereas the lowest values were found in areas of higher erosion rates (in the midstream and downstream transect and on the slopes). This variability within the valleys was traced back to the geomorphology and thermo-erosional processes. The results of this study showed that those thermo-erosional processes have an impact on the SOC storage within thermo-erosional valleys as well as on the degradation and availability of this stored OC.

ZUSAMMENFASSUNG

Die anhaltende Klimaveränderung hat einen großen Einfluss auf die Arktis und ihre Permafrostböden. Diese tauen durch die verstärkte Erwärmung und werden, zum Beispiel durch Thermoerosion, degradiert. Dadurch wird der im Permafrost gebundene organische Kohlenstoff und Stickstoff in die Atmosphäre zurückgeführt und dem biogeochemischen Kreislauf wieder zur Verfügung gestellt.

In dieser Arbeit wird die räumliche Verteilung von organischem Kohlenstoff und seiner Freisetzung in drei Thermoerosionstälern im Lena Delta untersucht, das vom Yedoma Eiskomplex unterlagert ist. Dafür wurden Permafrostproben auf ihren Gehalt von organischem Kohlenstoff und Stickstoff sowie auf im Boden gespeicherten organischen Kohlenstoff und das Kohlenstoff zu Stickstoff Verhältnis (C/N-Verhältnis) untersucht. Um die Auswirkung von Thermoerosionsprozessen auf die räumliche Verteilung dieser Parameter abzuschätzen wurden die erhaltenen Datensätze in verschiedene Kategorien (Transekte, geomorphologische Einheiten und Tiefe) eingeteilt und auf ihre Unterschiedlichkeit getestet.

Im Mittel waren in den drei untersuchten Tälern in den ersten 100 cm zwischen 19.7 ± 13.9 kg $\cdot$ m^{-2} und 27.0 ± 15.3 kg $\cdot$ m^{-2} organischer Kohlenstoff gespeichert, der mittlere Stickstoffgehalt lag zwischen 0.3 ± 0.1 wt% und 0.4 ± 0.2 wt%. Das mittlere C/N-Verhältnis lag zwischen 15.3 ± 3.4 und 17.2 ± 2.6. Die untersuchten Parameter zeigten große Unterschiede in ihrer Verteilung innerhalb der Täler auf. Ihre höchsten Werte wurden meist in Bereichen der Täler gefunden, die geringe Erosionsraten aufwiesen (im oberen Talbereich und im Hochland des Tales), wohingegen die niedrigsten Werte in Bereichen mit höheren Erosionsraten gefunden wurden (im unteren Talbereich und an den Hängen). Diese Variabilität innerhalb der Täler geht auf ihre Morphologie und unterliegenden Thermoerosionsprozessen zurück. Die Ergebnisse dieser Arbeit zeigen, dass diese Prozesse einen Einfluss auf die Verteilung von organischem Kohlenstoff und seine Degradierung haben.

TABLE OF CONTENTS

LIST OF FIGURES

LIST OF TABLES

LIST OF ABBREVIATIONS

OC .....organic carbon

TOC .....total organic carbon

TN .....total nitrogen

SOC .....soil organic carbon

C/N-ratio .....total organic carbon to total nitrogen ratio

C .....carbon

GHG.....greenhouse gases

CO_2 .....carbon dioxide

CH_4 .....methane

AL .....active layer

IPY .....International Polar Year

m a. s. l. .....meter above sea-level

KUR/KUR16-TEV1 .....investigated thermo-erosional valley on Kurungnakh Island

SOB/SOB16-TEV3 .....investigated thermo-erosional valley on Sobo-Sise Island

BYK/BYK16-TEV5 .....investigated thermo-erosional valley on Bykovsky Peninsula

DEM.....digital elevation model

N .....nitrogen

1 Introduction

The recent climate change is stronger in the Arctic than the global average (AMAP 2017). The average temperatures in the Arctic are predicted to rise by 4 °C until 2040, which is more than twice of the projected warming of the northern hemisphere (OVERLAND et al. 2017). About 24 % of the Earth's land surface is underlain by permafrost, which is particularly widespread in the Arctic (ZHANG et al. 2008). The periglacial environment reacts especially sensitive to climate change (ROMANOVSKY et al. 2010), which has consequences on geomorphological, hydrological and biological processes (OLIVA & FRITZ 2018). These include increasing permafrost temperatures, active layer deepening, decreasing extend of the area underlain by permafrost and degradation of permafrost (OLIVA & FRITZ 2018, ROMANOVSKY et al. 2017, GROSSE et al. 2011a, NELSON et al. 2001).

The ground in permafrost regions stores approximately twice as much carbon (C) than there is contained in the current atmosphere. These large reservoirs of C pools are vulnerable towards changes due to climate change (SCHUUR et al. 2015). Permafrost thawing is causing organic matter decomposition. This releases organic carbon (OC) into the ecosystem leading to an increasing release of the greenhouse gases (GHG) carbon dioxide (CO_2) and methane (CH_4) into the atmosphere. As a consequence, a positive feedback to global warming is created (STRAUSS et al. 2017).

The soil organic carbon (SOC) storage of permafrost is, amongst others, influenced by geomorphological processes. OBU et al. 2017 showed that there is less OC stored in areas influenced by higher erosion rates, which indicates a relation of SOC storage to the surface morphology (OBU et al. 2017). The distribution of OC was studied in representative landforms of permafrost landscapes, such as thermokarst lakes (LENZ et al. 2016, WALTER ANTHONY et al. 2014), drained thermokarst lake basins (FUCHS et al. 2018, LENZ et al. 2015) and retrogressive thaw slumps (RAMAGE et al. 2018, TANSKI et al. 2017). However, the impact on degradation and decomposition of another characteristic feature in permafrost landscapes is still not sufficiently investigated: thermo-erosional valleys. These degradational landforms are generally observed in continuous permafrost regions (GODIN et al. 2014) formed by the combination of thermal and mechanical action of moving water (FRENCH 2007, VAN EVERDINGEN 2005). The effects of thermo-erosion on the distribution and decomposition rates of C within thermo-erosional valleys are still relatively unknown.

This study will contribute to a better understanding of the impacts of thermo-erosional processes on organic matter stocks of near-surface ice-rich permafrost on the third terrace of the Lena River Delta. Its aim is to quantify the organic matter composition of three thermo-erosional valleys to reveal differences in its distribution within and between the valleys.

The main objectives of this thesis are:

- to quantify the distribution of total organic carbon (TOC) content, total nitrogen (TN) content, SOC storage and total organic carbon to total nitrogen ratio (C/N-ratio) in three thermo-erosional valleys on Kurungnakh Island, Sobo-Sise Island and Bykovsky Peninsula
- to highlight differences in the distribution of these biogeochemical parameters (per transect, geomorphological unit and depth)
- to estimate the role of thermo-erosional processes on degradation and decomposition of C

2 Scientific background

2.1 Permafrost

Permafrost is defined as “ground (soil or rock, including enclosed ice and organic matter) that remains at or below 0 °C for at least two consecutive years” (VAN EVERDINGEN 2005). Approximately 24 % of the Earth’s land surface is underlain by permafrost (ZHANG et al. 2008), which is especially widespread in the Arctic region (Figure 1) (AMAP 2012, ZHANG et al. 2008). Permafrost can be found as well at the continental shelves of the Arctic Ocean as in mountainous regions outside the Arctic (ZHANG et al. 2008).

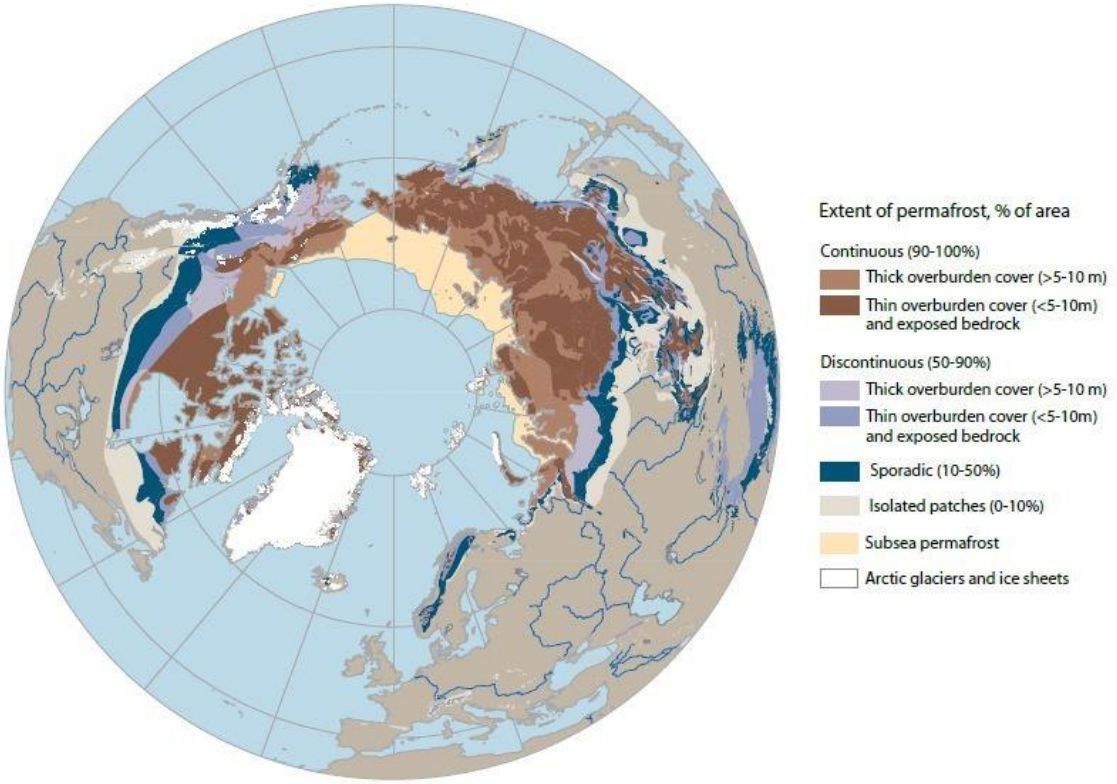

Figure 1: Distribution and properties of permafrost in the Northern Hemisphere (AMAP 2012).

Permafrost is differentiated between continuous, discontinuous, sporadic and isolated permafrost depending on the estimated portion of ground that it is underlaying (Figure 1) (FRENCH 2007, ZHANG et al. 2008). In the continuous permafrost zone 90 to 100 % is underlain by permafrost. Local unfrozen zones (called talik) usually exist beneath river channels and lakes (FRENCH 2007, VAN EVERDINGEN 2005). Much of the continuous permafrost was formed during or before the last glacial period (ROMANOVSKY et al. 2007). Within the discontinuous zone 50 to 90 % is covered by permafrost; the permafrost bodies are separated by taliks (FRENCH 2007, VAN EVERDINGEN 2005). Most of the discontinuous permafrost is younger than continuous permafrost; it was formed within the last several thousand years (ROMANOVSKY et al. 2007). In the sporadic zone permafrost covers 10 to

50 % of the area. Single bodies of permafrost are surrounded by unfrozen ground. Within the isolated zone only small patches of permafrost appear. These patches are widely surrounded by taliks (FRENCH 2007, VAN EVERDINGEN 2005). Continuous permafrost occurs mainly at high latitudes and has relatively high ice content, whereas discontinuous and sporadic permafrost and isolated permafrost zones are found in mountainous regions and at mid to low latitudes, containing relatively little ice. The farther southwards, the more discontinuous and sporadic the permafrost becomes (ZHANG et al. 2008).

Permafrost is overlain by an active layer (AL) (Figure 2). "This layer of ground […] is subject to annual thawing and freezing" (VAN EVERDINGEN 2005). The AL is usually approximately 20 to 150 cm thick (HEGINBOTTOM et al. 2012). The thickness depends on the air temperature, drainage, vegetation, rock or soil type, snow cover, the total water content and the orientation and degree of slope. The AL thickness is usually thinner in the High Arctic (less than 15 cm are possible) and gets thicker the farther south. Variations in the mean annual air temperature, soil moisture and snow cover can lead to different AL thickness from year to year (VAN EVERDINGEN 2005). The boundary between AL and permafrost is the permafrost table (Figure 2). Above, beneath and enclosed in the permafrost unfrozen zones appear (Figure 2) – these are called taliks (FRENCH 2007). These unfrozen bodies can occur due to local anomalies in hydrological, thermal, hydrogeological or hydrochemical conditions (VAN EVERDINGEN 2005).

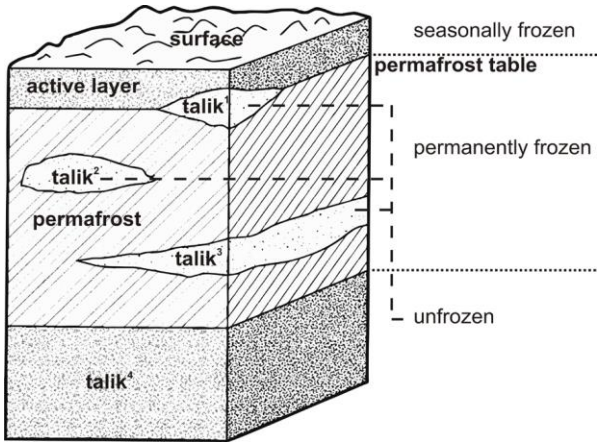

Figure 2: Vertical structure of the permafrost zone; talik[1] - supra-permafrost, talik[2] – closed talik, talik[3] – intra-permafrost, talik[4] – sub-permafrost (FRENCH 2007, modified by STRAUSS 2010).

One main characteristic that differentiates permafrost from unfrozen ground is the presence of ice in the ground (ROMANOVSKY et al. 2007). Ground ice refers to "all types of ice contained in freezing and frozen ground" (VAN EVERDINGEN 2005). Ground ice accounts from several tenths of per cent up to 90 % of the total permafrost volume (ROMANOVSKY et al. 2007). In high latitudes permafrost contains more ice (more than 20 % by volume) than in lower latitudes (ZHANG et al. 2008). Frozen soil that contains ice has a similar mechanical strength as bedrock. This means that the stability of an ecosystem in permafrost regions is depending on the stability of ground ice. With the loss of permafrost, the system would lose its stability (ROMANOVSKY et al. 2007). According to MACKAY 1972 there are four types of ground ice: pore ice, segregated ice, vein ice and intrusive ice. For this study a special type of vein ice is from importance – ice wedges. An ice wedge is "a massive, generally wedge-shaped body with its apex pointing downwards, composed of foliated or vertically banded,

commonly white ice" (VAN EVERDINGEN 2005). Ice wedges are typical landforms of permafrost regions around the world (FRENCH 2007, MACKAY 1990). They form due to thermal contraction during winter seasons, which results in an open crack. In early spring the crack is filled with melt water, which freezes during the next winter. Repeated cracking at the same location leads to ice wedge growth from year to year (Figure 3) (FRENCH 2007, LACHENBRUCH 1963, MACKAY 1990).

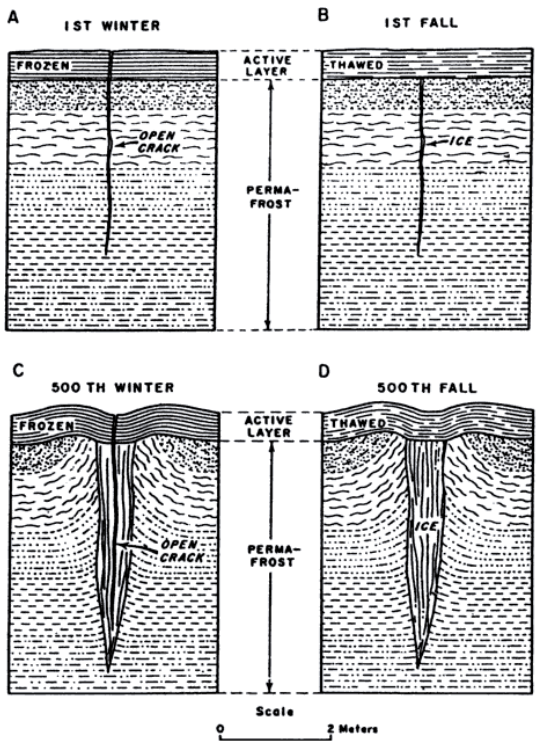

Figure 3: Scheme of the evolution of an ice wedge according to contraction cracks (LACHENBRUCH 1963).

Epigenetic ice wedges form after the sediment deposition, whereas syngenetic ice wedges form roughly at the same time as the surrounding sediments accumulate (Figure 4) (FRENCH 2007, MACKAY 1990). Epigenetic ice wedges are typically younger than the enclosed sediment. They are usually growing wider rather than deeper and have a specific wedge shape (Figure 4). The oldest ice of an epigenetic ice wedge is on the outside edges (FRENCH 2007, MACKAY 1990, VAN EVERDINGEN 2005). Syngenetic ice wedges grow both in width and height at the same time as the deposited sediments (Figure 4) (FRENCH 2007, MACKAY 1990). Therefore, the age of the ice on the outside edges increases from top to bottom (VAN EVERDINGEN 2005). Its shape and size is a function of the vertical as well as the horizontal growth rates. High sediment accumulation and low ice-vein accretion leads to thinner ice wedges; whereas due to low sedimentation and higher ice-accretion rates the ice wedges become wider (FRENCH 2007, MACKAY 1990). That is the reason why the form of syngenetic ice wedges is indeed wedge-shaped but more irregular (VAN EVERDINGEN 2005).

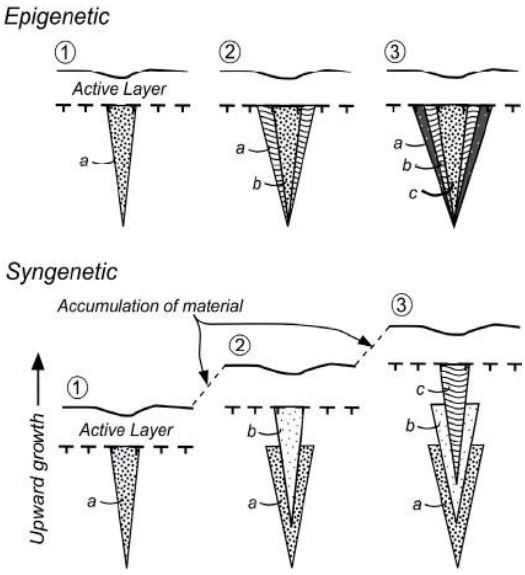

Figure 4: Schematic diagram of the growth of epigenetic and syngenetic ice wedges; Point in time: (1) first, (2) second, (3) third; ice wedge at (a) first, (b) second, (c) third point of time (MACKAY 1990).

2.2 Yedoma

Originally the word “Yedoma” was used by native Yakutian people describing relief features in East Siberian lowlands that developed due to thermokarst depressions. “Yedoma”/”е дома” means “corroded earth” (KANEVSKIY et al. 2011, TOMIRDIARO 1982 – cited in STRAUSS 2010). The modern translation of “Yedoma” –Ice Complex– is related to the massive ice content in the soil (KANEVSKIY et al. 2011). In this thesis the term is used as stratigraphic unit – Yedoma is an ice-rich and silty deposit formed in the Late Pleistocene (KANEVSKIY et al. 2011, SCHIRRMEISTER et al. 2013). The terms “Ice Complex” and “Yedoma” are often used synonymous (SCHIRRMEISTER et al. 2013). Because of its high organic content (e. g. decomposed animal remains and fossil plants) Yedoma is from importance and interest (chapter 2.3 & 2.4) since the early 19th century (SCHIRRMEISTER et al. 2011a).

The deposits can be up to 50 m thick and are widely distributed in the Arctic region (KANEVSKIY et al. 2011, SCHIRRMEISTER et al. 2002, STRAUSS et al. 2017). In Siberia it occurs on a total area of approximately 1 million km² (Figure 5). It also appears in Alaska (second largest area of Yedoma), but information about its distribution is still limited (KANEVSKIY et al. 2011).

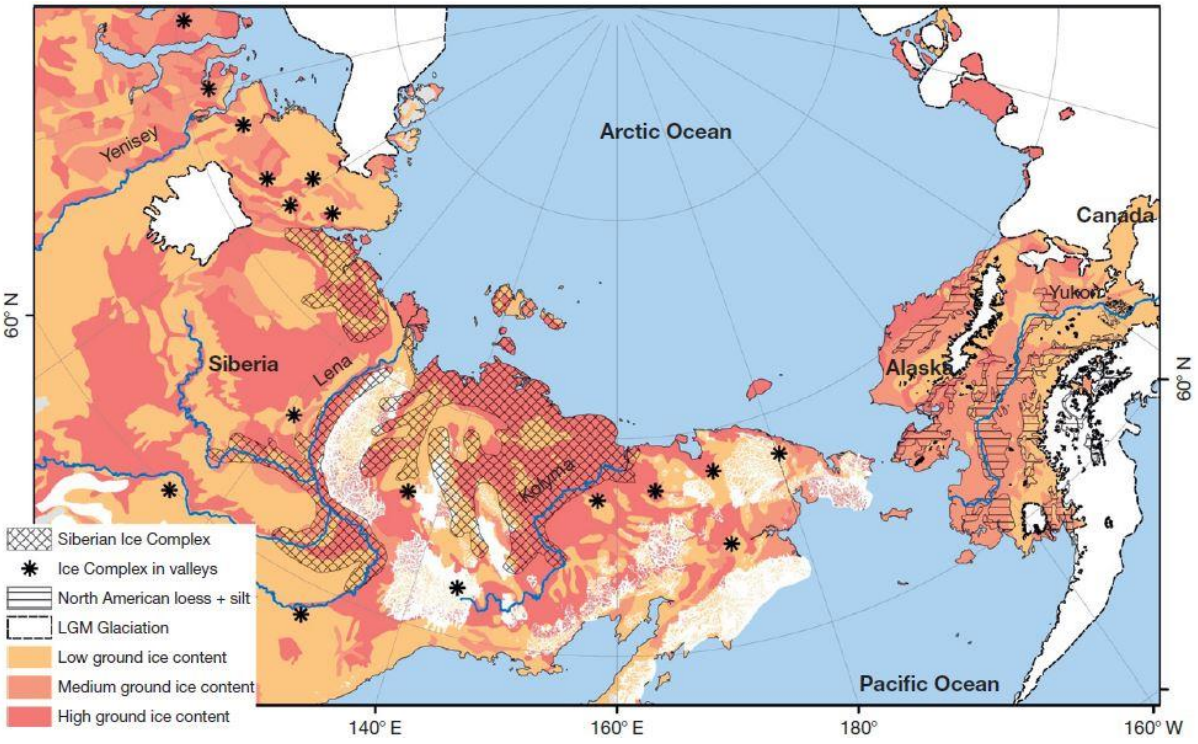

Figure 5: Distribution of ice-rich permafrost deposits and the extent of the Yedoma Ice Complex in Arctic and Subarctic lowlands (SCHIRRMEISTER et al. 2013).

According to KUNITSKY et al. 2002 the formation of the Ice Complex is a combination of cryogenic weathering, transport and accumulation of material and relief-shaping in cold and arid climate conditions. In perennial snow fields in topographically protected areas (among hills and low mountain ranges, terrain edges as valleys, steep slopes or cryoplanation

terraces) mixtures of fine-grained sediments, windblown snow and plants were accumulated. Due to intense freeze-thaw cycles underneath the snowfields and around their margins, wet conditions prevailed that led to frost weathering and therefore to the formation of additional fine-grained sediment. Runoff by seasonal meltwater transported some of this sediment that contained organic matter downslope. Further transportation to foreland plains or large alluvial fans occurred due to a variety of processes, such as alluvial, colluvial, solifluction or aeolian. This led to different types of depositions with different grain-size compositions. Together with the sediment aggradation in the flat accumulation areas syngenetic, polygonal ice-wedge systems were formed. Repeated over thousands of years these processes resulted in the formation of thick Yedoma depositions on wide plains (SCHIRRMEISTER et al. 2013).

2.3 Climate change and permafrost

Over the past 50 years the Arctic has warmed more than twice as the global rate. The spatial pattern of temperature shows an increase in cold and warm seasons (Figure 6) (OVERLAND et al. 2017). Arctic amplification is a term that defines the state when temperature trend and variability in the Arctic region tend to be larger than for the northern hemisphere and the global average. For the past decade (2000-2009) the arctic amplification is stronger during autumn and winter seasons than during spring and summer (Figure 6) (SERREZE & BARRY 2011). In the Arctic the average temperatures for the colder seasons are predicted to rise by 4 °C until 2040 (OVERLAND et al. 2017). During the past decade the highest temperatures of the instrumental records were reached in the Arctic. Palaeotemperature-reconstructions show that the recent summer temperatures of the Arctic are higher than at any time during the past 2000 years (WALSH et al. 2011).

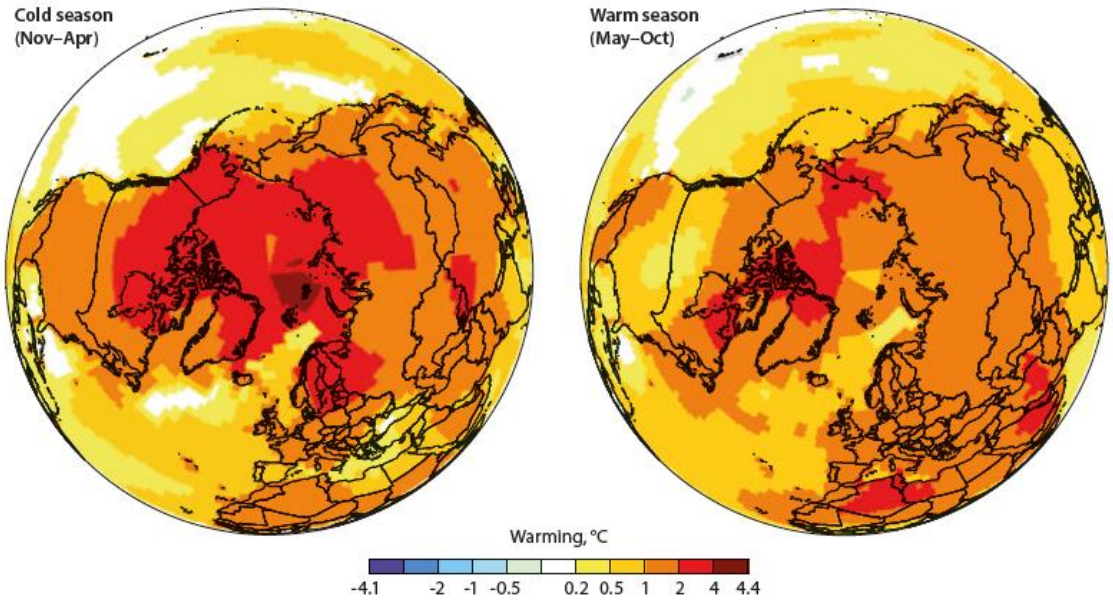

Figure 6: Spatial pattern of Arctic warming for the period 1961-2014 in the cold season (November-April) and warm season (May-October) (OVERLAND et al. 2017, on the basis of NASA GISTEMP).

The ongoing Arctic warming has certainly an effect on permafrost regions with consequences on hydrological, geomorphological and biological processes (OLIVA & FRITZ 2018). Because of its dynamically changing surface properties due to vegetation, snow, AL thickness, soil, surface- and groundwater the vulnerability and resilience of permafrost is complicated (GROSSE et al. 2011a). The increasing air temperature also impacts the temperature of permafrost. Since 2007-08 (the International Polar Year – IPY), the global mean permafrost temperature rose by 0.31 ± 0.10 °C per decade (OLIVA & FRITZ 2018). The colder permafrost of the continuous permafrost zone (in the Arctic and High Arctic) is exposed to the greatest increase, which can be more than 0.5 °C higher than during the IPY. In warmer permafrost regions (the southern and central Mackenzie Valley, the Alaskan Interior or the discontinuous permafrost zone of Siberia) the increase of permafrost temperature was smaller; 0.2 °C more compared to the IPY (ROMANOVSKY et al. 2017). The rising air and permafrost temperatures are favoring the deepening of the AL (OLIVA & FRITZ 2018). In contrast to the permafrost temperature, the AL thickness responds more to short-term variations of the climate and therefore shows a greater interannual variability (variations in summer temperatures). Long-term observations also indicate an increasing trend in AL thickness (ROMANOVSKY et al. 2017). By 2200 the AL thickness is projected to increase by 53-97 cm (SCHAEFER et al. 2011). The trend in the climate warming also has effects on the extent of permafrost and could significantly reduce the surface underlain by permafrost. Depending on the rate of climate warming near-surface permafrost could be reduced by 37 to 81 % and will retreat into higher latitudes and elevations. Most recent permafrost regions will be affected by the warming climate leading to degradation or even its disappearance (OLIVA & FRITZ 2018).

The areas that are underlain by ice-rich permafrost are of especial significance. Thawing of ice-rich permafrost causes strong feedbacks to the stability of the ground surface, microtopography, ecosystem function, hydrology and the C cycle (GROSSE et al. 2011a). It can lead to deformation and subsidence of level surfaces forming irregular thermokarst terrain. The effects range from local impact by subsidence beneath individual structures to extensive and deep depressions that developed in response to a long-term climate change (NELSON et al. 2001).

2.4 Carbon in permafrost

During the late Quaternary the decomposition rate of organic matter in the Arctic was slower than the plant growth, sedimentation and freezing rates (STRAUSS et al. 2015) due to low soil temperatures and poor soil drainage (HUGELIUS et al. 2014). As a result of processes such as cryoturbation, deposition of peat and repeated accumulation and stabilization of organic-rich material permafrost SOC (plant and animal remains) was deposited in mineral soils, peat depositions, silty organic- and ice-rich deposits (Yedoma), deltaic deposits and other

unconsolidated depositions from the Quaternary (HUGELIUS et al. 2014, SCHUUR et al. 2015). The ground in permafrost regions stores approximately twice as much C than there is contained in the current atmosphere (SCHUUR et al. 2015). About 50 % of the global SOC is stored in permafrost. Across the northern circumpolar permafrost region SOC stocks in the first three meters of soil, deltaic depositions and Yedoma permafrost depositions are estimated on 1307 ± 170 Pg (1 Pg = 1 billion tons); 999 Pg of this is stored in permafrost terrain (defined as the storage in High Arctic Soils/Gelisols and in deposits below 3 m depth) (HUGELIUS et al. 2014).

The effects of climate change on permafrost discussed in chapter 2.3 have an impact on the C storage. The large reservoirs of C pools in the permafrost regions are vulnerable towards changes due to a warming climate (SCHUUR et al. 2015). Organic matter decomposition caused by permafrost thawing releases OC to the ecosystem. This increases the release of the GHGs CO_2 and CH_4 to the atmosphere and therefore causes a positive feedback to global warming (Figure 7) (STRAUSS et al. 2017). This can accelerate climate change but the timing and magnitude of the GHG gas emissions and their impact on climate change is still uncertain. SCHUUR et al. 2015 assume that this happens more likely gradual and continual than abruptly and massive. SCHAEFER et al 2011 predict a release of 190 ± 64 Gt of permafrost C into the atmosphere until 2200. However, their simulation did not include the permafrost warming induced by the permafrost C feedback and some regions were excluded. This estimate is therefore underestimating the real C release due to permafrost thaw. The strength of the permafrost C feedback depends on the impact of thawing permafrost. With a larger loss of permafrost extend the release of C will be larger. On top of that, if the permafrost carbon feedback is once initiated it is irreversible and strong and can change the Arctic permafrost from a C sink to a C source (SCHAEFER et al. 2011).

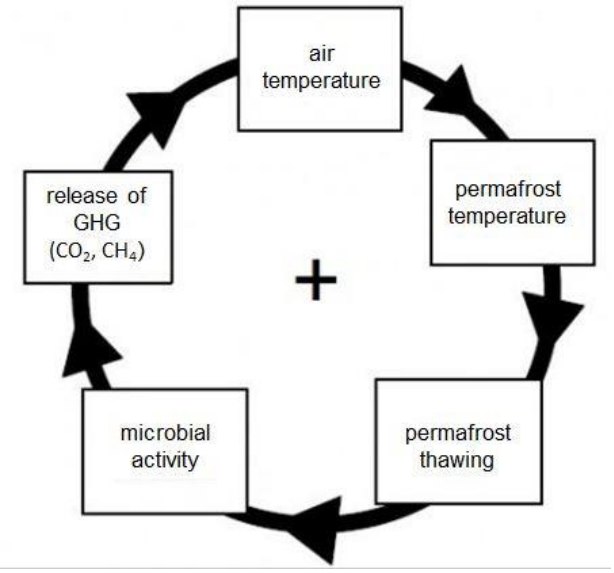

Figure 7: The positive permafrost carbon feedback cycle (STRAUSS et al. 2017, modified).

2.5 Permafrost degradation

With the ongoing global climate warming permafrost degradation is widespread in the Arctic (JORGENSON et al. 2001). According to VAN EVERDINGEN 2005 permafrost degradation is “a naturally or artificially caused decrease in the thickness and/or areal extent of permafrost”. It

can be caused by several reasons, for example by changes in terrain conditions or climate warming. These disturbances can have either natural or anthropogenic reasons (VAN EVERDINGEN 2005). The consequences of this degradation are deepening of the AL, reduction of the areal extent (ROMANOVSKY et al. 2017, VAN EVERDINGEN 2005) or the complete disappearance of permafrost (VAN EVERDINGEN 2005). Degrading permafrost can stand in relation with many processes, for example thermokarst, thermo-erosion, thermal abrasion or thermal denudation (ROMANOVSKY et al 2017). Depending on the ecological and climatic background and the permafrost characteristics (ground ice content and ground temperature) there are different possibilities permafrost may degrade. STRAUSS et al. 2017 differentiated between: a – ground warming and an increase in unfrozen water content, b – long-term thickening of the AL, c – thermo-erosion along coasts, rivers and lake shores, and d – rapid thaw due to thermokarst and thermo-erosional processes in lowlands, wetlands and hillslopes. According to MORGENSTERN 2012 the two main types of permafrost degradation are thermokarst and thermo-erosion.

In the different permafrost zones (continuous, discontinuous, sporadic) the climate-ecosystem interaction varies (SHUR & JORGENSON 2007). Areas of discontinuous, relatively warm and thin permafrost are especially prone to the impacts of climate change (JORGENSON et al. 2001). Due to permafrost degradation, changes in the vegetation composition, hydrologic cycle and function of the ecosystem were detected. This also influences the CH_4 and CO_2 fluxes (chapter 2.4) (JORGENSON et al. 2001, LAWRENCE & SLATER 2005). The destroying effect of degrading permafrost on settlements and infrastructure is also well known (NELSON et al. 2002, ROMANOVSKY et al. 2017).

2.6 Thermo-erosion and thermo-erosional valleys

Thermo-erosion is “the erosion of ice-bearing permafrost by the combined thermal and mechanical action of moving water” (VAN EVERDINGEN 2005), which includes the transport of the thawed sediments (VAN EVERDINGEN 2005). Depending on the direction the thermo-erosion acts there are two types that can be distinguished: linear (into depth) and lateral (sideways) (MORGENSTERN 2012). It can occur along the coasts, where it promotes coastal erosion (GÜNTHER et al. 2013), along river banks resulting in high erosion rates (COSTARD et al. 2003) and on surfaces of ice-rich sediments where it causes the rapid formation of thermo-erosional valleys and gullies (MORGENSTERN 2012, GODIN et al. 2014).

Due to surface runoff by snowmelt, summer precipitation or thawing permafrost on ice-rich permafrost there is a concentration of moving water along ice wedges causing preferential thawing, which results in the formation of gullies and valleys (FRENCH 2007). The rates of these thermo-erosional processes can vary from year to year. It depends on the local snow

depth, the speed the snow cover needs for melting and the surface runoff (GODIN & FORTIER 2012). Thermo-erosional valleys in ice-rich areas have the potential to restructure Arctic drainage networks, which leads to great changes in runoff volumes and timings. There is also a possible increase in sediment and nutrient transport to rivers and the sea (ROWLAND et al. 2010). Thermo-erosional valleys are distributed over wide areas in the Arctic and act as important snow accumulation areas. Furthermore, they have a significance influence on sediment, water and organic matter transport from permafrost to coastal waters at local scale (MORGENSTERN 2012).

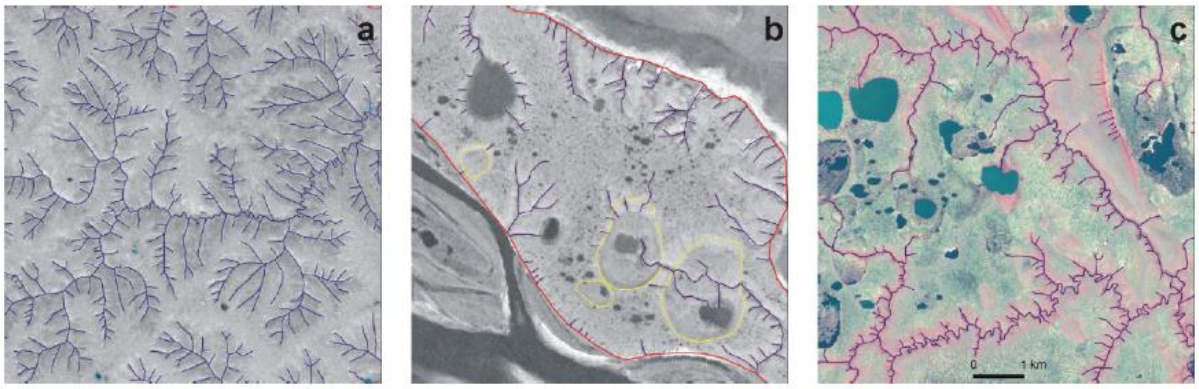

Figure 8: Different morphological valley types. a – extensive dendritic valleys; b – short parallel valleys along the margin of the Ice Complex, short radial valleys around thermokarst lakes; c – extensive longitudinal valleys with sharp meanders and short contributing valleys (MORGENSTERN 2012).

The morphology and spatial distribution of thermo-erosional valley systems basically depends on the relief gradient, the size of the catchment and the previous degradation of the initial surface of the Ice Complex by thermokarst (MORGENSTERN 2012). As a consequence, there are three different morphological valley types (Figure 8). Extensive dendritic valley systems have formed on large, broad Ice Complex plains, where a large catchment and a huge amount of water led to the formation of large permanent streams and channels (Figure 8a). Short parallel valley systems have formed on small remains of the Ice Complex. Those valleys are predominantly short but have cut deep into steep cliffs (Figure 8b). Extensive longitudinal valley systems with short tributaries have mainly evolved on low surfaces that have been degraded by extensive thermokarst (Figure 8c) (MORGENSTERN 2012). In the Lena River Delta short thermo-erosional valleys are most common. They can be up to 2 km long and sometimes have short tributary valleys (Figure 8b). The valleys are typically parallel aligned along the steep cliffs that show a sudden transition between the Yedoma upland and the channels and floodplains of the delta (MORGENSTERN 2012).

In addition to the differentiation of the morphological valley types, MORGENSTERN 2012 also observed eight different types of valley profiles (Table 1).

Table 1: Different types of valley profiles and their corresponding hydrological features (MORGENSTERN 2012).

Category	Occurrence	Characteristics	Hydrologic regime
short, straight gullies	on alas and thermokarst lake slopes	radially arranged around lakes and alasses; V- to U-shaped; steep gradient; up to a few meters deep and wide; dense, fresh vegetation	intermittent streams
drainage pathways in alasses	on alas floors	connect residual and secondary thermokarst lakes in partly drained alasses with the stream network outside the alasses; slightly indented into the alas floor; low gradient; up to a few meters wide; dense, fresh vegetation	intermittent and small permanent streams
V-shaped ravines	along steep coasts and cliffs; often due to lake drainage	V-shaped; steep to moderate gradient, up to tens of meters deep and wide; vegetation cover on floor and lower slopes often disturbed	intermittent streams
V-shaped valleys	in upper parts of the watersheds on Yedoma uplands	mostly tributary valleys; V-shaped; moderate to low gradient, up to tens of meters deep and hundreds of meters wide; intact vegetation cover	intermittent streams
U-shaped valleys	on Yedoma uplands	U-shaped; low gradient, up to tens of meters deep and several to tens of meters wide; flat valley floor with fresh vegetation	intermittent and small permanent streams
valleys of permanent streams and rivers	lower parts of long streams close to their mouth	U-shaped; low gradient, up to tens of meters deep and hundreds of meters to kilometers wide; broad floors with distinct floodplains; often bare sediment exposed; oxbow and small thermokarst lakes	permanent meandering streams
water tracks	on gently sloping Yedoma uplands; on large slightly inclined alas floors	arranged in parallel; low gradient; not or only slightly indented into the surface; dense, fresh vegetation	poorly developed runoff systems

3 Regional setting and study site

3.1 Lena River Delta

The Lena River Delta, located in the Laptev Sea (Figure 10), is the largest Arctic delta and the third largest in the world. The delta covers an area of approximately 32,000 km² and is characterized by a huge network of large and small rivers, channels and streams with more than 1,000 islands (ARE & REIMNITZ 2000, WALKER 1998, SCHNEIDER et al. 2009). The delta has an extend of 190 km from south to north (72.0-73.8°N) and 250 km from west to east (122.0-129.5°E) (BOLSHIYANOV et al. 2015). With an annual discharge of 520 $km^3 \cdot a^{-1}$ and a sediment load of 21 $Mt \cdot a^{-1}$ the Lena River is the major terrestrial source of water and sediment for the Laptev Sea (ARE & REIMNITZ 2000).

The delta is underlain by continuous permafrost with a thickness of 500-700 m (ROMANOVSKII et al. 2004), its seasonal thaw depth is 30-50 cm (BOLSHIYANOV et al. 2015). It was formed during the Middle to Late Pleistocene when the global sea-level was lower and the Lena River had its delta farther north. The accumulation of the recent Ice Complex was favored by relatively flat and extensive surfaces with a very low hydrological gradient, a poorly developed drainage system and the cold and dry climate of the Pleistocene (SCHIRRMEISTER et al. 2011a). For further details see chapter 2.2.

The Lena River Delta is located in a neotectonic zone with high seismic activity (ARE & REIMNITZ 2000) caused by a rift system in the eastern Laptev Sea that separates the North American and Eurasian plates (SCHIRRMEISTER et al. 2011a). This is characterized by vertical block movements that can locally exceed up to 60 m on Pleistocene and Holocene time scales (ARE & REIMNITZ 2000, SCHIRRMEISTER et al. 2011a). The main drivers are the extension of the Arctic Mid-Ocean Ridge into the Laptev Sea and uplift of the Siberian coast ridges, which both have a huge influence on the river characteristics (SCHWAMBORN et al. 2002). A tectonic boundary running from north to south separates the western and the eastern section of the delta along the Tumatskaya branch (Figure 9). The neotectonic activity in the Lena River Delta is documented until recent times (Figure 9) (SCHWAMBORN et al 2002).

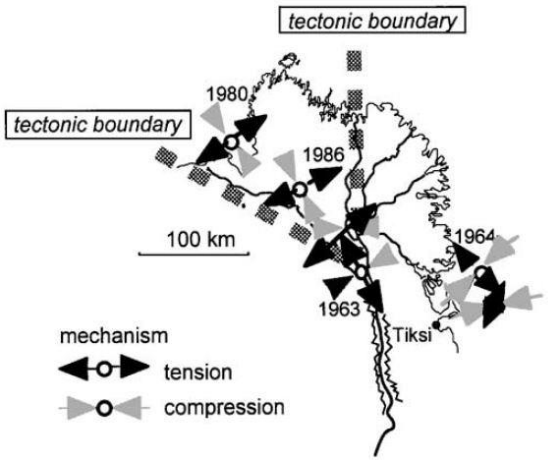

Figure 9: Tectonic boundaries of the Lena River Delta. The dates show the occurrence of recent earthquakes with a magnitude from 5-6 (SCHWAMBORN et al. 2002).

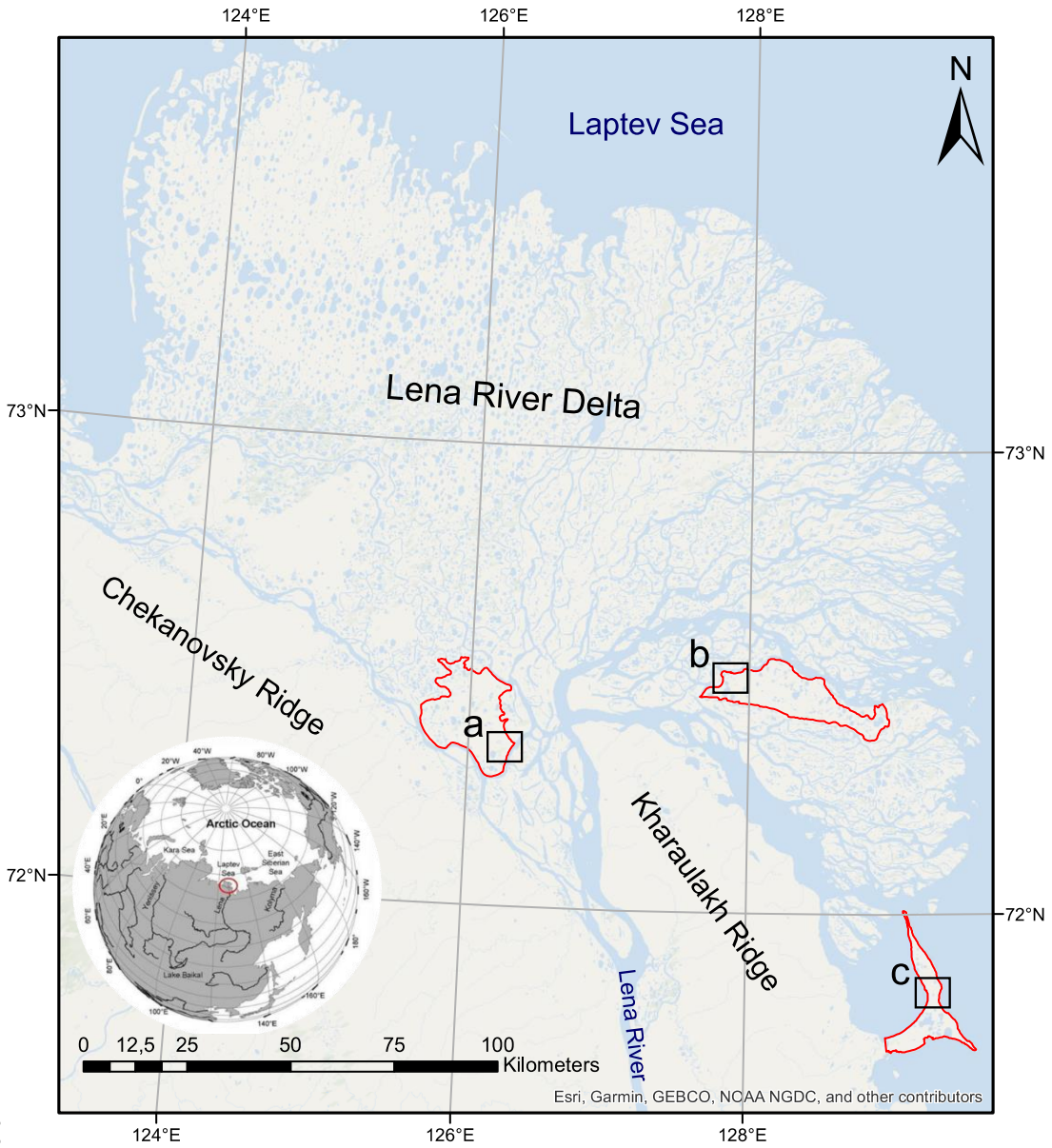

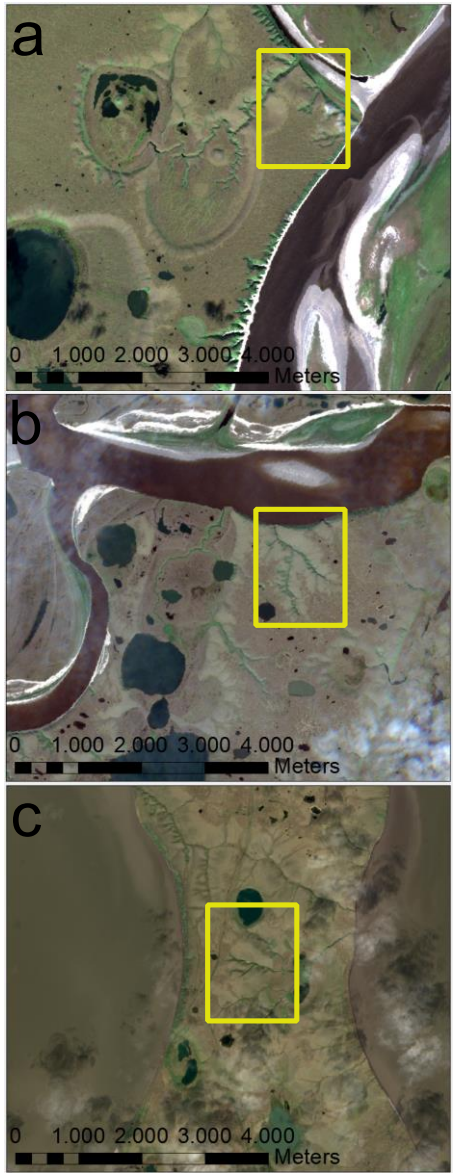

Figure 10: Location of the study areas within the Lena River Delta. Marked in red are the three study sites: a – Kurungnakh Island; b – Sobo-Sise Island; c – Bykovsky Peninsula. Black boxes mark the location of the satellite images on the right side, the yellow boxes in the satellite images mark the exact location of the three studied thermo-erosional valleys (see also Figure 12, Figure 14 & Figure 17) (sources: map: ArcGIS basemap "Oceans", WGS 1984, UTM Zone 52N; satellite images: Sentinel 2A, acquisition dates: a – 23 August 2016, b, c – 20 August 2016, band combination 3-2-1).

The Lena River Delta can be subdivided into three geomorphological terraces (Figure 11) that differ in stratigraphy and genesis. The first terrace covers the main part of the eastern delta and includes the active floodplains with surface elevations between 1-12 m above sea-level (m a. s. l.). It is the youngest part of the delta and was formed during the Holocene, the western part in the Early Holocene and the eastern part in the Late Holocene (SCHWAMBORN et al. 2002). The first terrace is characterized by patterned ground formed due to ice wedge polygons and relatively ice-rich sediments (SCHNEIDER et al. 2009) and mainly stretches along the main river channels in the central and eastern parts of the delta (SCHIRRMEISTER et al. 2011b). The surface elevation of the second terrace ranges from 11-30 m a. s. l. and is located in the north-western part of the delta (Figure 11). It was formed between the Late Pleistocene and the Early Holocene and is characterized by sandy sediments with low ice content (SCHNEIDER et al. 2009). One characteristic feature of the second terrace are the NNW-SSE-oriented thermokarst depressions often containing lakes (SCHIRRMEISTER et al. 2011b). The third terrace is the oldest part of the Lena River Delta with heights ranging between 30-60 m a. s. l. (SCHNEIDER et al. 2009). Because there is a considerable difference in elevation between the western and the eastern part of the terrace (more than 20 m) it can be subdivided into two areas (SCHWAMBORN et al. 2002). It has no fluvial-deltaic origin but its islands are erosional remnants of a Late Pleistocene plain that consist of fine-grained, ice-rich and organic-rich sediments (SCHNEIDER et al. 2009). The third terrace covers parts of the southern and southwestern areas of the Lena River Delta (Figure 11). Its surface is often dissected by thermokarst depressions that contain lakes and thermo-erosional valleys – typical degradation features that represent the morphology of ice-rich periglacial landscapes (SCHIRRMEISTER et al. 2011a).

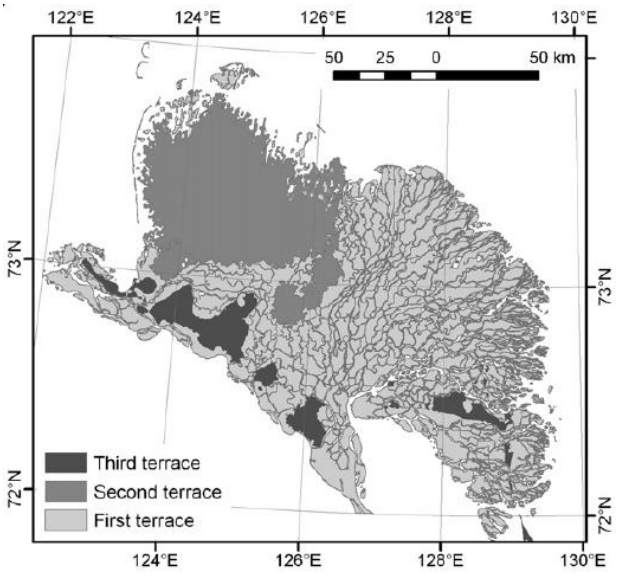

Figure 11: Distribution of the three main geomorphological terraces in the Lena River Delta (SCHNEIDER et al. 2009, based on SCHWAMBORN et al. 2002, adapted).

The climate in the region of the Lena River Delta is Arctic continental, characterized by low mean annual air temperatures of -13 °C. The mean temperature in January is -32 °C and in June 6.5 °C, with 190 mm the annual precipitation is low (SCHNEIDER et al. 2009). Between 1999 and 2011 the annual mean air temperature on Samoylov Island in the Lena River Delta was -12.5 °C. In these recorded years the coldest temperatures occurred in January (-30.3 °C) and February (-33.1 °C), whereas the warmest months were July and August with

mean monthly temperatures of 10.1 °C and 8.5 °C (BOIKE et al. 2013). Precipitation occurs mainly in summer between the middle of May and the end of September. Between 1999 and 2011 the summer precipitation varied between 52 mm and 199 mm with a mean precipitation of 125 mm. 70 % of these rainfall events were light with less than 1 mm of precipitation. Only one percent of the recorded rainfall events were heavy precipitation events with more than 16 mm (BOIKE et al. 2013). Due to its location on the border between the Siberian mainland and the Arctic Ocean, there is an exchange of warm and dry air masses and advection of cold and moist air masses, which causes variable weather conditions during the summer months (KUTZBACH et al. 2007).

Snow cover has an influence on the surface radiation characteristics. Because snow is a strong insulator it limits the heat exchange between the ground and the atmosphere, which is apart from that quite efficient. With a significant snow cover in winter the mean annual surface temperature is warmer than the mean annual air temperature due to the insulating effects of snow (STIEGLITZ et al. 2003). Patches of snow can also accumulate in small ravines and valleys and last for a few months (seasonal) or some years (perennial). When snow patches are melting the flowing meltwater can lead to surface erosion (KUNITSKY et al. 2002). The depth of snow shows high spatial variability because strong winds can redistribute the snow. Snow melting usually starts in May and by early June the snow cover is disappeared. This snow-free state remains until September (BOIKE et al. 2013).

In the Lena River Delta, plant growth is limited because of the rough climatic conditions mentioned earlier. Another narrowing factor is light – polar night begins in November and ends at the end of January whereas polar day lasts from March to August. The plant growing season in the summer lasts about three months (from the middle of June to the middle of September). That is why tundra vegetation is the predominant vegetation type in the Lena River Delta. It primarily consists of grasses, sedges, low shrubs, small flowering herbs, lichens and mosses (KUTZBACH et al. 2007).

3.2 Study sites

3.2.1 Kurunghakh Island

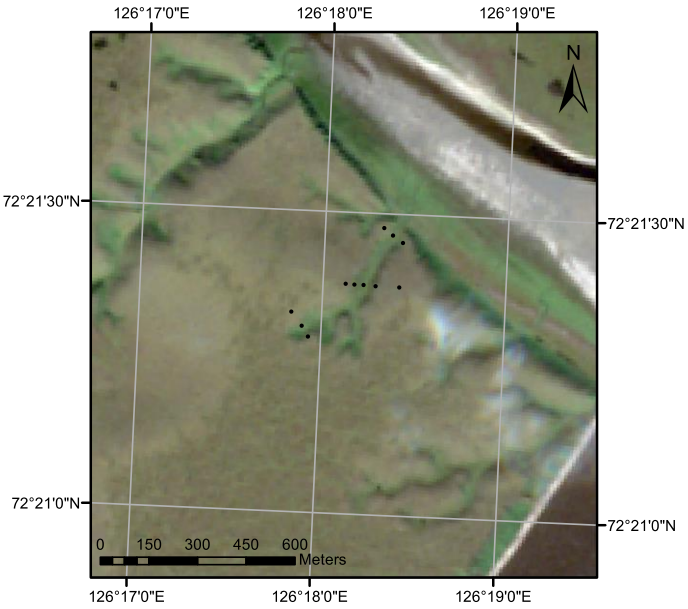

Figure 12: Satellite image of the studied thermo-erosional valley on Kurungnakh Island. The black dots mark the sampling locations (source: Sentinel 2A, acquisition date: 23 August 2016, band combination 3-2-1, WGS 1984, UTM Zone 52N).

Kurungnakh Island is located in the southern part of the Lena River Delta (Figure 10) and is partly exposed up to 40 m above the river level (BISCHOFF et al. 2011). It has an area of 260 km² (MORGENSTERN et al. 2011). The island is mainly composed of Late Quaternary sediments of the third terrace of the Lena River Delta. The circa 20 m thick Yedoma depositions are overlain by Holocene layers of 2-3 m thickness (BISCHOFF et al. 2011, WETTERICH et al. 2008). Kurungnakh Island is the easternmost part of the tectonically uplifted western Lena River Delta (MORGENSTERN et al. 2011). The surface of the island is characterized by thermokarst and thermo-erosional features (MORGENSTERN et al. 2011).

The studied thermo-erosional valley on Kurungnakh Island (KUR/KUR16-TEV1) is located on the eastern part of the island (Figure 10). It has a length of approximately 500 m and is the smallest valley of this study. The valley is draining into a branch of the Lena River (Figure 10, Figure 12). Because there are no active thermo-erosional processes the valley is stable (Figure 13).

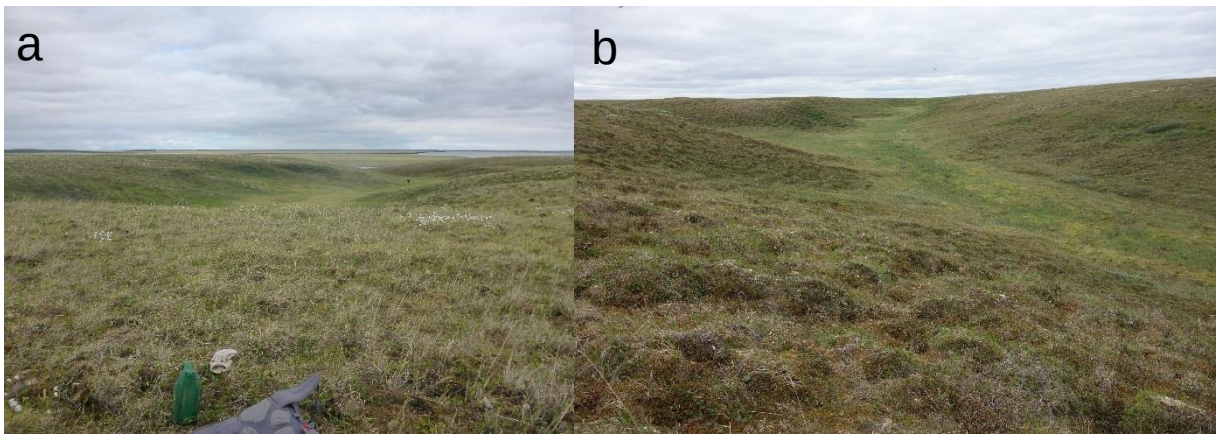

Figure 13: Photos of the thermo-erosional valley on Kurungnakh Island. a – view from upstream to downstream; b – view from downstream to upstream (Photos: J. Ramage (a), A. Morgenstern (b)).

3.2.2 Sobo-Sise Island

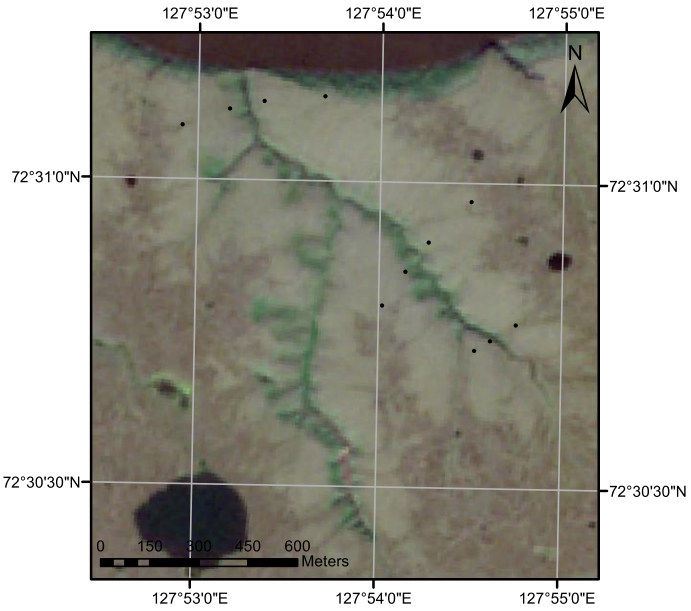

Figure 14: Satellite image of the studied thermo-erosional valley on Sobo-Sise Island. The black dots mark the sampling locations (source: Sentinel 2A, acquisition date: 20 August 2016, band combination 3-2-1, WGS 1984, UTM Zone 52N).

Sobo-Sise Island is located in the eastern part of the Lena River Delta (Figure 10) and is characterized by Yedoma deposits of the third geomorphological terrace of the delta. The east-west elongated island has a length of 45 km and an area of 336 km². It is situated between two of the main channels of the Lena River Delta. Besides the Yedoma upland Sobo-Sise Island is also characterized by degradational landforms such as thermokarst lakes, drained thaw lake basins and thermo-erosional valleys (FUCHS et al. 2018).

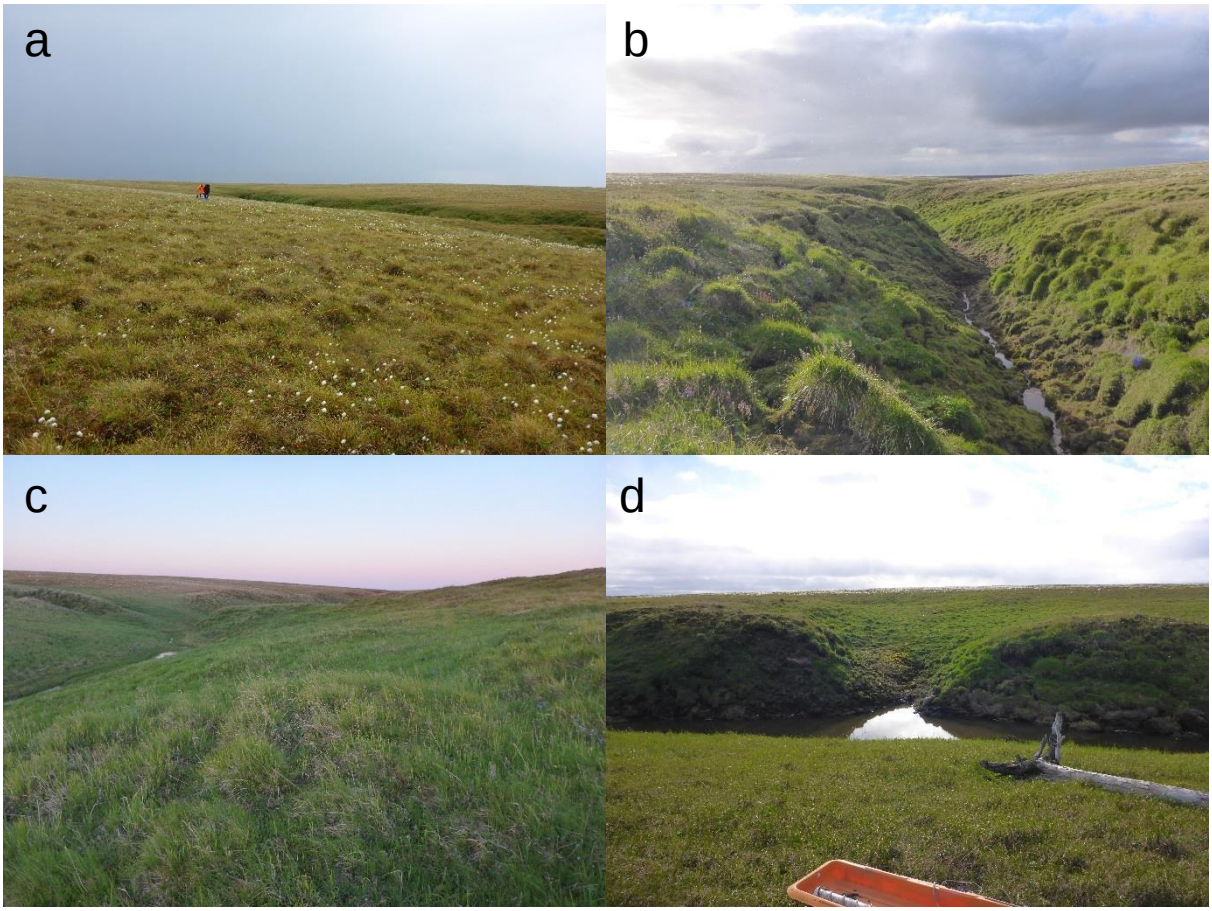

Figure 15: Photos of the thermo-erosional valley on Sobo-Sise Island. a – upstream; b – view from midstream to downstream; c – view from midstream to upstream; d – downstream (Photos: J. Ramage).

The thermo-erosional valley investigated on Sobo-Sise Island (SOB/SOB16-TEV3) is located at the north-western margin of the island (Figure 10). With a length of approximately 1.5 km it is the largest valley of this study. Just like KUR, this valley is also draining into a branch of the Lena River (Figure 10, Figure 14). The thermo-erosional processes in the valley are still active, a huge part of the valley carries water on its valley bed. (Figure 15b, c, d). It starts as a very small stream approximately at the midstream transect and gets broader downwards. The valley outlet is wide enough for navigating a small boat (Figure 16).

Figure 16: Outlet of the studied valley on Sobo-Sise Island (Photo: J. Ramage).

3.2.3 Bykovsky Peninsula

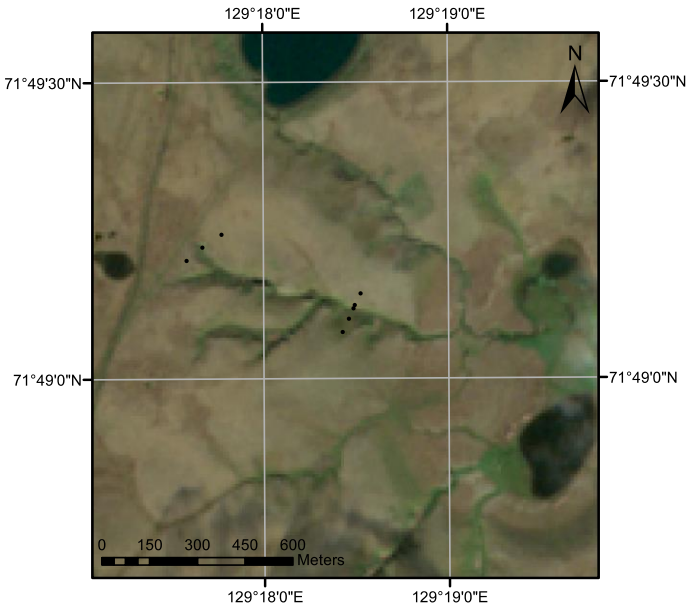

Figure 17: Satellite image of the studied thermo-erosional valley on Bykovsky Peninsula. The black dots mark the sampling locations (source: Sentinel 2A, acquisition date: 20 August 2016, band combination 3-2-1, WGS 1984, UTM Zone 52N).

The Bykovsky Peninsula is located at the foot of Kharaulakh Ridge and the tip of one of the outflow channels of the Lena River Delta (Figure 10). The peninsula is orientated NNW-SSE and its north-eastern coast is exposed to the Laptev Sea (LANTUIT et al. 2011). Bykovsky Peninsula has an area of 167 km² and is a narrow tongue of land with widths between 1 and 4 km (FUCHS et al. 2018). It is underlain by extensive Yedoma deposits covered by a Holocene layer consisting of reworked sediments from the Ice Complex enriched with organic matter in thick peat horizons (LANTUIT et al. 2011). The surface is characterized by low-lying depressions formed by thermokarst that cover about 46 % of Bykovsky Peninsula, another 6 % is occupied by thermo-erosional valleys (GROSSE et al. 2005). In contrast to Kurungnakh Island and Sobo-Sise Island the Bykovsky Peninsula is owing to its location strongly affected by rapid coastal erosion and inundation (FUCHS et al. 2018).

The studied thermo-erosional valley on the Bykovsky Peninsula (BYK/BYK-TEV5) is located at its central part (Figure 10). It has a length of approximately 1 km. In contrast to KUR and SOB, this valley is draining into a drained thermokarst lake basin (Figure 17). The valley has not stabilized completely, particularly in upstream area there are some thermo-erosional processes occurring (Figure 18a). The downstream part does not show active thermo-erosion (Figure 18b).

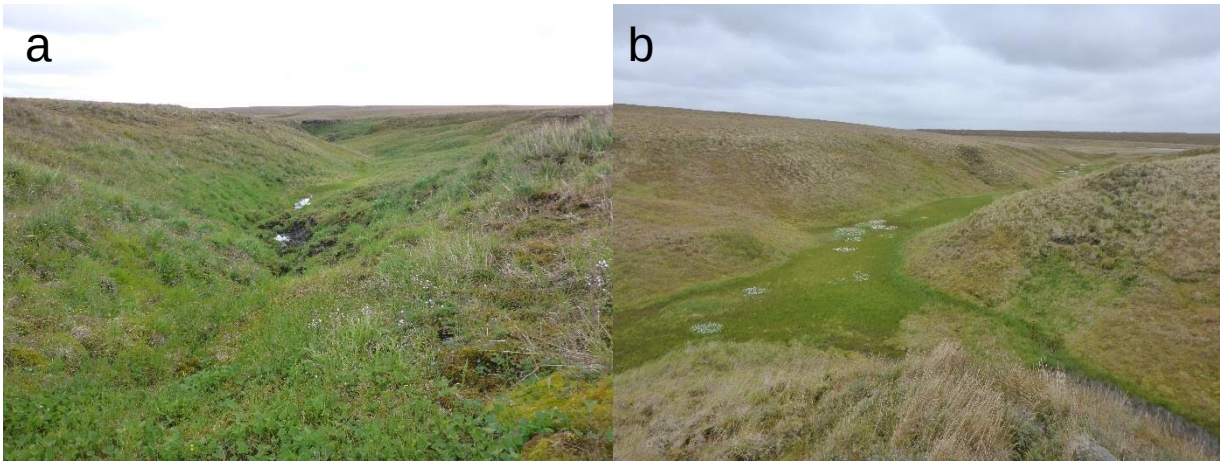

Figure 18: Photos of the thermo-erosional valley on Bykovsky Peninsula. a – upstream; b – downstream (Photos: J. Ramage).

4 Methods

4.1 Field work

The samples from the thermo-erosional valleys analyzed in this thesis were taken during the Lena Expedition 2016 by Justine Ramage assisted by Sebastian Wetterich, Georgy Maximov, Anne Morgenstern and Guido Grosse. During this expedition the three study sites in the Lena River Delta (Kurungnakh Island, Sobo-Sise Island and Bykovsky Peninsula – chapter 3.2) were visited.

For the sampling of the valleys a transect sampling scheme was developed (Figure 19). It consists of three cross-profiles through the valley that cover its upper, middle and lower part. Along those transects the drilling locations (black dots in Figure 19) were set on the Yedoma upland, on the slopes and at the valley

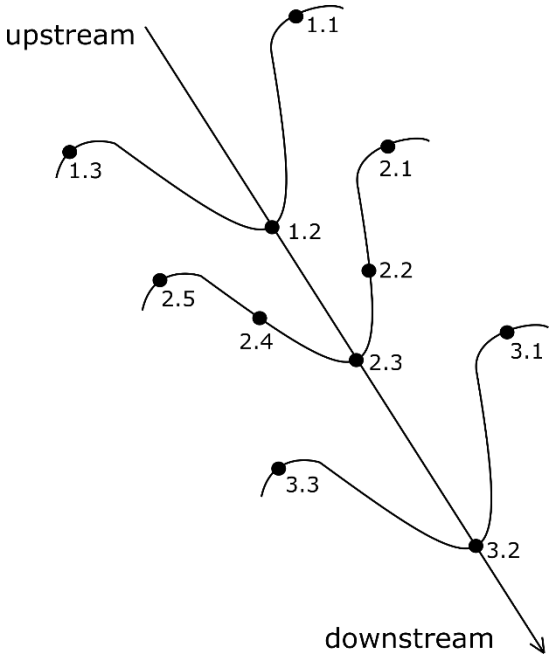

Figure 19: Valley transect sampling scheme with three cross-profiles on the example of the valley on Kurungnakh Island. Black dots mark the sampling locations (1.1-1.3: upstream transect, 2.1-2.5: midstream transect, 3.1-3.3: downstream transect).

bottom (Figure 19). The sampling procedure in the three studied valleys differed slightly due to either different valley conditions or organizational circumstances.

At every drilling location soil pits were excavated down to the permafrost (Figure 20a). The vegetation was cut with a knife, the AL was sampled with a fixed volume core cutter that was inserted horizontally into the wall of the open soil pit (Figure 20a). Depending on how many soil horizons could be determined, two to three AL samples were collected. Afterwards a SIPRE permafrost corer of 76 mm in diameter was drilled into the permafrost to approximately 1 m depth (Figure 20c). The core was split into different sections based on visual inspection and described qualitatively (material, ice content, cryostructure) (Figure 20b, d). If the core was ceased by an ice wedge, the sampling procedure was stopped. That is why some of the cores are less than 1 m in length. The different sections from the cores were packed into plastic bags and weighed. After the field work was done, the samples -still frozen- were transported from Russia to Germany.

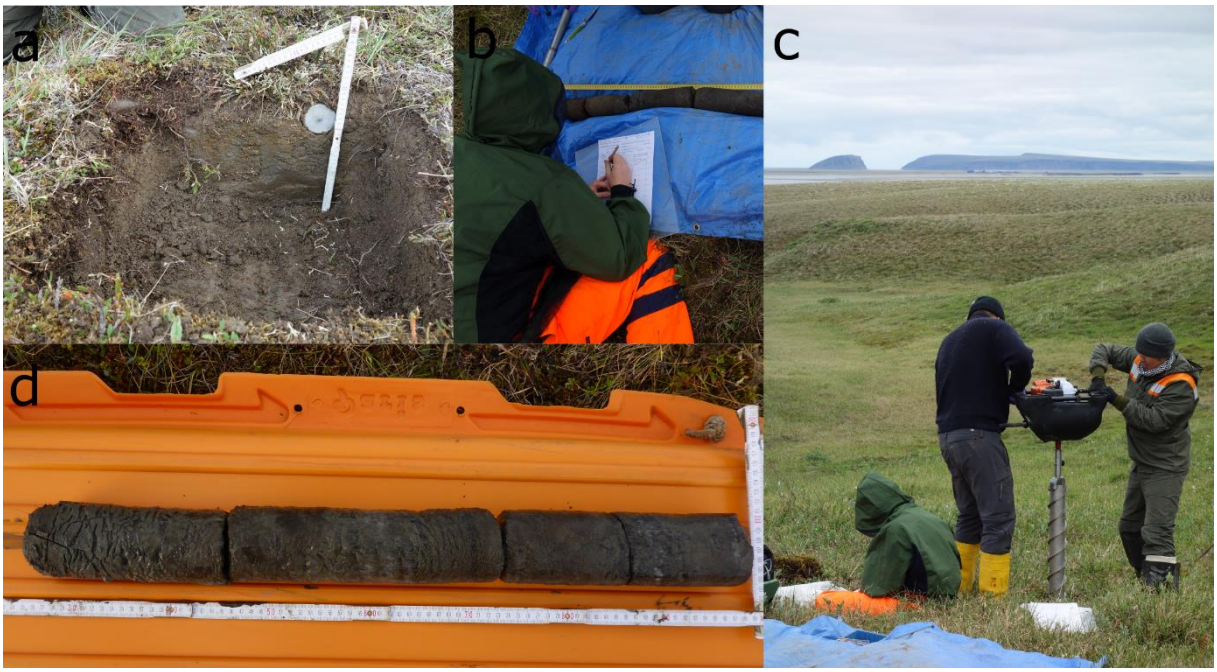

Figure 20: Field work during the Lena Expedition 2016. a – soil pit with a fixed volume core cutter; b – qualitative description of a core during field work; c – drilling of the permafrost with the SIPRE permafrost corer; d – permafrost core subdivided into different sections (Photos: A. Morgenstern (a, b, c), J. Ramage (d)).

4.2 Laboratory work

The samples were still frozen after the arrival in the laboratory of the Alfred Wegener Institute in Potsdam. As a first step of preparation for the laboratory analyses, the samples were freeze-dried for 72 hours (Sublimator 3-4-5, Zirbus technology). Afterwards the dry weight was determined. Finally, the samples were homogenized manually and a representable sub-sample was taken for further analyses (chapter 4.2.2).

4.2.1 Determination of water content and bulk density

The moisture content as well as the bulk density belong to the most relevant physical properties of permafrost (FRENCH 2007). With determining the wet weight as well as the weight after freeze-drying the water content of the samples was calculated (Equation 1).

$$W = \frac{m_w}{m_d} \cdot 100\ \% \qquad \textbf{Equation 1}$$

W	water content [%]
m_w	sample wet weight [g]
m_d	sample dry weight [g]

The bulk density describes the volumetric properties of the soil (SCHEFFER & SCHACHTSCHABEL 2010) and indicates its compaction. To calculate the bulk density the volume of the sample is required (Equation 2).

$$V = \pi \cdot r^2 \cdot h \qquad \textbf{Equation 2}$$

V	volume of the sample [cm^3]
r	radius of the corer [cm]
h	height of the sample segment [cm]

Afterwards the bulk density was calculated by dividing the weight of the dry sample by the total soil volume (Equation 3).

$$\rho_b = \frac{m_d}{V} \qquad \textbf{Equation 3}$$

ρ_b	bulk density [$g \cdot cm^{-3}$]
m_d	sample dry weight [g]
V	volume of the sample [cm^3]

4.2.2 Measurement of total carbon, total nitrogen total organic carbon

For measuring the TC, TN and the TOC contents the sub-samples were grinded and homogenized by a planetary mill (Pulverisette 5, Fritsch). The measurement of TC and TN as well as TOC is based on combustion. To determine TC and TN 5 mg of each sample was transferred into tin capsules twice together with tungsten(VI)-oxide. The tungsten(VI)-oxide ensures the complete oxidation of the sample at high temperatures (>900 °C). For calibrating the elemental analyzer used for this measurement (Vario EL III, Elementar) a blank capsule and a series of standards was added for each series of measurement. To ensure correct analytical values control standards were added after every 15 samples. The percentage of TC and TN was calculated based on the weight of the measured sample. The detection limit of the elemental analyzer for TN is 0.1 wt%.

TOC was measured by a different elemental analyzer (Vario Max C, Elementar). The principle is quite similar, but the samples are burned at lower temperatures (ca. 550 °C) so

the inorganic carbon is not detected. According to the TC content determined in the previous measurement 15 to 100 mg was weighed into crucibles.

4.3 Data processing

4.3.1 Analysis of the valley morphometry

For a better understanding of the processes going on in the valleys their morphometry needs to be obtained. Therefore, a digital elevation model (DEM) was used. In this study the Arctic DEM with a spatial resolution of 2 m (provided by the Polar Geospatial Center from the University of Minnesota) was used. The DEM was imported in ArcGIS and elevation profiles along the sampled transects were generated. The DEM was the base for the morphometric description of the three studied thermo-erosional valleys.

4.3.2 Total organic carbon to total nitrogen ratio

The C/N-ratio is an indicator for the mineralization rate of the organic matter (STRAUSS 2010). Thus, the C/N-ratio shows the degree of decomposition of the organic matter contained in the soil (Table 2). This is based on the assumption that the metabolic activity of the microorganisms primarily releases C and leaves the nitrogen (N) compounds behind (PALMTAG et al. 2016). The C/N-ratio can be used as well for predicting C loss from soils over time (SCHÄDEL et al. 2014).

Table 2: Approach to classify TOC/TN values (WALTHERT et al. 2004; cited in STRAUSS 2010).

TOC/TN-ratio	Description	Rate of mineralization
<10	very narrow	high
10-12	narrow	
13-16	moderately narrow	moderate
17-20	moderate	
21-25	moderately wide	
26-35	wide	low
>35	very wide	

To calculate the C/N-ratio of a sample its TOC value was divided by its TN value (Equation 4). The obtained value is non-dimensional.

$$C/N = \frac{TOC}{TN}$$

Equation 4

C/N	C/N-ratio
TOC	Total Organic Carbon [wt%]
TN	Total Nitrogen [wt%]

4.3.3 Soil organic carbon storage

The SOC storage was calculated based on the equation provided in HUGELIUS et al. 2010 (Equation 5). The TOC was derived by the elemental analysis (chapter 4.2.2), the bulk density (ρ_b) was calculated beforehand (chapter 4.2.1). The coarse fraction (CF) was zero because the sample was grinded before measuring with the elemental analyzer.

$$SOC = TOC \cdot \rho_b \cdot (1 - CF) \cdot h \cdot 10 \quad \textbf{Equation 5}$$

SOC	Soil Organic Carbon [kg · m^{-2}]
TOC	Total Organic Carbon [wt%]
ρ_b	bulk density [g · cm^{-3}]
CF	coarse fraction (> 2 mm diameter)
h	height of the sample segment [cm]

4.3.4 Preparation of the data for statistical approaches

Before the obtained data set can be analyzed it is necessary to homogenize the data to make sure that it is comparable. To ensure this, each core was split into segments of 10 cm in length (0-10 cm, 10-20 cm, …, 90-100 cm). Some of the samples already fulfilled this condition, others needed to be adapted. For segments shorter than 10 cm this was done by Equation 6. If a core was ceased by an ice wedge and was therefore shorter than 1 m, the last measured value was extrapolated for the remaining segments.

$$x_i = \frac{(h_1 \cdot x_1) + (h_2 \cdot x_2)}{10} \quad \textbf{Equation 6}$$

x_i	homogenized value
h_1	height of the first sample segment [cm]
x_1	original value of the first sample segment
h_2	height of the second sample segment that lack to 10 cm ($h_1 + h_2 = 10$ cm) [cm]
x_2	original value of the second sample segment

This was done for all measured geochemical parameters as well as for the C/N-ratio and the SOC storrage.

For the statistical analyses the homogenized data was normalized afterwards (Equation 7). That means the transformation of the dataset between the values 0 and 1, which ensures comparability. Per parameter the minimum and maximum value was determined from all its values from all studied thermo-erosional valleys. Therefore, the results are comparable among each other.

$$z_i = \frac{x_i - \min(x)}{\max(x) - \min(x)} \quad \textbf{Equation 7}$$

z_i	normalized value
x_i	homogenized value
min(x)	minimum value of the dataset
max(x)	maximum value of the dataset

4.3.5 Statistical approaches

According to the aims of this study the dataset was subdivided into different categories (Table 3). On the basis of this subdivision the significant difference between the obtained values was tested.

Table 3: Subdivision of the cores per valley into the investigated categories.

	transect			geomorphological unit			depth		
	up-stream	mid-stream	down-stream	Yedoma upland	slope	bed	0-30 cm	0-50 cm	0-100 cm
KUR16-TEV1	1.1	2.1	3.1	1.1	2.2	1.2	for each core individually		
	1.2	2.2	3.2	1.3	2.4	2.3			
	1.3	2.3	3.3	2.1		3.2			
		2.4		2.5					
		2.5		3.1					
				3.3					
SOB16-TEV3	1.1	2.1	3.1	1.1	2.2	1.2	for each core individually		
	1.2	2.2	3.2	1.3	2.4				
	1.3	2.3	3.3	2.1	3.2				
		2.4	3.4	2.4	3.4				
				3.1					
				3.4					
BYK16-TEV5	1.1		2.0	1.1	2.1	1.2	for each core individually		
	1.2		2.1	1.3	2.3	2.2			
	1.3		2.2	2.0					
			2.3	2.4					
			2.4						

The different datasets were first tested on their normal distribution. In this study the Shapiro-Wilk test was used, which has the advantage to work for small sample populations (n>30) (RAZALI & WAH 2011). The null hypothesis H_0 (the dataset is normally distributed) gets accepted when p>0.05. Because this did not apply for any of the studied parameters, the alternative hypothesis (the dataset is not normally distributed) was accepted.

On this basis the Kruskal-Wallis test was used for testing the significant difference. This test does not require a normal distribution of the samples and can be used for three or more sampled groups (McKnight & Najab 2010). For additional information on the relations between the single parameters, the Dunn's posthoc test was operated.

5 Results

5.1 Morphometry of the thermo-erosional valleys

5.1.1 Thermo-erosional valley on Kurungnakh Island

KUR is draining into a branch of the Lena River with a difference in elevation of 40 m. Its outlet is facing into the north-eastern direction. The Yedoma upland of the valley has an elevation gradient towards the coast of Kurungnakh Island of 30 m. A smaller valley is merging with KUR from the north-western direction of its outlet (Figure 12, Figure 21). Three transects of the valley were sampled – upstream, midstream and downstream (see chapter 4.1 for details). The upstream transect is located at the headwater of the valley and is across a first order stream, whereas the mid- and downstream transects are across a third order stream of the valley. The downstream transect is located near the outlet of KUR (Figure 21). The thermo-erosional valley is part of a short parallel valley system that has formed on small remains of the Ice Complex. According to Morgenstern 2012 (chapter 2.6) these are typical for the Lena River Delta.

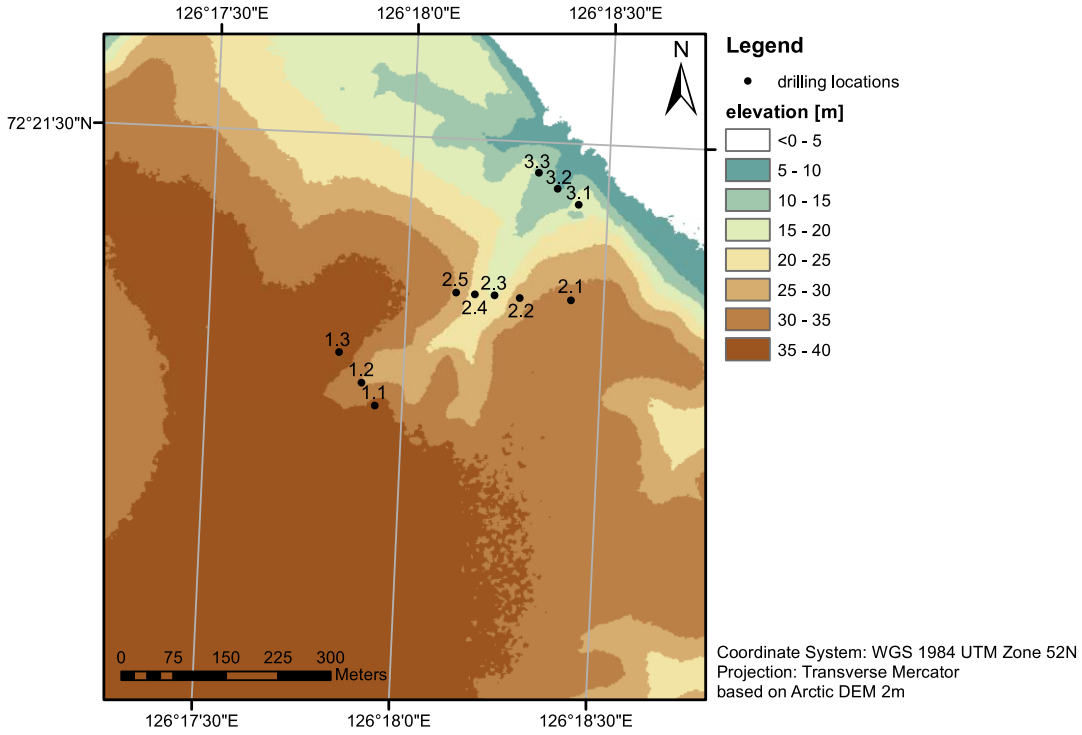

Figure 21: Elevation map of KUR with the sampling locations. The white area is showing the branch of the Lena River KUR is draining into.

Along the sampled transects elevation profiles were generated to observe the profile characteristics (Figure 22). All three valley profiles show a V-shape with slightly differences in topography.

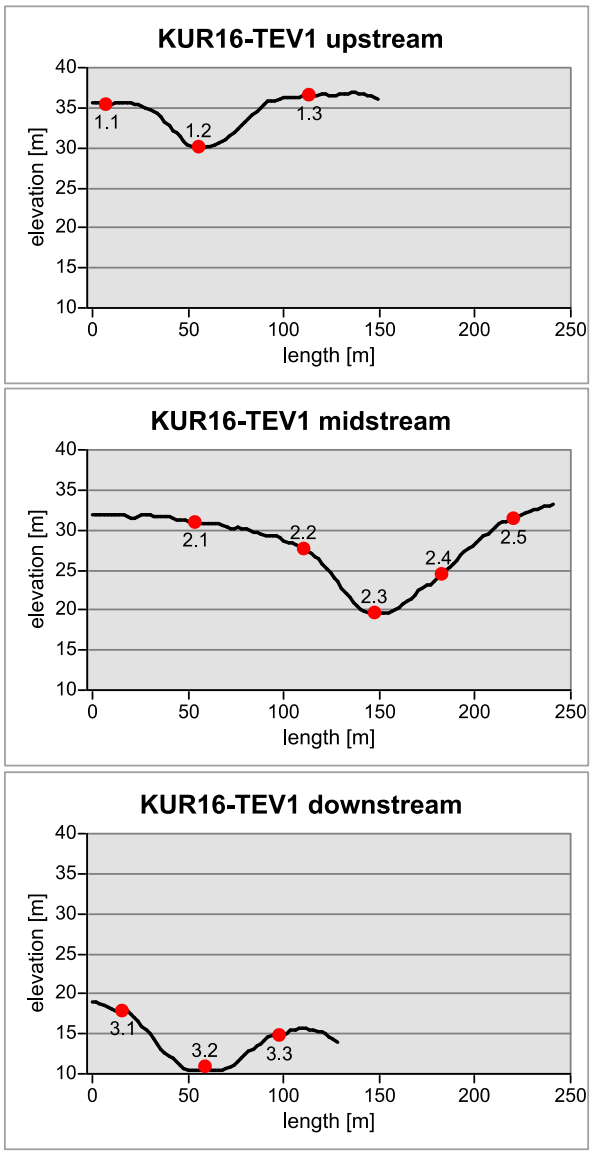

Figure 22: Elevation profile along the three transects of KUR. The red dots mark the sampling locations (based on the Arctic DEM with 2 m resolution).

The upstream transect of KUR has a width of approximately 100 m and a difference in elevation between the upland and the valley bed of about 5 m. The Yedoma upland has an elevation of 36 to 37 m a. s. l. The slope angles in the upstream area range between 1 to 22°; the north-western facing slope is with 3 to 22° slightly steeper than the south-eastern facing slope with 1 to 17°. The north-western facing slope has a slight concave shape whereas the south-eastern-facing slope is elongated (Figure 22).

The Yedoma upland of the midstream transect of KUR is 32 to 34 m a. s. l., lower than the upstream transect. The midstream transect is 200 m long and has a difference in elevation between the upland and the valley bed of about 15 m. The slope angles in this transect range between 1 to 30°, the difference in slope steepness is clearly visible. The elongated north-western facing slope angles range between 6 to 28°, whereas the slope angles of the convex south-eastern facing slope range between 3 to 17°. (Figure 22).

The downstream transect of KUR is located near the valley outlet. With around 20 m a. s. l. the Yedoma upland of this transect has the lowest elevation of the three transects. It is about 100 m long and has a difference in elevation between the upland and the valley bed of about 10 m. The slope angles range between 3 to 22°; the north-western facing slope is with 2 to 22° just slightly steeper than the south-eastern facing with 3 to 17°. Both slopes have a convex shape. The Yedoma upland located on the south-eastern side of downstream transect is higher elevated than on its north-western side (Figure 22).

5.1.2 Thermo-erosional valley on Sobo-Sise Island

SOB is draining into a branch of the Lena River with an elevation difference of 25 m. The valley outlet is facing into the northern direction. The elevation gradient from the headwater to the valley outlet is 21 m (Figure 23). Along the valley three transects were sampled – upstream, midstream and downstream. The upstream and midstream transects are located across a first order stream, the downstream transect across a third order stream. The upstream transect is located at the headwater of SOB, whereas the downstream transect is located near the outlet of the valley (Figure 23).

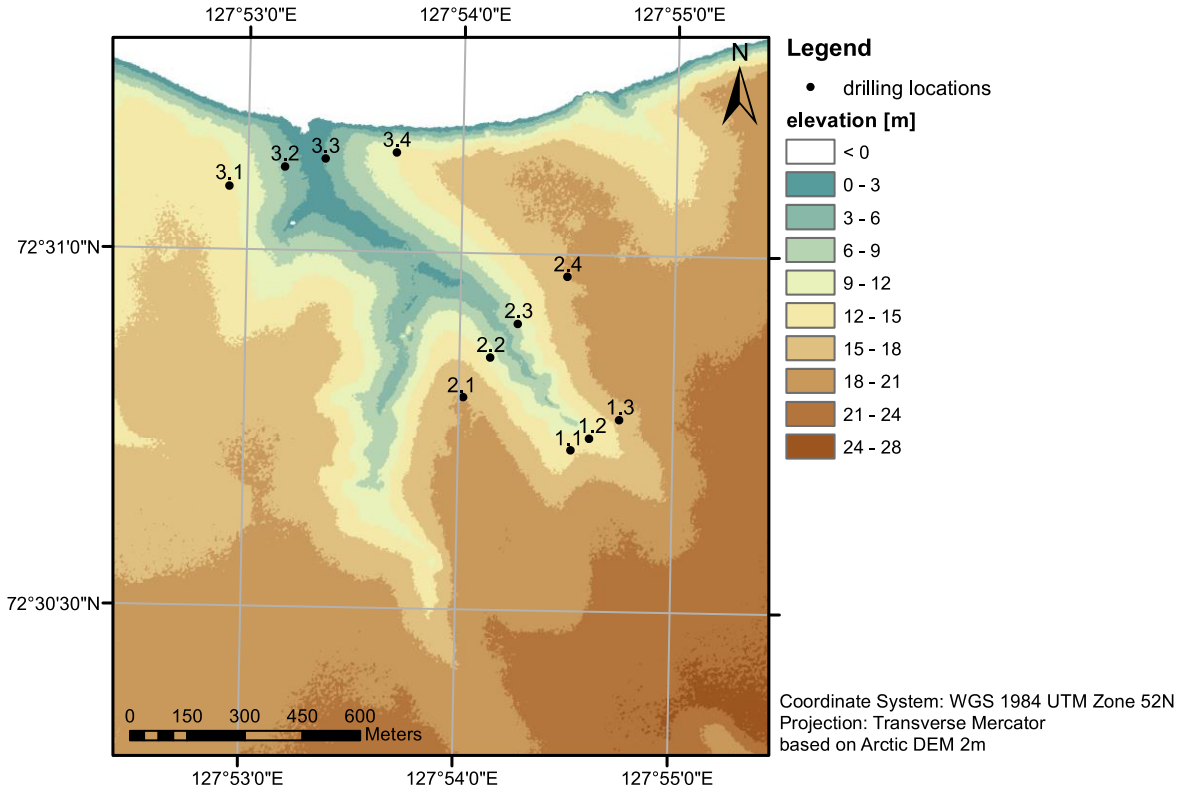

Figure 23: Elevation map of SOB with the sampling locations. The white area is showing the branch of the Lena River SOB is draining into.

The upstream transect of SOB is relatively flat, whereas its midstream and downstream transect have a V-shape (Figure 24).

The upstream transect of SOB is 400 m long and has a difference in elevation between the upland and the valley bed of about 12 m. The Yedoma upland has an elevation between 17 and 20 m a. s. l. The slopes of the transect have slope angles between 1 to 11°, the south-western facing slope is with 1 to 11° slightly steeper than the north-eastern facing with 1 to 7°. Both slopes have a convex shape (Figure 24).

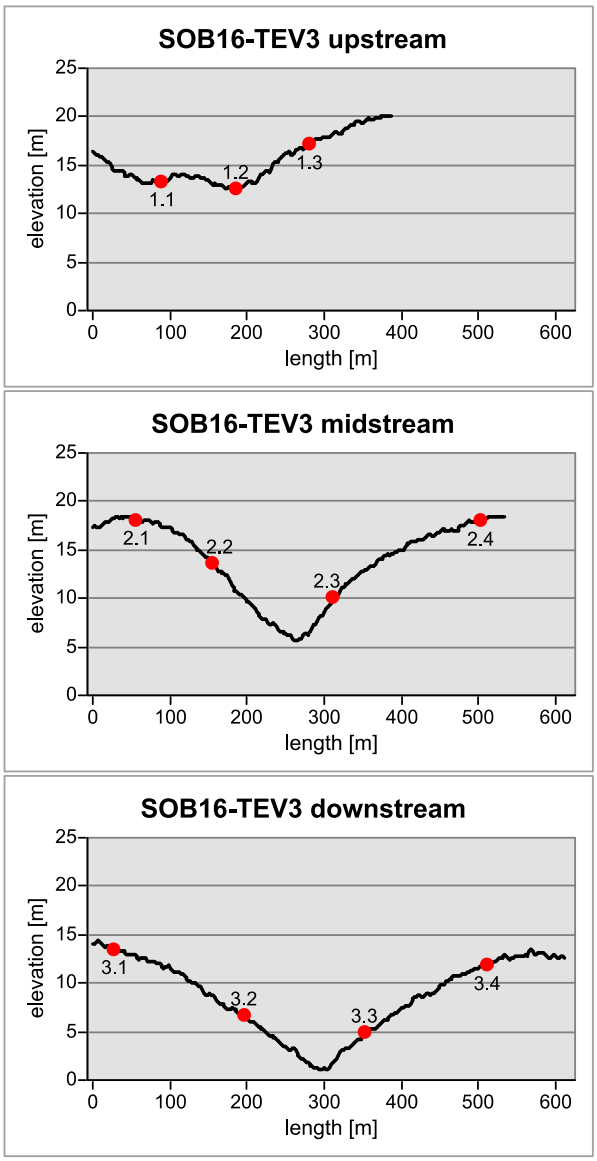

Figure 24: Elevation profile along the three transects of SOB. The red dots mark the sampling locations (based on the Arctic DEM with 2 m resolution).

The midstream transect of SOB has a length of 500 m and a difference in elevation between the upland and the valley bed of about 15 m. On both sides of the transect the Yedoma upland has an elevation of 17 m a. s. l. The slope angles of both slopes range between 1 to 20°, the south-eastern facing slope has a convex shape whereas the north-western facing is elongated (Figure 24).

The downstream transect of SOB is 600 m long and has a difference in elevation between the upland and the valley bed of about 15 m. The Yedoma upland has an elevation of 13 to 15 m a. s. l. The slope angles of the downstream transect range between 1 to 11°, the south-eastern as well as the north-western facing slope has a convex shape (Figure 24).

5.1.3 Thermo-erosional valley on Bykovsky Peninsula

In contrast to KUR and SOB, BYK is draining into a drained thermokarst lake basin. It is a lateral valley of a larger valley system that is flowing into the basin (Figure 17, Figure 25). From its headwater to the outlet it has a difference in elevation of approximately 35 m and its outlet is facing eastwards. In this valley two transects were sampled – upstream and downstream. The upstream transect is located at the headwater of the valley and crosses a first order stream, whereas the downstream transect is located near the outlet of BYK and crosses a third order stream (Figure 25).

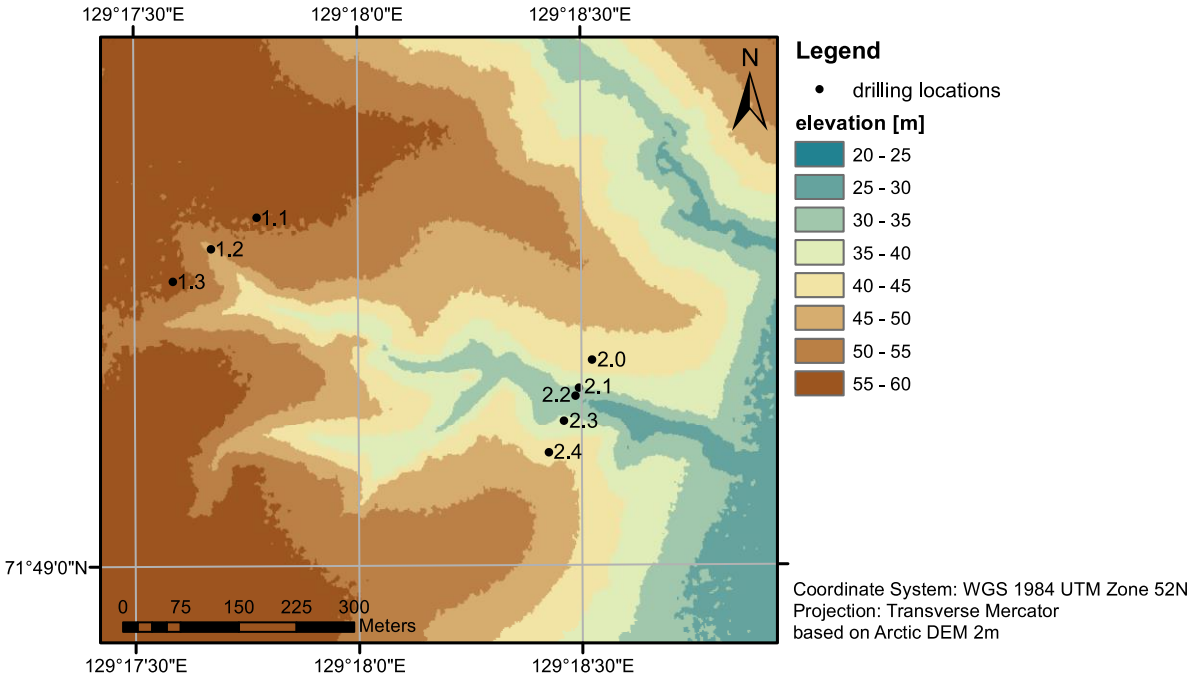

Figure 25: Elevation map of BYK with the sampling locations.

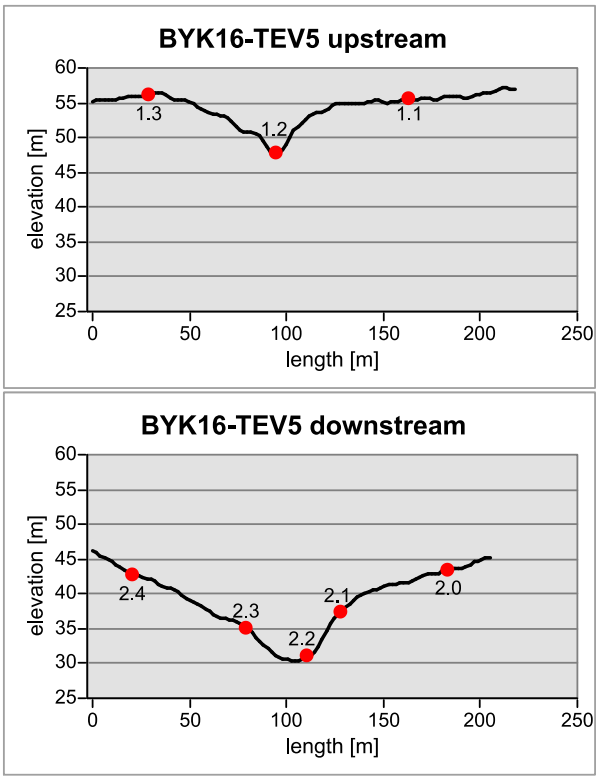

Figure 26: Elevation profile along the two transects of BYK. The red dots mark the sampling locations (based on the Arctic DEM with 2 m resolution).

The elevation profiles along the two transects of this valley show that both sampled transects are V-shaped (Figure 26).

The upstream transect of BYK is about 150 m long and has a difference in elevation between the upland and the valley bed of about 7 m. Its Yedoma upland is at an elevation of 55 m a. s. l. With slope angles between 5 to 21° the south-western facing slope is steeper than the north-eastern facing slope that has slope angles between 3 to 16°. Both slopes are convex (Figure 26).

The downstream transect of BYK has a length of 200 m and has a difference in elevation between the upland and the valley bed of about 15 m. The upland that has an elevation of about 45 m a. s. l. Like the upstream transect, the two slopes of the downstream transect have different slope angles. The southern facing slope is with slope angles between 5 to 28° steeper than the northern facing slope with 5 to 16°. The southern facing slope is

convex, whereas the northern facing slope appears elongated with a slight tendency to a convex shape (Figure 26).

5.2 Active layer depths

During the fieldwork the AL depth at each sampling site was determined. The comparison of the average AL depth of all investigated thermo-erosional valleys showed that KUR had with 17.1 ± 6.5 cm the lowest mean AL depth (ranging between 9 to 28 cm), BYK had with 39.3 ± 6.5 cm the highest mean AL depth (ranging between 26 to 50 cm) and the mean AL in SOB was 24.5 ± 12.1 cm (ranging between 5 to 40 cm).

In KUR the mean AL depth increased the with proximity to the valley outlet. In the upstream area the mean AL depth was 3.0 ± 0.0 cm, whereas in the lower part it was 21.0 ± 2.4 cm (Table 4). The AL depth in SOB showed a similar trend. The upper part of the valley had an AL depth of 6.7 ± 2.4 cm and increased towards the midstream transect (41.7 ± 5.7 cm). The average AL depth of the midstream and the downstream transect of SOB was quite similar (Table 4). The observed values in BYK showed again a clear trend of increasing AL depth with proximity to the outlet of the valley (34.0 ± 5.7 cm to 42.4 ± 4.6 cm) (Table 4). The increasing trend towards the valley outlet was also reflected in the averaged AL depth per transect of all valleys (Table 4).

Table 4: Summary of the mean AL depths of the three investigated thermo-erosional valleys as well as the aggregated values for all three valleys per transect. The mean values are given with ± standard deviation.

	KUR	SOB	BYK	all valleys
upstream	3.0 ± 0.0	6.7 ± 2.4	34.0 ± 5.7	16.6 ± 12.9
midstream	19.6 ± 5.8	41.7 ± 5.7		24.8 ± 8.2
downstream	21.0 ± 2.4	41.3 ± 6.5	42.4 ± 4.6	33.3 ± 9.9

Because the mean AL depths of the geomorphological units in KUR did not show large differences, there is no clear trend observable (Table 5). In contrast to this, the values of SOB showed up differences between the investigated units. The highest mean value was observed at the slope (36.3 ± 3.9 cm), the lowest at the valley bed (5.0 ± 0.0 cm) and the value of the Yedoma upland was in between (19.8 ± 9.1 cm) (Table 5). The mean AL depths of BYK were slightly different. The highest value was observed at the valley bed (44.5 ± 5.5 cm), the lowest on the Yedoma upland (35.0 ± 5.5 cm) and the slope was in between (42.5 ± 1.5 cm) (Table 5). The summary of the mean AL depths per geomorphological unit for all three observed valleys showed the highest value at the slopes and lower values at the Yedoma upland and on the valley bed that are quite similar (Table 5).

Table 5: Summary of the mean AL depths of the three investigated thermo-erosional valleys as well as the aggregated values for all three valleys per geomorphological unit. The mean values are given with ± standard deviation.

	KUR	SOB	BYK	all valleys
Yedoma upland	17.3 ± 7.4	19.8 ± 9.1	35.0 ± 5.5	22.7 ± 10.5
slope	17.5 ± 4.5	36.3 ± 3.9	42.5 ± 1.5	33.1 ± 10.1
bed	16.3 ± 5.4	5.0 ± 0.0	44.5 ± 5.5	23.8 ± 16.0

5.3 Spatial distribution of carbon and nitrogen

In this chapter the results from the laboratory and the data analysis are presented for each investigated thermo-erosional valley. The results from the laboratory and information about the characteristics of the cores collected in the field can be found in Appendix 1, Appendix 2 and Appendix 3. The results of the significant difference tests mentioned in the following section are summarized in Appendix 4, Appendix 5, Appendix 6 and Appendix 7.

For all studied thermo-erosional valleys, the values of TOC ranged between 1.2 and 37.5 wt%, both the minimum and maximum value was detected in SOB. The highest value of TN (1.2 wt%) was measured in BYK, whereas the lowest TN value (<0.1 wt%) was detected in KUR as well as in SOB. The resulting C/N-ratios ranged between 9.1 and 71.2, its minimum value was found in KUR and its maximum value in SOB. The minimum value of SOC (1.6 $kg \cdot m^{-2}$) was found in SOB, whereas its maximum value (148.5 $kg \cdot m^{-2}$) was detected in KUR.

5.3.1 Thermo-erosional valley on Kurungnakh Island

5.3.1.1 Transects

With the exception of TOC, all studied parameters of KUR showed a decreasing trend the farther they are located from the outlet of the valley (Table 6, Appendix 8).

The upstream transect had the highest mean TOC values (6.8 ± 4.1 wt%), the lowest mean TOC values were detected in the midstream transect (4.8 ± 3.0 wt%) (Table 6). The significant difference test of the individual values showed that the values of the midstream transect were significantly lower than the values of the upstream transect.

The mean TN values of KUR ranged between <0.1 and 0.7 wt%, the mean values of the transects were relatively similar (Table 6). However, the significant difference test of the unique TN values per transect showed up that the upstream values were significantly higher than the midstream values.

The mean C/N-ratios of the transects of KUR were relatively similar (Table 6) and did not show significant differences. The ranges of the C/N-ratios of the three investigated transects were relatively equal (Appendix 8).

The averaged SOC storage is the highest in the upstream transect (35.9 ± 11.5 kg · m^{-2}) and decreased with proximity to the outlet of the valley (Table 6). The SOC values were significantly higher in the upstream transect than the values of the midstream and downstream transect. The highest determined SOC storage was found in the downstream transect (148.5 kg · m^{-2}), although the mean values of this transect are the lowest compared to the other two transects (Appendix 8).

Table 6: Summary of the aggregated geochemical parameters for each transect of KUR. The mean values are given with ± standard deviation.

	TOC [wt%]	TN [wt%]	C/N	SOC [kg · m^{-2}]
upstream	6.8 ± 4.1	0.4 ± 0.1	17.6 ± 4.3	35.9 ± 11.5
midstream	4.8 ± 3.0	0.3 ± 0.1	16.4 ± 3.7	23.8 ± 10.8
downstream	5.5 ± 2.7	0.3 ± 0.1	16.5 ± 4.3	16.5 ± 32.7

5.3.1.2 Geomorphological units

For all investigated parameters of KUR, the slopes had the lowest values, whereas the values of the Yedoma upland and the valley bed were quite similar (Table 7, Appendix 9).

The mean values of TOC and TN were lowest at the slopes (3.9 ± 1.7 wt% and 0.2 ± 0.1 wt%, respectively), whereas the Yedoma upland and the valley bed had higher and quite similar values (Table 7). For both, TOC and TN, the values of the upland and the valley bed were significantly higher than the ones of the slopes.

The C/N-ratio also had its lowest mean value at the slope (15.4 ± 1.7), but in contrast to TOC and TN the mean values of the upland (15.9 ± 3.8) and the valley bed (19.4 ± 4.6) differed (Table 7). The significant difference test showed that the C/N-ratios of the valley bed were significantly higher than on the upland and the slope.

The mean SOC storage was, like TOC and TN, the lowest at the slope (24.7 ± 9.3 kg · m^{-2}) and had higher mean values at the Yedoma upland and the valley bed that were relatively similar (Table 7). Between the values of SOC of the three different geomorphological units there was no significant difference. In contrast to the valley bed, the SOC values of the upland had a wide range with a maximum value of 148.5 kg · m^{-2} (Appendix 9).

Table 7: Summary of the aggregated geochemical parameters for each geomorphological unit of KUR. The mean values are given with ± standard deviation.

	TOC [wt%]	TN [wt%]	C/N	SOC [kg · m^{-2}]
Yedoma upland	5.5 ± 3.5	0.3 ± 0.1	15.9 ± 3.8	30.7 ± 25.5
slope	3.9 ± 1.7	0.2 ± 0.1	15.4 ± 1.7	24.7 ± 9.3
bed	6.7 ± 3.4	0.3 ± 0.1	19.4 ± 4.6	28.9 ± 10.8

5.3.1.3 Distribution at depth

For the investigated parameters of KUR there was a decreasing trend with increasing depth of TOC, TN and the C/N-ratio, whereas the SOC storage showed an increasing trend with increasing depth (Table 8, Appendix 10).

The mean TOC values decreased with increasing depth from 6.9 ± 5.2 wt% to 5.5 ± 3.4 wt%. The mean TN values did not show great variations (Table 8), but the distribution of the values showed a decreasing trend with depth (Appendix 10). Also, the C/N-ratio showed a decreasing trend with increasing depth from 19.1 ± 5.7 to 16.7 ± 4.1 (Table 8). Appendix 11 shows the distribution of TOC, TN and the C/N-ratio of the individual cores of KUR.

In contrast to TOC, TN and the C/N-ratio, the mean SOC values increased with depth from 22.3 ± 14.7 to 29.1 ± 20.2 kg · m^{-2} (Table 8). The values of the SOC storage showed also different distributions in different depths. The 0-30 cm and 0-50 cm segments had narrower ranges (2.6 to 55.5 kg · m^{-2} and 2.6 to 59.2 kg · m^{-2}, respectively), whereas the 0-100 cm segments showed up a broader range (2.6 to 148.5 kg · m^{-2}) (Appendix 10).

The significant difference test of the individual values of the segments did not show any differences between the segments for all investigated geochemical parameters.

The comparison of AL and permafrost showed higher mean values for TOC, TN and the C/N-ratio compared to the mean values of the permafrost. The C/N-ratios of the AL were significantly higher than the values of the permafrost. In contrast to this, the SOC storage was significantly lower in the AL and higher in the permafrost (Table 8).

Table 8: Summary of the aggregated geochemical parameters for different depths of KUR (0-30 cm, 0-50 cm, 0-100 cm, active layer (AL), permafrost (PF)). The mean values are given with ± standard deviation.

	TOC [wt%]	TN [wt%]	C/N	SOC [kg · m^{-2}]
0-30 cm	6.9 ± 5.2	0.3 ± 0.2	19.1 ± 5.7	22.3 ± 14.7
0-50 cm	6.0 ± 4.3	0.3 ± 0.1	17.8 ± 4.9	25.9 ± 13.7
0-100 cm	5.5 ± 3.4	0.3 ± 0.1	16.7 ± 4.1	29.1 ± 20.2
AL	8.9 ± 6.2	0.4 ± 0.2	21.4 ± 6.4	13.8 ± 10.0
PF	4.9 ± 1.9	0.3 ± 0.1	15.8 ± 2.7	32.1 ± 20.3

5.3.2 Thermo-erosional valley on Sobo-Sise Island

5.3.2.1 Transects

The investigated parameters per transect of SOB showed the lowest values of TOC, TN and the C/N-ratio in the midstream transect and similar values for the upstream and downstream transects. The SOC storage did not show great variation between the three transects (Table 9, Appendix 12).

The mean TOC values of the upstream (5.8 ± 5.7 wt%) and downstream (5.5 ± 6.3 wt%) transects were relatively equal, the mean value of the midstream transect is lower (4.1 ± 2.9 wt%). For TN the mean values did not show great differences (Table 9), but the distribution of its values per transect showed up lower values in the midstream transect and higher values in the upstream and downstream transect (Appendix 12). Neither the TOC nor the TN values of the different transect showed significant differences.

The midstream transect had a lower mean C/N-ratio compared to the upstream and downstream transect (Table 9). The midstream transect had significantly lower values for the C/N-ratio than upstream and downstream.

The distribution of the TOC values and the C/N-ratios of the upstream and downstream transect showed high ranges with high maximum values (TOC – upstream: 31.6 wt%, downstream: 37.6 wt%; C/N: upstream: 40.9, downstream: 71.2) (Appendix 12).

The SOC storages of the three transects were relatively similar, without significant differences (Table 9). In addition, the values of the different transects did not show great variation in the distribution of the stored OC (Appendix 12).

Table 9: Summary of the aggregated geochemical parameters for each transect of SOB. The mean values are given with ± standard deviation.

	TOC [wt%]	TN [wt%]	C/N	SOC [kg · m^{-2}]
upstream	5.8 ± 5.7	0.3 ± 0.2	16.6 ± 5.3	18.5 ± 12.3
midstream	4.1 ± 2.9	0.3 ± 0.1	14.5 ± 3.3	18.1 ± 13.2
downstream	5.5 ± 6.3	0.3 ± 0.1	17.1 ± 9.6	22.2 ± 15.3

5.3.2.2 Geomorphological units

In SOB, TOC, TN and the C/N-ratio showed up lower values at the slopes and higher values at the Yedoma upland and the valley bed. The SOC storage was highest at the upland, whereas the slopes and the valley bed had lower and relatively similar values (Table 10, Appendix 13).

The mean TOC value was highest at the Yedoma upland (6.6 ± 6.3 wt%) and lowest at the slopes (2.7 ± 1.2) (Table 10), the TOC values of the slopes were significantly lower than the values of the upland and the valley bed. The Yedoma upland showed up a wide maximum range of TOC with a maximum value of 37.6 wt% (Appendix 13).

The mean TN values did not show great variation (Table 10), but the distribution of the values per geomorphological unit showed lower values at the slopes than at the upland and the valley bed (Appendix 13). The TN values of the slopes were significantly lower than of the upland and valley bed.

Also, the C/N-ratio of the slopes (13.5 ± 1.9) is significantly lower than the ratio of the upland (17.7 ± 8.7) and the valley bed (16.1 ± 1.0) (Table 10). Just like for the TOC, the C/N-ratio did show a wide maximum range at the Yedoma upland with a maximum value of 71.2 (Appendix 13).

The lowest mean value of SOC was found at the valley bed (12.4 ± 11.7 kg · m^{-2}), the highest at the upland (25.3 ± 14.8 kg · m^{-2}) (Table 10). The values of the upland were significantly higher than on the slopes and the valley bed.

Table 10: Summary of the aggregated geochemical parameters for each geomorphological unit of SOB. The mean values are given with ± standard deviation.

	TOC [wt%]	TN [wt%]	C/N	SOC [kg · m^{-2}]
Yedoma upland	6.6 ± 6.3	0.3 ± 0.1	17.7 ± 8.7	25.3 ± 14.8
slope	2.7 ± 1.2	0.2 ± 0.1	13.5 ± 1.9	13.1 ± 8.0
bed	5.7 ± 3.6	0.3 ± 0.2	16.1 ± 1.0	12.4 ± 11.7

5.3.2.3 Distribution at depth

With increasing depth, the TN, TOC and C/N-ratio decreased, whereas SOC storage increased (Table 11, Appendix 14).

The highest mean value of TOC was found in the first investigated segment (0-30 cm: 7.6 ± 8.5 wt%), the lowest in the last segment (0-100 cm: 5.1 ± 5.2 wt%) (Table 11). The maximum value of 37.6 wt% was found in the first 30 cm (Appendix 14). The mean values of TN did not show much difference (Table 11), the distribution of the values showed higher values in the first segment compared to the second and third segment (Appendix 14). Also, the mean C/N-ratio decreased with depth from 19.4 ± 11.5 to 16.0 ± 6.8 (Table 11). All three parameters did not show significant differences between the segments. The distribution of the values of TOC, TN and the C/N-ratio was relatively similar in the second and third segment (Appendix 14).

Appendix 15 is showing the distribution of TOC, TN and the C/N-ratio of the individual cores of SOB.

In contrast to the TOC, TN and the C/N-ratio, the SOC storage increased with increasing depth from 11.9 ± 9.6 kg · m^{-2} to 19.7 ± 13.9 kg · m^{-2} (Table 11). The values of the first segment were significantly higher than the values of the second and third segment.

In comparison with the permafrost, the AL had higher TN, TOC values and a higher C/N-ratio, but without significant difference. In contrast to this, the SOC storage of the AL was significantly lower compared to the permafrost (Table 11).

Table 11: Summary of the aggregated geochemical parameters for different depths of SOB (0-30 cm, 0-50 cm, 0-100 cm, active layer (AL), permafrost (PF)). The mean values are given with ± standard deviation.

	TOC [wt%]	TN [wt%]	C/N	SOC [kg · m^{-2}]
0-30 cm	7.6 ± 8.5	0.3 ± 0.2	19.4 ± 11.5	11.9 ± 9.6
0-50 cm	6.1 ± 7.0	0.3 ± 0.2	17.5 ± 9.3	18.0 ± 15.8
0-100 cm	5.1 ± 5.2	0.3 ± 0.1	16.0 ± 6.8	19.7 ± 13.9
AL	8.4 ± 9.4	0.3 ± 0.2	20.3 ± 12.8	8.7 ± 2.9
PF	4.1 ± 2.0	0.3 ± 0.1	14.7 ± 1.6	23.1 ± 14.2

5.3.3 Thermo-erosional valley on Bykovsky Peninsula

5.3.3.1 Transects

All four investigated geochemical parameters in BYK showed higher values in the upstream transect compared to the downstream transect (Table 12, Appendix 16).

The mean TOC content of the upstream transect (10.6 ± 4.7 wt%) was higher than the content of the downstream transect (4.7 ± 2.1 wt%) (Appendix 16). The mean TN value was higher at the upstream transect (0.6 ± 0.2 wt%) compared to the downstream transect (0.3 ± 0.1 wt%) (Table 12). The mean C/N-ratio decreased with proximity to the valley outlet from 19.2 ± 2.5 to 15.9 ± 1.7 (Table 12). Also, the SOC storage showed a higher mean value at the upstream transect compared to the downstream transect (Table 12).

The significant difference test of the individual values of the parameters showed that all four parameters were significantly higher at the upstream transect.

Table 12: Summary of the aggregated geochemical parameters for each transect of BYK. The mean values are given with ± standard deviation.

	TOC [wt%]	TN [wt%]	C/N	SOC [kg · m^{-2}]
upstream	10.6 ± 4.7	0.6 ± 0.2	19.2 ± 2.5	37.6 ± 17.6
downstream	4.7 ± 2.1	0.3 ± 0.1	15.9 ± 1.7	20.8 ± 9.1

5.3.3.2 Geomorphological units

The lowest values of all four parameters were found at the slopes, whereas the Yedoma upland and the valley bed showed higher values (Table 13, Appendix 17).

The mean TOC value of the slope is with 4.1 ± 2.4 wt% lower than on the upland (8.2 ± 4.2 wt%) and the valley bed (7.1 ± 5.0 wt%) (Table 13). The TOC values of the slopes were significantly lower compared to the upland and the valley bed.

Also, the TN mean TN value was lowest at the slopes (0.3 ± 0.2 wt%) and higher at the Yedoma upland (0.5 ± 0.2 wt%) and the valley bed (0.4 ± 0.2 wt%) (Table 13), the individual values of the geomorphological units were significantly lower at the slopes compared to the Yedoma upland.

The mean C/N-ratio was lowest at the slope (15.3 ± 2.1), the mean C/N-ratio of the upland and the valley bed was relatively similar (18.1 ± 2.7 and 17.3 ± 1.5, respectively) (Table 13). The C/N-ratio of the slopes was significantly lower than the C/N-ratio at the upland and the valley bed.

The mean SOC storage was lowest at the slopes and higher at the Yedoma upland and the valley bed (Table 13). The individual values of the slopes showed significant differences to the values of the upland.

Table 13: Summary of the aggregated geochemical parameters for each geomorphological unit of BYK. The mean values are given with ± standard deviation.

	TOC [wt%]	TN [wt%]	C/N	SOC [kg · m^{-2}]
Yedoma upland	8.2 ± 4.2	0.5 ± 0.2	18.1 ± 2.7	31.4 ± 16.6
slope	4.1 ± 2.4	0.3 ± 0.2	15.3 ± 2.1	18.4 ± 8.4
bed	7.1 ± 5.0	0.4 ± 0.2	17.3 ± 1.5	27.1 ± 14.5

5.3.3.3 Distribution at depth

In this valley, the TN, TOC and C/N-ratio were relatively equal distributed with almost no difference between the investigated depths. The SOC storage showed increasing values with increasing depth (Table 14, Appendix 18).

The mean TOC values of the three segments did not show great differences (0-30 cm: 6.8 ± 5.0 wt%, 0-50 cm: 6.9 ± 4.5 wt%, 0-100 cm: 6.9 ± 4.4 wt%) (Table 14), the individual values are relatively equal distributed (Appendix 18).

The mean TN values did not show differences at all (Table 14), the distribution of the values showed slightly lower values in the first 30 cm compared to the other two investigated segments (Appendix 18).

Like TOC and TN, the C/N-ratio did not show great differences, the mean values ranged between 17.2 ± 2.6 and 17.9 ± 3.8 (Table 14).

None of the three parameters showed significant differences between the three segments. The distribution with depth showed some fluctuations in some cores of the valley, but most cores did not show great variations in depth (Appendix 19).

In contrast to this, the mean SOC storage showed an increase with increasing depth from 14.0 ± 7.8 kg · m^{-2} to 27.1 ± 15.3 kg · m^{-2} (Table 14). The SOC values of the third investigated segment was significantly higher than the values of the first and second segment.

The mean TOC of the AL is with 6.6 ± 4.7 wt% slightly lower than of the permafrost with 7.1 ± 4.2 wt%, the mean TN values showed no differences. The AL showed a slightly higher C/N-ratio (17.4 ± 3.5) compared to the permafrost (17.0 ± 1.6) (Table 14). The individual values of TOC, TN and the C/N-ratio did not show significant differences between AL and permafrost. In contrast to this, the SOC was significantly lower in the AL and higher in the permafrost (Table 14).

Table 14: Summary of the aggregated geochemical parameters for different depths of BYK (0-30 cm, 0-50 cm, 0-100 cm, active layer (AL), permafrost (PF)). The mean values are given with ± standard deviation.

	TOC [wt%]	TN [wt%]	C/N	SOC [kg · m^{-2}]
0-30 cm	6.8 ± 5.0	0.4 ± 0.2	17.9 ± 3.8	14.0 ± 7.8
0-50 cm	6.9 ± 4.5	0.4 ± 0.2	17.4 ± 3.3	20.2 ± 14.1
0-100 cm	6.9 ± 4.4	0.4 ± 0.2	17.2 ± 2.6	27.1 ± 15.3
AL	6.6 ± 4.7	0.4 ± 0.2	17.4 ± 3.5	15.3 ± 8.2
PF	7.1 ± 4.2	0.4 ± 0.2	17.0 ± 1.6	34.9 ± 13.9

5.3.4 Differences between the thermo-erosional valleys

Summarized for all three investigated thermo-erosional valleys, KUR had with 5.1 ± 3.4 wt% the lowest mean TOC content and with 15.3 ± 3.4 the lowest mean C/N-ratio. The mean SOC storage of KUR was with 26.7 ± 20.2 kg · m^{-2} the second highest (Table 15), the highest SOC storage of all three values was found in BYK (148.5 kg · m^{-2}) (Figure 27). The mean TN content did not differ from the mean TN content of SOB (Table 15). Additionally, the distribution of the individual TN values of both valleys was relatively equal (Figure 27).

The mean TOC value of SOB had almost no difference to the value of KUR (Table 15), but the individual values of SOB had a wider range with a higher maximum value (37.6 wt%) (Figure 27). The mean C/N-ratio of SOB is with 16.0 ± 6.8 the second highest (Table 15), with 71.2 the highest C/N-ratio of this study was found in this valley (Figure 27). With a mean value of 19.7 ± 13.9 kg · m^{-2} SOB had the lowest SOC storage (Table 15, Figure 27).

BYK had the highest mean values of all studied geochemical parameters (Table 15). With 1.2 wt% the highest TN value was found in BYK (Figure 27).

Table 15: Summary of the aggregated geochemical parameters for each of the three thermo-erosional valleys (Kurungnakh Island (KUR), Sobo-Sise Island (SOB) and Bykovsky Peninsula (BYK)). The mean values are given with ± standard deviation and for 0-100 cm depth.

	TOC [wt%]	TN [wt%]	C/N	SOC [kg · m^{-2}]
KUR	5.1 ± 3.4	0.3 ± 0.1	15.3 ± 3.4	26.7 ± 20.2
SOB	5.1 ± 5.2	0.3 ± 0.1	16.0 ± 6.8	19.7 ± 13.9
BYK	6.9 ± 4.4	0.4 ± 0.2	17.2 ± 2.6	27.0 ± 15.3

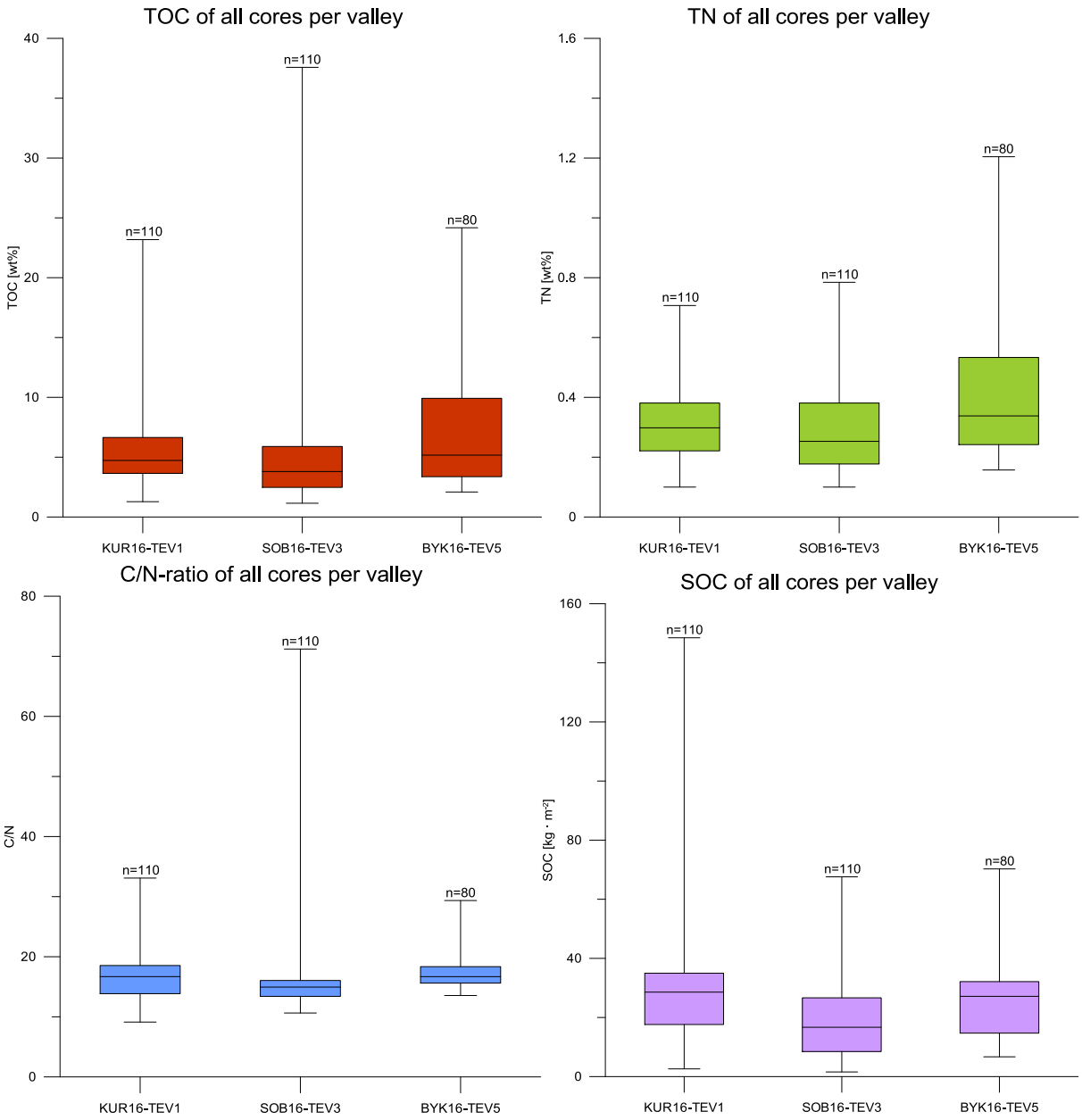

Figure 27: Distribution of TOC, TN, C/N-ratio and SOC storage per investigated thermo-erosional valley.

5.3.4.1 Transects

The summarized parameters showed the highest mean values for all parameters upstream, whereas the lowest mean values (with the exception of TN) were found midstream (Table 16).

The highest mean TOC value was found upstream (7.6 ± 5.3 wt%) and the lowest midstream (4.5 ± 3.0 wt%). The mean TN values of the three transect did not show great variations, the mean values of midstream and downstream were equal (0.3 ± 0.1 wt%). The mean C/N-ratio ranged between 15.5 ± 3.7 and 17.8 ± 4.3, where the lowest mean value was found midstream and the highest upstream. For the SOC storage the same distribution was found;

the maximum mean value of 30.7 ± 16.5 kg · m^{-2} was determined upstream and the lowest mean value of 21.3 ± 12.3 kg · m^{-2} midstream (Table 16).

The significant difference test showed that the upstream values of the parameters were significantly higher compared to midstream and downstream. The mean values of midstream and downstream were relatively equal, for TOC, the C/N-ratio and the SOC storage the mean values downstream were slightly higher than for midstream (Table 16), but without significant difference.

Table 16: Summary of the aggregated geochemical parameters for each transect of all three investigated thermo-erosional valleys. The mean values are given with ± standard deviation.

	TOC [wt%]	TN [wt%]	C/N	SOC [kg · m^{-2}]
upstream	7.6 ± 5.3	0.4 ± 0.2	17.8 ± 4.3	30.7 ± 16.5
midstream	4.5 ± 3.0	0.3 ± 0.1	15.5 ± 3.7	21.3 ± 12.3
downstream	5.2 ± 4.1	0.3 ± 0.1	16.5 ± 6.1	23.8 ± 20.0

5.3.4.2 Geomorphological units

All four investigated geochemical parameters had their lowest mean values at the slope. The mean values of the Yedoma upland and the valley bed were higher and relatively equal (Table 17).

The lowest mean TOC value was found at the slope (3.4 ± 1.8 wt%), whereas the mean values of the Yedoma upland and the valley bed were higher but relatively similar (upland: 6.6 ± 5.0 wt%, valley bed: 6.7 ± 4.1 wt%). The mean TN values showed a similar trend with the lowest mean value at the slope (0.2 ± 0.1 wt%). In this case, the mean values of the upland and the valley bed were the same (0.4 ± 0.2 wt%). Also, the mean C/N-ratio was lowest at the slope (14.4 ± 2.1) and higher at the Yedoma upland and the valley bed (upland: 17.1 ± 6.0, valley bed: 18.1 ± 3.6). The same trend was represented by the mean SOC storage with 17.3 ± 9.7 kg · m^{-2} at the slope and 28.8 ± 20.0 kg · m^{-2} at the upland and 25.6 ± 13.6 kg · m^{-2} at the valley bed (Table 17).

The significant difference test of all values per geomorphological unit showed for TOC, TN and the SOC storage that the values of the slope were significantly lower than the values of the upland and the valley bed. The individual values of the C/N-ratio showed significant differences between all three investigated categories.

Table 17: Summary of the aggregated geochemical parameters for each geomorphological unit of all three investigated thermo-erosional valleys. The mean values are given with ± standard deviation.

	TOC [wt%]	TN [wt%]	C/N	SOC [kg · m^{-2}]
Yedoma upland	6.6 ± 5.0	0.4 ± 0.2	17.1 ± 6.0	28.8 ± 20.0
slope	3.4 ± 1.8	0.2 ± 0.1	14.4 ± 2.1	17.3 ± 9.7
bed	6.7 ± 4.1	0.4 ± 0.2	18.1 ± 3.6	25.6 ± 13.6

5.3.4.3 Distribution at depth

Summarized for all three investigated thermo-erosional valleys, the mean TOC and C/N-ratio showed a decrease with increasing depth, whereas the mean SOC storage showed an increasing trend. The mean TN values did not change with depth (Table 18).

The mean TOC values decreased with depth from 7.2 ± 6.6 wt% to 5.7 ± 4.4 wt%. The mean TN values of the three investigated segments (0.3 ± 0.2 wt%) did not change with depth. Like TOC, the mean C/N-ratio showed a decreasing trend with increasing depth from 18.9 ± 8.0 to 16.5 ± 5.0. In contrast to this, the mean SOC storage increased with increasing depth. The first segment had a mean value of 16.3 ± 12.3 kg · m^{-2}, while the mean value of the third segment was 25.0 ± 17.3 kg · m^{-2} (Table 18).

The individual values of the C/N-ratio showed significantly lower values in the 0-100 cm segment compared to the 0-30 cm segment. The mean TN content did not change with depth (Table 18), the individual values of the three segments did not show significant differences. In contrast to this, the mean SOC storage increased with increasing depth (Table 18).

For the AL the TOC, TN and C/N-ratio showed higher mean values than the permafrost, whereas the SOC storage had a lower mean value in the AL compared to the permafrost (Table 18). The individual values of TOC and TN did not show significant differences between al and permafrost, the values of the C/N-ratio and SOC storage were significantly different.

Table 18: Summary of the aggregated geochemical parameters for different depths of all three investigated thermo-erosional valleys (0-30 cm, 0-50 cm, 0-100 cm, active layer (AL), permafrost (PF)). The mean values are given with ± standard deviation.

	TOC [wt%]	TN [wt%]	C/N	SOC [kg · m^{-2}]
0-30 cm	7.2 ± 6.6	0.3 ± 0.2	18.9 ± 8.0	16.3 ± 12.3
0-50 cm	6.3 ± 5.5	0.3 ± 0.2	17.6 ± 6.6	21.5 ± 15.0
0-100 cm	5.7 ± 4.4	0.3 ± 0.2	16.5 ± 5.0	25.0 ± 17.3
AL	7.8 ± 7.0	0.4 ± 0.2	19.3 ± 8.6	12.7 ± 8.0
PF	5.0 ± 2.8	0.3 ± 0.2	15.7 ± 2.3	29.3 ± 17.6

6 Discussion

This study is based on 30 sites located in three thermo-erosional valleys in the Lena River Delta and shows variability in soil characteristics within and between the valleys. Its main aim was to determine differences in the spatial distribution of TOC, TN, the C/N-ratio and the SOC storage in the three thermo-erosional valleys. The underlying hypothesis of this thesis was that thermo-erosional processes have an influence on the distribution of C and N within the resulting landforms. The following discussion of the results of this study will examine the different spatial distribution of the analyzed geochemical parameters with distance to the valley outlet, within geomorphological units and with depth. On top of that, the role of thermo-erosional processes on degradation and decomposition of C will be estimated.

6.1 Data discussion

At first the quality of the obtained data needs to be illustrated to ensure its resilience. There are several factors that could have had an influence on the accuracy of the results of this study.

The three studied valleys were sampled at different points in time between the end of June and end of August (Appendix 1, Appendix 2, Appendix 3). This led to deeper thawing depths in the valleys that were sampled later (SOB, BYK). On top of that, the obtained AL depths were not the maximum but intermediate thaw depths. Because of this, samples that are actually belonging to the AL were allocated to permafrost, which impacts the comparison of the values between AL and permafrost.

Some of the cores were ceased by ice wedges and consequently shorter than 1 m. In this case, the values of the investigated geochemical parameters were extrapolated down to 1 m to ensure comparability among each other. This affects the distribution in depth of the data and may have led to inaccurate results.

Furthermore, the sampling of the three thermo-erosional valleys was not consistent (Figure 21, Figure 23, Figure 25). In KUR and SOB three transect were sampled (upstream, midstream, downstream), whereas in BYK only along two transects samples were taken (upstream, downstream) because of time reasons. In addition, the sampling of the geomorphological units investigated in this study was unequal, on the one hand within the individual valleys and on the other hand among one another. In KUR, only the midstream transect was sampled on the slopes, whereas in SOB in the midstream and downstream transect the slopes were cored. Because a huge part of SOB carried water, coring was not possible at the valley bed of the midstream and downstream transect. That is why in SOB only one core was taken at the valley bed. The different sampling procedures in the valleys have an impact on the accuracy and comparability of the results.

6.2 Impacts of thermo-erosion on local scale

Previous studies revealed different distributions of C and N as well as SOC storage rates on local scale due to geomorphological and topographical processes (FUCHS et al. 2018, OBU et al. 2017, (OLEFELDT et al. 2016), PIZANO et al. 2014, HARMS et al. 2014, SHELEF et al. 2017, SIEWERT et al. 2015). Also within this study, spatial differences of the investigated geochemical parameters depending on their position were detected (chapter 5.3).

6.2.1 Spatial and vertical distribution

Thermo-erosional processes have an influence on the SOC storage of permafrost, which is represented in the results of this study. The highest values of all parameters were found on the upland and in the upstream transects of the valleys (also referred to as undisturbed). In both cases the terrain was influenced by none or just very light thermo-erosional processes and thin AL. In contrast to this, the areas of the valleys that were and are influenced by higher thermo-erosion rates (slopes, midstream and downstream transects; also referred to as disturbed) were characterized by lower values and thicker AL. The SOC of the undisturbed area is higher than in the disturbed area of the valleys. Furthermore, previous studies in the Lena River Delta also showed higher SOC values for the Yedoma upland. For Kurungnakh Island SIEWERT et al. 2016 had a mean value of 36.9 ± 11.1 kg · m^{-2}, which is considerably higher than the mean value of KUR (26.7 ± 20.2 kg · m^{-2}). FUCHS et al. 2018 investigated geomorphological landforms on Sobo-Sise Island and Bykovsky Peninsula. Their mean SOC value for the Yedoma upland of Sobo-Sise Island was with 25.7 ± 16.1 kg · m^{-2} higher than the mean value of SOB with 19.7 ± 13.9 kg · m^{-2}, whereas their mean SOC value of the Yedoma upland of Bykovsky Peninsula was with 28.1 ± 18.4 kg · m^{-2} almost similar to the mean value of BYK (27.0 ± 15.3 kg · m^{-2}). These results point out that thermo-erosional processes have a negative influence on the SOC

storage in permafrost. According to MORGENSTERN 2012 thermo-erosional valleys have an influence on sediment and organic matter transport from permafrost to coastal waters at local scale. The eroded sediment including organic matter is transported through the Lena River into coastal waters.

Besides its influence on the SOC storage of permafrost, thermo-erosion also affects the degradation and decomposition of C, which can be seen at the C/N-ratio. The C/N-ratio in this study is predominantly moderate with some exceptions. In the areas of the valleys with higher erosion rates the C/N-ratio was lower (in the disturbed areas of the valley). For the Yedoma upland of Kurungnakh Island SCHIRRMEISTER et al. 2011a found values of the C/N-ratio ranging between 15 and 18 for the first meter, which covers roughly the results of this study. SCHIRRMEISTER et al. 2011a also investigated a site on Bykovsky Peninsula and found values of the C/N-ratio ranging between 15 and 20. FUCHS et al. 2018 found a mean C/N-ratio of 10.8 ± 3.5 for the Yedoma upland on Bykovsky Peninsula. The results of this study were higher than the study of FUCHS et al. 2018 and conform with the results of SCHIRRMEISTER et al. 2011a.For Sobo-Sise Island FUCHS et al. 2018 also investigated sites on the Yedoma upland and slopes. The mean C/N-ratio of the upland was 12.2 ± 6.8 and for the slopes 10.7 ± 2.9. In this study the C/N-ratio of SOB was slightly higher but showed a similar trend of a higher C/N-ratio at the upland and a lower one at the slopes. This trend is visible for all three investigated valleys, which means more degraded and decomposed C at the slopes compared to the upland. Additionally, the C/N-ratio decreased with increasing depth. FUCHS et al. 2018 found similar results for thermokarst deposits on Sobo-Sise Island and Bykovsky Peninsula, but with slightly lower values for the C/N-ratio (the mean values range between 10.7 ± 2.9 and 13.2 ± 7.8). STRAUSS et al. 2015 found even smaller values for the C/N-ratio in thermokarst deposits on the Buor-Khaya Peninsula (located south-eastern of the study region of this study) with median values ranging between below 8 and 10. The difference of both studies to this study is the investigated depth. FUCHS et al. 2018 investigated the first two meters, STRAUSS et al. 2015 studied partly way deeper sediments with depths up to 11.7 m. The inclusion of sediments from greater depths results in lower mean values for the C/N-ratio because of its decreasing trend with increasing depth that was found in both studies (FUCHS et a. 2018, STRAUSS et al. 2015), as well as in this study. The higher values of the C/N-ratio in the upper parts indicate the accumulation of fresher material that has not been mineralized yet.

Besides C the soils of the three study sites also contain N. The undisturbed areas of the investigated valleys contain more N than the disturbed areas. In their study, FUCHS et al. 2018 found similar values of TN on Sobo-Sise Island and Bykovsky Peninsula compared to this study. However, RAMAGE 2018 found higher values of TN in three Arctic valleys on Herschel Island, Canada but with similar trends in distribution within the valleys compared to

this study. N is often the limiting factor for plant growth in tundra environments. Due to permafrost thawing the availability of N is increased, which may increase primary production and the release of GHG emissions from permafrost soils (FUCHS et al. 2018). Relocation and mixing of N due to thermo-erosional processes could increase drainage and aeriation of soils, which may promote mineralization of N and nitrification (HARMS et al. 2014). The increased availability of N due to the formation of thermo-erosional landforms could have acute local consequences for aquatic ecosystems (HARMS et al. 2014).

The mean AL depth increased with proximity to the valley outlet and was thickest at the slopes. FUCHS et al. 2018 predicted that with further deepening of the AL the C availability will increase. Therefore, the SOC stored beneath the AL is from importance for future remobilization of C (FUCHS et al. 2018). An estimation for the study sites of Sobo-Sise Island and Bykovsky Peninsula shows a thaw-out of 700,00 t of C by AL deepening of 10 cm (FUCHS et al. 2018). A regional study in north-eastern Siberia contains scenarios of AL deepening of more than 100 cm by the end of the 21st century (SAZONOVA et al. 2004). The results of this study show higher SOC values in the permafrost compared to the AL. The stored OC in the permafrost will be potentially released by future thawing. This shows that thermo-erosional processes have an influence on AL thickening and thereby contributes to remobilization of C.

Based on the results of this study, the thermo-erosional processes seem to increase with proximity to the valley outlet. In contrast to this, GODIN & FORTIER defined in their study three different zones of a thermo-erosional gully on Bylot Island, Canada. The head of the gully was characterized by very active thermo-erosional processes, the central part by low to moderate thermo-erosional processes and the outlet by very low thermo-erosional processes (GODIN & FORTIER 2010). GODIN & FORTIER analyzed a small and active thermo-erosional gully, whereas in this study larger landforms were studied. KUR and BYK were (nearly) stabilized valleys, in SOB active thermo-erosional processes were found in the lower part of the valley. Based on this, it is probable that with growth, extension and stabilization of the thermo-erosional landforms the erosional processes change.

6.2.2 Processes of slope movement

According to BERHE et al. 2007 soil erosion includes three processes: detachment, transport and deposition of material. By these processes the soil gets relocated to the foot of the slope (BERHE et al. 2007, SHELEF et al. 2017). This can also be seen in the results of this study. At the slopes the lowest values of the geochemical parameters were found, whereas at the valley beds higher values were detected. The material got eroded, transported downslope

and accumulated. According to HOBBIE et al. 2000 the topographic position is an important factor that controls the C storage.

On the slopes the lowest values of all parameters were detected. Similar results were found in the studies of RAMAGE 2018 for three Arctic Valleys on Herschel Island, Canada and FUCHS et al. 2018 for different geomorphological units on Sobo-Sise Island and Bykovsky Peninsula. Surface disturbances change the physical and biological processes, which has an impact on the C cycling (PIZANO et al. 2014). Due to thawing of ice-rich soil the ground surface destabilizes, which leads to mass wasting of soil and sediment and thermo-erosional landforms are formed (PIZANO et al. 2014). The erosion leads to exposure of lower soil layers to aeriation and increased microbial activity, which causes decomposition of organic matter and degradation of C (OBU et al. 2017). This explains on the one hand the lower C/N-ratios and on the other hand the lower values of SOC storage at the slopes.

After the erosion of the sediment it is accumulated at the foot of the slope after downslope soil transport due to soil creep and fluvial processes (SHELEF et al. 2017). Compared to the eroded slope the conditions at this position in the valley are wetter and the aeration is reduced, which can slow down the decomposition (BERHE et al. 2007). This explains the higher values of the C/N-ratio at the valley bed compared to the slope. This process turns the valley bed into a sediment and nutrient sink (BERHE et al. 2007, LARSEN et al. 2016).

6.3 Impacts of thermo-erosion on regional and global scale

The three investigated thermo-erosional valleys of this study showed up little differences in the mean values of the studied geochemical parameters, with the exception of the SOC storage. SOB (19.7 ± 13.9 kg $\cdot$ m^{-2}) showed up a smaller mean value than KUR (26.7 ± 20.2 kg $\cdot$ m^{-2}) and BYK (27.0 ± 15.3 kg $\cdot$ m^{-2}). There are two possible reasons for this difference. In SOB there are active thermo-erosional processes that can have an influence on the SOC storage. KUR has already stabilized and in BYK just little thermo-erosional processes were detected. Additionally, in SOB the valley beds were not sampled in the midstream and downstream transects because of the water stream at the valley bed. In both transects the slopes were sampled resulting in four coring sites. Due to the erosional processes mentioned before (chapter 6.2.2) the SOC storage is lower at the slopes compared to the valley bed. This has an influence on the mean SOC storage of SOB because in KUR and BYK only two coring sites were at slopes.

As already mentioned in chapter 2.6, thermo-erosional valleys are widely distributed in the Arctic (MORGENSTERN 2012). The results of this thesis show that thermo-erosional processes have an influence on the SOC storage as well as on degradation and decomposition of C.

The soils of the northern permafrost region store huge amounts of SOC that is prone to remobilization due to permafrost degradation (HUGELIUS et al. 2014, STRAUSS et al. 2017). The key processes of permafrost degradation are AL deepening, thermokarst formation and thermo-erosion (GROSSE et al. 2011b, HUGELIUS et al. 2014). Deepening of the AL mainly affects soils near the surface (HARDEN et al. 2012, HUGELIUS et al. 2014), whereas thermo-erosion has a deeper impact. Due to thermo-erosional processes SOC that is stored at greater depths can be remobilized and mineralized. Both processes can affect permafrost landscapes over decadal timescales (HUGELIUS et al. 2014). Inclusion of the permafrost C feedback (chapter 2.4) into Earth System Models results in the potential of a large positive climate feedback from the permafrost region (SCHAEFER et al. 2011, SCHNEIDER VON DEIMLING et al. 2015). SCHNEIDER VON DEIMLING et al. 2015 did not include thermo-erosional processes into their model but predicted a potential enhancement of permafrost C fluxes due to these processes.

7 Conclusion

This study gives an overview about the spatial distribution and degradation of C and N in three thermo-erosional valleys in the Lena River Delta. The average SOC storages of the three valleys for 0-100 cm ranged between 19.7 ± 13.9 kg · m^{-2} and 27.0 ± 15.3 kg · m^{-2}, the mean TN content between 0.3 ± 0.1 wt% and 0.4 ± 0.2 wt%. The average C/N-ratio was ranging between 15.3 ± 3.4 and 17.2 ± 2.6. The variability of SOC storages and C/N-ratio within the investigated valleys was traced back on the geomorphology and thermo-erosional processes. In general, areas within the valleys with lower erosion rates had higher SOC storages and less degraded C, whereas areas with higher erosion rates stored less SOC and more degraded C.

In summary, this study provides a regional overview of the distribution and degradation of C of thermo-erosional valleys within the Lena River Delta. Further investigations in other regions across the Arctic are necessary to give a more precise estimate of the role of thermo-erosional valleys on the C availability for the positive C feedback cycle. In addition, for a better understanding of the heterogeneous distribution of the SOC storage and the C/N-ratio within the valleys the driving geomorphological and thermo-erosional processes need to be observed. A possible approach for this would be dating of the sediment for a better understanding of the temporal dynamics within the valleys.

REFERENCES

AMAP (2012): Arctic Climate Issues 2011: Changes in Arctic Snow, water, ice and permafrost (SWIPA). Arctic Monitoring and Assesment Programme. Oslo.

AMAP (2017): Snow, Water, Ice and Permafrost in the Arctic (SWIPA). Arctic Monitoring and Assesment Programme (AMAP). Oslo.

ARE, F. & REIMNITZ, E. (2000): An Overview of the Lena River Delta Setting: Geology, Tectonics, Geomorphology, and Hydrology. In: Journal of Coastal Research. Vol. 16(4). pp. 1083-1093.

BERHE, A. A.; HARTE, J.; HARDEN, J. W. & TORN, M. S. (2007): The Significance of the Erosion-induced Terrestrial Carbon Sink. In: Bioscience. Vol. 57(4). pp. 337-346.

BISCHOFF, J.; MANGELSDORF, K.; GATTINGER, A.; SCHLOTER, M.; KURCHATOVA, A. N.; HERZSCHUH, U. & WAGENER, D. (2013): Response of methanogenic archaea to Late Pleistocene and Holocene climate changes in the Siberian Arctic. In: Global Biogeochemical Cycles. Vol. 27. pp. 305-317.

BOLSHIYANOV, D.; MAKAROV, A. & SAVELIEVA, L. (2015): Lena River delta formation during the Holocene. In: Biogeoscience. Vol. 12. pp. 579-593.

BOIKE, J.; KATTENSTROH, B.; ABRAMOVA, K.; BORNEMANN, N.; CHETVEROVA, A.; FEDOROVA, I.; FRÖB, K.; GRIGORIEV, M.; GRÜBER, M.; KUTZBACH, L.; LANGER, M.; MINKE, M.; MUSTER, S.; PIEL, K.; PFEIFFER, E.-M.; STOOF, G.; WESTERMANN, S.; WISCHNEWSKI, K.; WILLE, C. & HUBBERTEN, H.-W. (2013): Baseline characteristics of climate, permafrost and landcover from a new permafrost observatory in the Lena River Delta, Siberia. In: Biogeoscience. Vol. 10. pp. 2105-2128.

COSTARD, F.; DUPEYRAT, L.; GAUTIER, E. & CAREY-GAILHARDIS, E. (2003): Fluvial thermal erosion investigations along a rapidly eroding river bank: Application to the Lena River (Central Siberia). In: Earth Surface Processes and Landforms. Vol. 28. pp. 1349-1359.

FRENCH, H. M. (2007): The Periglacial Environment. Third Edition. John Wiley & Sons, Ltd. Chichester.

FUCHS, M.; GROSSE, G.; STRAUSS, J.; GÜNTHER, F.; GRIGORIEV, M.; MAXIMOV, G. M. & HUGELIUS, G. (2018): Carbon and nitrogen pools in thermokarst-affected permafrost landscapes in Arctic Siberia. In: Biogeoscience. Vol. 15. pp. 953-971.

GODIN, E. & FORTIER, D. (2010): Geomorphology of thermo-erosional gullies – case study from Bylot Island, Nunavut, Canada. In: Proceedings of the 6th Canadian Permafrost Conference and 63rd Canadian Geotechnical Conference, Calgary. pp. 1540-1547.

GODIN, E. & FORTIER, D. (2012): Geomorphology of a thermo-erosion gully, Bylot Island, Nunavut; Canada. In: Canadian Journal for Earth Science. Vol. 49. pp. 979-986.

GODIN, E.; FORTIER, D. & COULOMBE, S. (2014): Effects of thermo-erosion gullying on hydrologic flow networks, discharge and soil loss. In: Environmental Research Letters. Vol. 9. pp. 1-10.

GROSSE, G.; SCHIRRMEISTER, L.; KUNITSKY, V. V. & HUBBERTEN, H.-W. (2005): The Use of CORONA Images in Remote Sensing of Periglacial Geomorphology: An Illustration from the NE Siberian Coast. In: Permafrost and Periglacial Processes. Vol. 16. pp. 163-172.

GROSSE, G.; ROMANOVSKY, V.; JORGENSON, T.; ANTHONY, K. W.; BROWN, J. & OVERDUIN, P. P. (2011a): Vulnerability and Feedbacks of Permafrost to Climate Change. In: Eos Transactions. Vol. 92(9). pp. 73-74.

GROSSE, G.; HARDEN, J.; TURETSKY, M.; MCGUIRE, A. D.; CAMILL, P.; TARNOCAI, C.; FROLKING, S.; SCHUUR, E. A. G.; JORGENSON, T.; MARCHENKO, S.; ROMANOVSKY, V.; WICKLAND, K. P.; FRENCH, N.; WALDROP, M.; BOURGEAU-CHAVEZ, L. & STRIEGL, R. G. (2011b): Vulnerability of high-latitude soil organic carbon in North America to disturbance. In: Journal of Geophysical Research. Vol. 116. G00K06.

GÜNTHER, F.; OVERDUIN, P. P.; SANDAKOV, A. V.; GROSSE, G. & GRIGORIEV, M. N. (2013): Short- and long-term thermo-erosion of ice-rich permafrost coasts in the Laptev Sea region. In: Biogeoscience. Vol. 10. pp. 4297-4318.

HARDEN, J. W.; KOVEN, C. D.; PING, C.-L.; HUGELIUS, G.; MCGUIRE, A. D.; CAMILL, P.; JORGENSON, T.; KUHRY, P.; MICHAELSON, G. J.; O'DONNELL, J. A.; SCHUUR, E. A. G.; TARNOCAI, C.; JOHNSON, K. & GROSSE, G. (2012): Field information links permafrost carbon to physical vulnerabilities of thawing. In: Geophysical Research Letters. Vol. 39. L15704.

HARMS, T. K.; ABBOTT, B. W. & JONES, J. B. (2014): Thermo-erosion gullies increase nitrogen available for hydrologic export. In: Biogeochemistry. Vol. 117. pp. 299-311.

HEGINBOTTOM, J. A.; BROWN, J.; HUMLUM, O. & SVENSSON, H. (2012): Permafrost and Periglacial Environments. In: WILLIAMS, R. S. & FERRIGNO, J. G. (ed.) (2012): State of the Earth's Cryosphere at the Beginning of the 21st Century: Glaciers, Global Snow Cover, Floating Ive, and Permafrost and Periglacial Environments – Satellite Image Atlas of Glaciers of the World. 78 p.

HOBBIE, S. E.; SCHIMEL, J. P.; TRUMBORE, S. E. RANDERSON, J. R. (2000): Controls over carbon storage and turnover in high-latitude soils. In: Global Change Biology. Vol. 6. pp. 196-210.

HUGELIUS, G.; KUHRY, P.; TARNOCAI, C. & VIRTANEN, T. (2010): Soil Organic Carbon Pools in a Periglacial Landscape: a Case Study from the Central Canadian Arctic. In: Permafrost and Periglacial Processe. Vol. 21. pp. 16-29.

HUGELIUS, G.; STRAUSS, J.; ZUBRZYCKI, S.; HARDEN, J. W.; SCHUUR, E. A. G.; PING, C.-L.; SCHIRRMEISTER, L.; GROSSE, G.; MICHAELSON, G. J.; KOVEN, C. D.; O'DONNELL, J. A.; ELBERLING, B.; MISHRA, U.; CAMILL, P.; YU, Z.; PALMTAG, J. & KUHRY, P. (2014): Estimated stocks of circumpolar permafrost carbon with quantified uncertainty ranges and identified data gaps. In: Biogeoscience. Vol. 11. pp. 6573-6593.

JORGENSON, M. T.; RACINE, C. H.; WALTERS, J. C. & OSTERKAMP, T. E. (2001): Permafrost degradation and ecological changes associated with a warming climate in Central Alaska. In: Climate Change. Vol. 48. pp. 551-579.

KANEVSKIY, M.; SHUR, Y.; DORTIER, D.; JORGENSON, M. T. & STEPHANI, E. (2011): Cryostratigraphy of late Pleistocene syngenetic permafrost (yedoma) in northern Alaska, Itkillik River exposure. In: Quaternary Research. Vol. 75. pp.584-596.

KUNITSKY, V. V.; SCHIRRMEISTER, L.; GROSSE, G. & KIENAST, F. (2002): Snow Patches in Nival Landscapes and Their Role for the Ice Complex Formation in the Laptev Sea Coastal Lowlands. In: Polarforschung. Vol. 70. pp. 53-67.

KUTZBACH, L.; WILLE, C. & PFEIFFER, E.-M. (2007): The exchange of carbon dioxide between wet arctic tundra and the atmosphere at the Lena River Delta, Northern Siberia. In: Biogeoscience. Vol. 4. pp. 869-890.

LACHENBRUCH, A. H. (1963): Contraction theory of ice wedge polygons: A qualitative discussion. In: Permafrost International Conference. National Academy of Sciences – National Research Counsil. Lafayette. pp. 63-71.

LANTUIT, H.; ATKINSON, D.; OVERDUIN, P. P.; GRIGORIEV, M.; RACHOLD, V.; GROSSE, G. & HUBBERTEN, H.-W. (2011): Coastal erosion dynamics on the permafrost-dominated Bykovsky Peninsula, north Siberia, 1951-2006. In: Polar Research. Vol. 30(1). pp. 1-21.

LARSEN, A.; HECKMANN, T.; LARSEN J. R. & BORK, H.-R. (2016): Gully catchments as a sediment sink, not just a source: Results from a long-term (~12 500 year) sediment budget. In: Earth Surface Processes and Landforms. Vol. 41. pp. 486-498.

LAWRENCE, D. M. & SLATER, A. G. (2005): A projection of severe near-surface permafrost degradation during the 21st century. In: Geophysical Research Letters. Vol. 32. pp. 1-5.

LENZ, J.; GROSSE, G.; JONES, B. M.; WALTER ANTHONY, K. M.; BOBROV, A. & WULF, S. (2015): Mid-Wisconsin to Holocene Permafrost and Landscape Dynamics based on a Drained Lake Basin Core from the Northern Seward Peninsula, Northwest Alaska. In: Permafrost and Periglacial Processes. Vol. 27. pp. 56-75.

LENZ, J.; JONES, B. M.; WETTERICH, S.; TJALLINGII, R.; FRITZ, M.; ARP, C. D.; RUDAYA, N. & GROSSE G. (2016): Impacts of shore expansion and catchment characteristics on lacustrine thermokarst records in permafrost lowlands, Alaska Arctic Coastal Plain. In: Arktos. Vol. 2(25). pp. 1-15.

MACKAY, J. R. (1972): The Worls of Underground Ice. In: Annals of the Association of the American Geographers. Vol. 62: 1. pp. 1-22.

MACKAY, J. R. (1990): Some Observations on the Growth and Deformation of Epigenetic, Syngenetic and Anti-Syngenetic Ice Wedges. In: Permafrost and Periglacial Processes. Vol. 1. pp. 15-29.

MCKNIGHT, P. E. & NAJAB, J. (2010): Kruskal-Wallis Test. In: The Corsini Encyclopedia of Psychology. Vol. 1.

MORGENSTERN, A.; GROSSE, G.; GÜNTHER, F.; FEDEROVA, I. & SCHIRRMEISTER, L. (2011): Spatial analyses of thermokarst lakes and basins in Yedoma landscapes of the Lena Delta. In: The Cryosphere Discussions. Vol. 5. pp. 1495-1545.

MORGENSTERN, A. (2012): Thermokarst and thermal erosion: Degradation of Siberian ice-rich permafrost. Dissertation Thesis. Potsdam.

NELSON, F. E.; ANISIMOV, O. A. & SHIKLOMANOV, N. I. (2001): Subsidence risk from thawing permafrost. In: Nature. Vol. 410. p. 889.

NELSON, F. E.; ANISIMOV, O. A. & SHIKLOMANOV, N. I. (2002): Climate Change and Hazard Zonation in the Circum-Arctic Permafrost Regions. In: Natural Hazards. Vol. 26. pp. 203-225.

OBU, J.; LANTUIT, H.; MYERS-SMITH, I.; HEIM, B.; WOLTER, J. & FRITZ. M. (2017): Effect of Terrain Characteristics on Soil Organic Carbon and Total Nitrogen Stocks in Soils of Herschel Island, Western Canadian Arctic. In: Permafrost and Periglacial Processes. Vol. 28. pp. 92-107.

OLEFELDT, D.; GOSWAMI, S.; GROSSE, G.; HAYES, D.; HUGELIUS, G.; KUHRY, P.; MCGUIRE, A. D.; ROMANOVSKY, V. E.; SANNEL, A. B. K.; SCHUUR, E. A. G. & TURETSKY, M. R. (2016): Circumpolar distribution and carbon storage of thermokarst landscapes. In: Nature Communications. pp. 1-11.

OLIVA, M. & FRITZ, M. (2018): Permafrost degradation on a warmer Earth: Challenges and perspectives. In: Current Opinion in Environmental Science & Health. Vol. 5. pp. 14-18.

OVERLAND, J.; WALSH, J. & KATTSOV, V. (2017): Trends and feedbacks. In: Snow, Water, Ice and Permafrost in the Arctic (SWIPA). Arctic Monitoring and Assesment Programme (AMAP). Oslo. pp. 65-102.

PALMTAG, J; RAMAGE, J.; HUGELIUS, G.; GENTSCH, N.; LASHCHINSKY, A.; RICHTER, A. & KUHRY, P. (2016): Controls on the storage of organic carbon in permafrost soil in northern Siberia. In: European Journal of Soil Science. Vol. 67. pp. 478-491.

PIZANO, C.; BARÓN, A. F.; SCHUUR, E. A. G.; CRUMMER, K. G. & MACK, M. C. (2014): Effects of thermo-erosional disturbance on surface soil carbon and nitrogen dynamics in upland arctic tundra. In: Environmental Research Letters. Vol. 9. pp. 1-13.

RAMAGE, J. (2018): Impact of hillslope thermokarst on the nearshore carbon budget along the Yukon Coast, Canada. Dissertation Thesis. Potsdam.

RAMAGE, J. L.; IRRGANG, A. M.; MORGENSTERN, A. & LANTUIT, H. (2018): Increasing coastal slump activity impacts the release of sediment and organic carbon into the Arctic Ocean. In: Biogeoscience. Vol. 15. pp. 1483-1495.

RAZALI, N. M. & WAH, Y. B. (2011): Power comparisons of Shapiro-Wilk, Kolmogorov-Smirnov, Lilliefors and Anderson-Darling tests. In: Journal of Statistical Modeling and Analytics. Vol. 2(1). pp. 21-33.

ROMANOVSKII, N. N.; HUBBERTEN, H.-W.; GAVRILOV, A. V.; TUMSKOY, V. E. & KHOLODOV, A. L. (2004): Permafrost of the east Siberian Arctic shelf and coastal lowlands. In: Quternary Science Reviews. Vol. 23. pp. 1359-1369.

ROMANOVSKY, V. E.; GRUBER,S.; JIN, H.; MARCHENKO, S. S.; SMITH, S. L.; TROMBOTTO, D. & WALTER, K. M. (2007): Frozen Ground. In. Global Outlook for Ice & Snow. UNEP. pp. 181-200.

ROMANOVSKY, V. E.; SMITH, S. L. & CHRISTIANSEN, H. H. (2010): Permafrost Thermal State in the Polar Northern Hemisphere during the International Polar Year 2007-2009: a Synthesis. In: Permafrost and Periglacial Environments. Vol. 21. pp. 106-116.

ROMANOVSKY, V. E.; ISAKSEN, K.; DROZDOV, D.; ANISIMOV, O.; INSTANES, A.; LEIBMAN, M.; MCGUIRE, A. D.; SHIKLOMANOV, N.; SMITH, S.; WALKER, D.; GROSSE, G.; JONES, B. M.; JORGENSON, M. T.; KANEVSKIY, M.; KIZYAKOV, A.; LEWKOWICZ, A.; MALKOVA, G.; MARCHENKO, S.; NICOLSKY, D. J.; STERLETSKIY, D. & WESTERMANN, S. (2017): Changing permafrost and its impacts. In: Snow, Water, Ice and Permafrost in the Arctic (SWIPA). Arctic Monitoring and Assesment Programme (AMAP). Oslo. pp. 65-102.

ROWLAND, J. C.; JONES, C. E.; ALTMANN, G.; BRYAN, R.; CROSBY, B. T.; GEERNAERT, G. L.; HINZMANN, L. D.; KANE, D. L.; LAWRENCE, D. M.; MANCINO, A.; MARSH, P.; MCNAMARA, J. P.; Romanovsky, V. E.; TONIOLO, H.; TRAVIS, B. J.; TROCHIM, E. & WILSON, C. J. (2010): Arctic Landscapes in Transition: Responses to Thawing Permafrost. In: Eos Transactions. Vol. 91(26). pp. 229-230.

SAZONOVA, T. S.; ROMANOVSKY, V. E.; WALSH, J. E. & SERGUEEV, D. O. (2004): Permafrost dynamics in the 20th and 21st centuries along the East-Siberian transect. In: Journal of Geophysical Research. Vol. 109. pp. 1-25.

SCHÄDEL, C.; SCHUUR, E. A. G.; BRACHO, R.; ELBERLING, B.; KNOBLAUCH, C.; LEE, H.; LUO, Y.; SHAVER, G. R. & TURETSKY, M. R. (2014): Circumpolar assessment of permafrost C quality and its vulnerability over time using long-term incubation data. In: Global Change Biology. Vol. 20. pp. 641-652.

SCHAEFER, K.; ZHANG, T.; BRUHWILER, L. & BARRET, A. P. (2011): Amount and timing of perma-frost carbon release in response to climate warming. In: Tellus. Vol. 63B. pp. 165-180.

SCHEFFER, F. & SCHACHTSCHABEL, P. (2010): Lehrbuch der Bodenkunde. Spektrum. Heidelberg. 16th edition. 569 p. (in German).

SCHIRRMEISTER, L.; SIEGERT, C.; KUZNETSOVA, T.; KUZMINA, S.; ANDREEV, A. KIENAST, F.; MEYER, H. & BOBROV, A. (2002): Paleoenvironmental and paleoclimatic records from permafrost deposits in the Arctic region of Northern Siberia. In: Quarternary International. Vol. 89. pp. 97-118.

SCHIRRMEISTER, L.; KUNITSKY, V.; GROSSE, G.; WETTERICH, S.; MEYER, H.; SCHWAMBORN, G.; BABIY, O.; DEREVYAGIN, A. & SIEGERT, C. (2011a): Sedimentary characteristics and origin of the Late Pleistocene Ice Complex on north-east Siberian Arctic coastal lowlands and islands – A review. In Quarternary International. Vol. 241 (1-2). pp. 3-25.

SCHIRRMEISTER, L.; GROSSE, G.; SCHNELLE, M.; FUCHS, M.; KRBETSCHEK, M.; ULRICH, M.; KUNITSKY, V.; GRIGORIEV, M.; ANDREEV, A.; KIENAST, F.; MEYER, H.; BABIY, O.; KLIMOVA, I.; BOBROV, A.; WETTERICH, S. & SCHWAMBORN, G. (2011b): Late Quaternary paleoenvironmental records from the western Lena Delta, Arctic Siberia. In: Palaeogeography, Palaeoclimatology, Palaeoecology. Vol. 299. pp. 175-196.

SCHIRRMEISTER, L.; FROESE, D.; TUMSKOY, V.; GROSSE, G. & WETTERICH, S. (2013): Yedoma: Late Pleistocene Ice-Rich Syngenetic Permafrost of Beringia. In: The Encyclopedia of Qaurternary Science. Vol. 3. pp. 542-552.

SCHNEIDER, J.; GROSSE, G. & WAGNER, D. (2009): Land cover classification of tundra environments in the Arctic Lena Delta based on Landsat 7 ETM+ data and its application for upscaling of methane emissions. In: Remote Sensing of Environment. Vol. 113. pp. 380-391.

SCHNEIDER VON DEIMLING, T.; GROSSE, G.; STRAUSS, J.; SCHIRRMEISTER, L.; MORGENSTERN, A.; SCHAPHOFF, S.; MEINSHAUSEN, M. & BOIKE, J. (2011): Observation-based modelling of permafrost carbon fluxes with accounting for deep carbon deposits and thermokarst activity. In: Biogeoscience. Vol. 12. pp. 3469-3488.

SCHUUR, E. A. G.; MCGUIRE, A. D.; SCHÄDEL, C.; GROSSE, G.; HARDEN, J. W.; HAYES, D. J.; HUGELIUS, G.; KOVEN, C. D.; KUHRY, P.; LAWRENCE, D. M.; NATALI, S. M.; OLEFELDT, D.; ROMANOVSKY, V. E.; SCHAEFER, K.; TURETSKY, M. R.; TREAT, C. C. & VONK, J. E. (2015): Climate change and the permafrost carbon feedback. In: Nature. Vol. 520. pp. 171-179.

SCHWAMBORN, G.; RACHOLD, V. & GRIGORIEV, M. N. (2002): Late Quaternary sedimentation history of the Lena Delta. In: Quaternary International. Vol. 89. pp. 119-134.

SERREZE, M. C. & BARRY, R. G. (2011): Processes and impacts of Arctic amplification: A research synthesis. In: Global and Planetary Change. Vol. 77. pp. 85-96.

SHELEF, E.; ROWLAND, J. C.; WILSON, C. J.; HILLEY, G. E.; MISHRA, U.; ALTMANN, G. L. & PING, C.-L. (2017): Large uncertainty in permafrost carbon stocks due to hillslope soil deposits. In: Geophysical Research Letters. Vol. 44(17). pp. 6134-6144.

SHUR, Y. L. & JORGENSON, M. T. (2007): Patterns of Permafrost Formation and Degradation in Relation to Climate and Ecosystems. In: Permafrost and Periglacial Processes. Vol. 18. pp. 7-19.

SIEWERT, M. B.; HANISCH, J.; WEISS, N.; KUHRY, P.; MAXIMOV, T. C. & HUGELIUS, G. (2015): Comparing carbon storage of Siberian tundra and taiga permafrost ecosystems at very high spatial resolution. In: Journal of Geophysical Research: Biogeoscience. Vol. 120(10). pp. 1973-1994.

SIEWERT, M. B.; HUGELIUS, G.; HEIM, B. & FAUCHERRE, S. (2016): Landscape controls and vertical variability of soil organic carbon storage in permafrost-affected soils of the Lena River Delta. In: Catena. Vol. 147. pp. 725-741.

STIEGLITZ, M.; DÉRY, S. J.; ROMANOVSKY, V. E. & OSTERKAMP, T. E. (2003): The role of snow cover in the warming of arctic permafrost. In: Geophysical Research Letters. Vol. 30(13). pp. 1-4.

STRAUSS, J. (2010): Late Quarternary environmental dynamics at the Duvanny Yar key section, Lower Kolyma, East Siberia. Diploma Thesis. Potsdam.

STRAUSS, J.; SCHIRRMEISTER, L.; MANGELSDORF, K.; EICHHORN, L.; WETTERICH, S. & HERZSCHUH, U. (2015): Organic-matter quality of deep permafrost carbon – a study from Arctic Siberia. In: Biogeoscience. Vol. 12. pp. 2227-2245.

STRAUSS, J.; SCHIRRMEISTER, L.; GROSSE, G.; FORTIER, D.; HUGELIUS, G.; KNOBLAUCH, C.; ROMANOVSKY, V.; SCHÄDEL, C.; SCHNEIDER VON DEIMLING, T.; SCHUUR, E. A. G.; SHMELEV, D.; ULRICH, M. & VEREMEEVA, A. (2017): Deep Yedoma Permafrost: A synthesis of depositional characteristics and carbon vulnerability. In: Earth-Science Reviews. Vol. 172. pp. 75-86.

TANSKI, G.; LANTUIT, H.; RUTTOR, S.; KNOBLAUCH, C.; RODOSAVLJEVIC, B.; STRAUSS, J.; WOLTER, J.; IRRGANG, A. M.; RAMAGE, J. & FRITZ, M. (2017): Transformation of terrestrial organic matter along thermokarst-affected permafrost coasts in the Arctic. In: Science of the Total Environment. Vol. 581-582. pp. 434-447.

TOMIRDIARO, S. V. (1982): Evolution of Lowland Landscapes in Northeastern Asia during Late Quarternary Time. In: Paleoecology of Beringia. pp. 29-37.

VAN EVERDINGEN, R. O. (ed.) (2005): Multi-language glossary of permafrost and related ground-ice terms. International Permafrost Association.

WALKER, H. J. (1998): Arctic Deltas. In: Journal of Coastal Research. Vol. 14(3). pp. 718-738.

WALSH, J. E.; OVERLAND, J. E.; GROISMAN, P. Y. & RUDOLF, B. (2011): Ongoing Climate Change in the Arctic. In: AMBIO: A Journal of the Human Environment. Vol. 40. pp. 6-16.

WALTHERT, l.; ZIMMERMANN, S.; LÜSCHER, P. & LUSTER, J. (2004): Waldböden der Schweiz – Grundlagen und Region Jura. Ott Verlag. 768 p.

WALTER ANTHONY, K. M.; ZIMOV, S. A.; GROSSE, G.; JONES, M. C.; ANTHONY, P. M.; CHAPIN III, F. S.; FINLAY, J. C.; MACK, M. C.; DAVYDOV, S.; FRENZEL, P. & FROLKING, S. (2014): A shift of thermokarst lakes from carbon sources to sinks during the Holocene epoch. In: Nature. Vol. 511. pp. 452-456.

WASHBURN, A. L. (1981): Periglaziale Forschung in Revue. In: Geologische Rundschau. Vol. 70. Springer. pp. 664-690.

WETTERICH, S.; KUZMINA, S.; ANDREEV, A. A.; KIENAST, F.; MEYER, H.; SCHIRRMEISTER, L.; KUZNETSOVA, T. & SIERRALTA, M. (2008): Palaeoenvironmental dynamics inferred from late Quaternary permafrost deposits on Kurungnakh Island, Lena Delta, Northeast Siberia, Russia. In: Quaternary Science Reviews. Vol. 27. pp. 1523-1540.

ZHANG, T.; BARRY, R. G.; KNOWLES, K.; HEGINBOTTOM, J. A. & BROWN, J. (2008): Statistics and characteristics of permafrost and ground-ice distribution in the Northern Hemisphere. In: Polar Geography. Vol. 31: 1-2. pp. 47-68.

APPENDIX

Appendix 1: Sample list of KUR with information gained during field work and results of the laboratory work.

Site	Sample	Depth [cm]	AL - PF	Coordinates N	Coordinates E	Date	Geomorpho-logical unit	Water Content [%]	Bulk Density [g/m³]	TOC [wt%]	TC [wt%]	TN [wt%]	C/N-ratio	SOC [kg · m⁻²]
KUR16-TEV1-1.1	1	0-9	AL	72°21'16.524"	126°17'53.448"	26.07.2016	upland	2.9752	0.1079	24.9771	23.8439	0.7338	34.0361	24.2631
	2	9-20	PF					1.7769	0.7202	7.0116	7.3624	0.4647	15.0875	55.5498
	3	20-30						1.7623	0.6929	5.1419	5.4253	0.3082	16.6856	35.6293
	4	30-40						2.0264	0.5984	5.6297	5.8751	0.3443	16.3530	33.6889
	5	40-50						2.1659	0.5611	5.6701	5.8014	0.2911	19.4802	31.8171
	6	50-63						2.3752	0.3944	5.0664	5.1291	0.2474	20.4786	25.9741
	7	63-76						2.0601	0.5781	5.0440	5.0789	0.2549	19.7881	37.9043
	8	76-90						1.9883	0.5365	7.8125	8.0587	0.4178	18.6973	58.6743
	9	90-106						2.1414	0.3603	7.3246	7.5049	0.3963	18.4832	42.2256
KUR16-TEV1-1.2	1	0-9	AL	72°21'18.144"	126°17'50.964"	26.07.2016	valley bed	2.7485	0.2368	16.0455	16.3952	0.6881	23.3176	34.1994
	2	9-19	PF					2.2710	0.4677	8.9725	9.5399	0.4786	18.7459	41.9665
	3	19-30						1.2870	1.1369	3.6658	3.8889	0.1702	21.5411	45.8428
	4	30-40						1.4813	0.9326	4.6944	4.8457	0.2307	20.3516	43.7804
	5	40-50						2.2087	0.5013	6.6789	7.0587	0.4478	14.9156	33.4796
	6	50-60						2.1585	0.6133	7.7346	8.1567	0.5603	13.8033	47.4385
	7	60-70						2.2074	0.5802	6.9839	7.3330	0.4878	14.3184	40.5217
	8	70-80						1.9362	0.6333	6.8340	7.4096	0.3878	17.6206	43.2784
	9	80-86						2.0082	0.5548	7.3186	7.6736	0.3780	19.3604	24.3611
	10	86-100						2.0124	0.5830	4.1808	4.3131	0.2284	18.3018	34.1219
KUR16-TEV1-1.3	1	0-9	AL	72°21'19.09"	126°17'48.84"	26.07.2016	upland	2.5282	0.2683	16.2074	16.4577	0.7572	21.4045	39.1292
	2	9-20	PF					1.4445	1.0516	3.4901	3.7639	0.1824	19.1385	40.3705
	3	20-30						1.5302	1.0661	5.0799	5.3373	0.3162	16.0633	54.1585
	4	30-36						2.0286	0.5902	9.8939	10.4414	0.6814	14.5198	35.0380
	5	36-50						2.5207	0.3778	4.1918	4.5004	0.2421	17.3108	22.1705
	6	50-61						1.8820	0.6991	4.8636	5.0248	0.2879	16.8927	37.4019
	7	61-70						1.9071	0.6464	4.7461	5.0135	0.2998	15.8334	27.6108
	8	70-76						1.9040	0.6461	5.6059	5.9649	0.3685	15.2128	21.7336

Site	Sample	Depth [cm]	AL - PF	Coordinates		Date	geomorpho-logical unit	Water Content [%]	Bulk Density [g/m³]	TOC [wt%]	TC [wt%]	TN [wt%]	C/N-ratio	SOC [kg · m^{-2}]
				N	E									
KUR16-TEV1-2.1	1	0-10	AL	72°21'22.86"	126°18'20.556"	27.07.2016	upland	2.0634	0.1213	13.4996	14.0733	0.5449	24.7756	16.3700
	2	10-13						1.5439	0.5760	3.8980	4.1900	0.2411	16.1678	6.7354
	3	13-20	PF					1.4713	0.9564	2.5268	2.8396	0.1901	13.2893	16.9163
	4	20-30						1.3213	1.0104	2.9382	3.2322	0.2240	13.1151	29.6887
	5	30-40						1.5910	0.8738	4.4173	4.7611	0.3289	13.4325	38.6000
	6	40-51						2.3483	0.5253	5.4292	5.7741	0.3906	13.9005	31.3703
	7	51-61						2.1499	0.5272	3.6502	3.8925	0.3033	12.0359	19.2418
KUR16-TEV1-2.2	1	0-8	AL	72°21'23.256"	126°18'13.842"	27.07.2016	slope	1.9414	0.2272	9.7031	10.7106	0.4922	19.7135	17.6386
	2	8-13						1.4539	0.4561	2.9981	3.2528	0.2139	14.0137	6.8372
	3	9-20	PF					4.0799	0.2450	5.3030	5.5731	0.2860	18.5436	14.2913
	4	20-30						1.3902	0.8230	3.5873	3.8822	0.2510	14.2902	29.5217
	5	30-40						1.9084	0.8377	3.4115	3.6083	0.2198	15.5177	28.5768
	6	40-50						2.4284	0.4272	3.3413	3.8766	0.2312	14.4533	14.2724
	7	50-60						2.2952	0.5173	2.9017	3.5107	0.2089	13.8878	15.0098
	8	60-70						2.0012	0.5614	3.4413	3.7267	0.2575	13.3663	19.3181
	9	70-84						1.8821	0.6166	4.6887	5.0083	0.3295	14.2304	40.4779
	10	84-101						2.1607	0.5361	4.0260	4.3141	0.2619	15.3753	36.6904
KUR16-TEV1-2.3	1	0-5	AL	72°21'23.292"	126°18'11.916"	27.07.2016	valley bed	4.9274	0.0351	18.6708	19.6125	0.5163	36.1606	3.2753
	2	5-13						5.9962	0.0641	17.4931	17.5159	0.5827	30.0203	8.9760
	3	13-22						4.1293	0.1148	10.5769	11.6606	0.4308	24.5506	10.9239
	4	22-30	PF					2.2794	0.4838	6.9139	7.6118	0.3881	17.8132	26.7591
	5	30-40						2.2516	0.5247	6.0420	6.4910	0.3457	17.4765	31.7047
	6	40-50						2.1794	0.5846	4.9812	5.1652	0.2765	18.0137	29.1199
	7	50-65						2.4631	0.4558	4.4612	4.7330	0.2630	16.9604	30.5022
	8	65-80						2.6837	0.3146	4.3770	4.6192	0.2562	17.0815	20.6549
	9	80-98						2.4599	0.4175	3.8025	4.0068	0.2135	17.8109	28.5748

Site	Sample	Depth [cm]	AL - PF	Coordinates		Date	geomorpho-logical unit	Water Content [%]	Bulk Density [g/m³]	TOC [wt%]	TC [wt%]	TN [wt%]	C/N-ratio	SOC [kg · m^{-2}]
				N	E									
KUR16-TEV1-2.4	1	0-12	AL	72°21'23.364"	126°18'9.072"	27.07.2016	slope	1.8339	0.2380	7.7729	8.0021	0.4710	16.5018	10.1755
	2	12-22						1.2920	0.6817	1.9206	2.1266	0.1443	13.3110	5.8920
	3	22-37	PF					1.1991	0.9583	1.4937	1.8508	0.1180	12.6565	21.4702
	4	37-50						1.2990	1.2141	1.7172	2.0089	0.1240	13.8522	27.1032
	5	50-62						1.7652	0.6957	3.6461	3.7458	0.2161	16.8715	30.4379
KUR16-TEV1-2.5	0	0-3	AL	72°21'23.616"	126°18'5.148"	26.07.2016	upland	1.3984	0.5628	5.4305	6.0037	0.2483	21.8686	9.1692
	1	3-28						1.2765	0.5398	1.8288	2.0730	0.1006	18.1797	5.4299
	2	3-28						1.2249	0.4922	1.8677	2.1666	< 0,10	18.6771	5.9754
	3	28-40	PF					1.4173	0.9734	5.0659	5.5641	0.3203	15.8184	59.1747
	4	40-50						2.0283	0.6013	7.4037	8.1730	0.4508	16.4233	44.5160
	5	50-60						2.2657	0.4616	5.3139	5.8188	0.2976	17.8539	24.5280
	6	60-70						2.6075	0.4144	6.6456	7.3175	0.3641	18.2538	27.5419
	7	70-77						2.3503	0.5047	8.4030	9.2790	0.4695	17.8973	29.6846
	8	77-90						2.3728	0.4401	2.2269	2.7759	0.1572	14.1703	12.7400
	9	90-100						2.4300	0.5640	2.7402	3.1866	0.2040	13.4326	15.4545
KUR16-TEV1-3.1	1	0-4	AL	72°21'27.18"	126°18'26.172"	27.07.2016	upland	1.8626	0.2039	12.3277	13.6550	0.4474	27.5515	10.0560
	2	4-14						1.3215	0.2901	1.6568	1.9867	0.1377	12.0276	4.8065
	3	14-24						1.3199	1.0898	2.2307	2.7063	0.1747	12.7700	24.3104
	4	24-34	PF					1.4927	1.0504	2.0630	2.5054	0.1757	11.7393	21.6684
	5	34-44						2.0363	0.5771	2.9982	3.4352	0.2380	12.5966	17.3041
	6	44-52						2.0502	0.5326	4.1838	4.6512	0.3089	13.5439	17.8257
	7	52-60						1.7890	0.6644	2.4958	2.9534	0.1919	13.0081	13.2661
	8	60-80						1.8736	0.6226	11.9218	12.6515	0.6430	18.5396	148.4614

Site	Sample	Depth [cm]	AL - PF	Coordinates		Date	geomorpho-logical unit	Water Content [%]	Bulk Density [g/m³]	TOC [wt%]	TC [wt%]	TN [wt%]	C/N-ratio	SOC [kg · m^{-2}]
				N	E									
KUR16-TEV1-3.2	1	0-15	AL	72°21'28.044"	126°18'22.284"	27.07.2016	valley bed	2.8020	0.0703	11.0819	12.5849	0.3362	32.9628	11.6885
	2	15-18						2.7088	0.3136	8.6155	9.5750	0.4804	17.9353	8.1048
	3	18-30	PF					2.3030	0.4523	6.8301	7.8287	0.3454	19.7756	37.0683
	4	30-40						2.0674	0.6013	5.0587	5.5545	0.2560	19.7622	30.4164
	5	40-50						1.8897	0.6826	4.8110	5.3103	0.2595	18.5373	32.8406
	6	50-62						2.3354	0.5023	5.3236	5.8838	0.2987	17.8214	32.0905
	7	62-72						2.6516	0.4057	4.9537	5.7603	0.3018	16.4137	20.0955
	8	72-84						2.5303	0.5953	5.1138	5.6387	0.3124	16.3710	24.3558
	9	84-90						2.9367	0.3384	4.3749	5.0094	0.2698	16.2159	8.8835
	10	90-100						2.6560	0.3550	3.9259	4.4721	0.2610	15.0434	13.9376
KUR16-TEV1-3.3	1	0-6	AL	72°21'28.98"	126°18'20.592"	27.07.2016	upland	1.7035	0.2266	10.1424	11.2707	0.4963	20.4363	13.7890
	2	6-21						1.2420	0.1358	1.2805	1.5991	< 0.10	12.8048	2.6085
	3	21-27	PF					1.3473	0.8523	3.3838	3.7210	0.2625	12.8886	17.3037
	4	27-40						1.8821	0.5924	3.8854	4.2950	0.3132	12.4068	29.9220
	5	40-50						1.9076	0.7644	5.1351	5.5242	0.3810	13.4783	39.2534
	6	50-58						2.3180	0.4238	5.8641	6.5406	0.4490	13.0599	19.8799
	7	58-70						2.4820	0.4360	6.7650	7.2012	0.4272	15.8369	35.3949
	8	70-80						2.8152	0.3712	6.9273	7.3087	0.4112	16.8476	25.7171
	9	80-90						2.0071	0.5302	7.0350	7.2363	0.3965	17.7438	37.3009
	10	90-100						2.4021	0.3936	5.6612	6.1345	0.3397	16.6632	22.2829

Appendix 2: Sample list of SOB with information gained during field work and results of the laboratory work.

Site	Sample	Depth [cm]	AL - PF	Coordinates N	Coordinates E	Date	Geomorpho-logical unit	Water Content [%]	Bulk Density [g/m³]	TOC [wt%]	TC [wt%]	TN [wt%]	C/N-ratio	SOC [kg · m⁻²]
SOB16-TEV3-1.1	1	0-5	AL	72°30'37.6"	127°54'44.3"	12.08.2016	upland	3.1786	0.0982	25.0780	28.7972	0.5609	44.7117	12.3180
	2	5-27	PF					1.2675	0.1565	1.6572	2.2058	0.1214	13.6539	5.7051
	3	28-40						1.4144	0.9402	2.2849	2.8738	0.1507	15.1658	25.7782
	4	40-50						2.0000	0.5592	5.7563	6.7159	0.3849	14.9539	32.1875
	5	50-60						1.9815	0.4971	3.8866	4.6492	0.2782	13.9691	19.3207
	6	60-72						1.9785	0.4002	3.5187	4.0217	0.2443	14.4028	16.8978
	7	72-85						2.0629	0.4934	6.2214	7.2782	0.4151	14.9870	39.9035
	8	85-97						2.4539	0.4316	5.9850	6.9933	0.4047	14.7882	30.9986
SOB16-TEV3-1.2	1	0-5	AL	72°30'95.6"	127°54'04.1"	12.08.2016	valley bed	5.1067	0.0987	20.3764	23.0192	1.0150	20.0758	10.0533
	2	5-28	PF					2.6696	0.0972	8.8139	10.4140	0.5541	15.9067	19.7138
	3	28-40						1.8259	0.4828	5.9341	6.9731	0.3330	17.8194	34.3788
	4	40-50						1.8730	0.6164	3.9061	4.5202	0.2415	16.1713	24.0771
	5	50-56						4.7644	0.0822	3.1867	3.6380	0.2078	15.3345	1.5723
SOB16-TEV3-1.3	1	0-10	AL	72°30'45.6"	127°55'02.1"	12.08.2016	upland	4.3018	0.0371	31.5755	34.5122	0.7721	40.8947	11.7014
	2	10-27	PF					1.2942	0.2008	2.1521	2.6660	0.1260	17.0783	7.3478
	3	27-40						1.5018	0.7483	2.1555	2.5893	0.1385	15.5576	20.9669
	4	40-48						2.5139	0.4619	4.0038	4.6002	0.2654	15.0856	14.7937
	5	48-60						1.8638	0.5502	3.7947	4.3951	0.2496	15.2002	25.0545
	6	60-70						2.2980	0.5313	9.1231	10.5305	0.6620	13.7813	48.4727
	7	70-80						2.1303	0.5673	5.4650	6.4042	0.4001	13.6581	31.0017
	8	80-90						2.3968	0.4079	3.0431	3.5073	0.1957	15.5494	12.4115
	9	90-100						2.2468	0.5083	5.4785	6.1848	0.3536	15.4923	27.8469
	10	100-114						2.0095	0.5927	4.6026	5.2207	0.2909	15.8207	38.1907
SOB16-TEV3-2.1	1	0-7	AL	72°30' 49.9"	127°53' 58.3"	14.08.2016	upland	2.9364	0.0739	24.7464	27.3891	0.6900	35.8619	12.8063
	2	7-30	PF					1.2665	0.1442	2.5564	3.0657	0.1593	16.0472	8.4757
	3	30-40						1.4980	0.9890	4.7284	5.3245	0.3042	15.5442	46.7614
	4	40-48						2.2011	0.5139	6.1224	7.0416	0.3836	15.9590	25.1722

Site	Sample	Depth [cm]	AL - PF	Coordinates		Date	Geomorpho-logical unit	Water Content [%]	Bulk Density [g/m³]	TOC [wt%]	TC [wt%]	TN [wt%]	C/N-ratio	SOC [kg · m^{-2}]
				N	E									
SOB16-TEV3-2.2	1	0-1	AL	72°30'56.4"	127°53'59.7"	14.08.2016	slope	1.6121	0.6162	7.6108	8.5611	0.4918	15.4768	4.6896
	2	1-40						1.2982	0.0758	2.0844	2.5570	0.1716	12.1495	6.1612
	3	40-75	PF					1.3283	0.0905	1.5101	1.8475	0.1223	12.3431	4.7817
	4	75-85						1.3949	1.0223	2.0226	2.5539	0.1558	12.9805	20.6767
	5	85-95						1.3838	1.2534	2.3394	2.8667	0.1795	13.0351	29.3219
	6	95-103						2.1238	0.5825	2.6834	3.1971	0.2039	13.1583	12.5041
	7	103-121						2.3832	0.4912	1.9554	2.4893	0.1693	11.5471	17.2884
SOB16-TEV3-2.3	1	0-3	AL	72°30'57.3"	127°54'02.5"	14.08.2016	slope	2.4820	0.3655	12.8281	14.1003	0.5838	21.9741	14.0648
	2	3-15						1.3427	0.2394	1.9163	2.2074	0.1870	10.2488	5.5046
	3	15-31						1.5066	0.1453	3.0921	3.4326	0.2805	11.0243	7.1872
	4	31-40	PF					1.4895	1.0491	3.2578	3.5660	0.2705	12.0452	30.7606
	5	40-50						1.5179	0.6131	2.7157	2.9884	0.2101	12.9247	16.6502
	6	50-65						2.2176	0.3883	2.9953	3.3201	0.2343	12.7834	17.4450
	7	65-75						1.9239	0.5535	3.2667	3.6404	0.2645	12.3501	18.0800
	8	75-82						2.0013	0.4852	3.1569	3.4978	0.2306	13.6883	10.7229
	9	82-92						1.7889	0.8052	3.9622	4.3541	0.3082	12.8578	31.9038
	10	92-96						1.9806	0.5646	4.1381	4.6167	0.3310	12.5017	9.3463
SOB16-TEV3-2.4	1	0-3	AL	72°31'03.1"	127°54'14.7"	12.08.2016	upland	3.3368	0.1389	28.8815	30.7721	0.6585	43.8619	12.0330
	2	3-24						1.2937	0.1717	2.2642	2.6997	0.1534	14.7559	7.3880
	3	24-42	PF					1.5806	0.8232	4.5622	4.8961	0.2973	15.3470	67.5965
	4	42-50						1.9023	0.7072	5.5302	5.8690	0.3492	15.8387	31.2870
	5	50-60						2.8412	0.2802	5.5141	5.7074	0.3532	15.6123	15.4526
	6	60-70						2.5446	0.4478	4.6903	5.0215	0.3139	14.9406	21.0018
	7	70-80						1.9915	0.4912	3.8283	4.1415	0.2562	14.9417	18.8040
	8	80-90						2.0862	0.3763	3.1095	3.4806	0.2214	14.0454	11.7007
	9	90-100						1.9294	0.5967	2.4736	2.9931	0.1983	12.4754	14.7593
	10	100-109						1.9707	0.6747	2.9480	3.3825	0.2202	13.3882	17.9000

Site	Sample	Depth [cm]	AL - PF	Coordinates		Date	Geomorpho-logical unit	Water Content [%]	Bulk Density [g/m³]	TOC [wt%]	TC [wt%]	TN [wt%]	C/N-ratio	SOC [kg · m^{-2}]
				N	E									
SOB16-TEV3-3.1	1	7-14	AL	72°31'6.96"	127°53'2.929"	12.08.2016	upland	7.1379	0.0545	37.5802	38.5541	0.5277	71.2097	14.3387
	2	14-27						3.8034	0.0892	12.0542	12.7069	0.7371	16.3544	13.9828
	3	27-40	PF					5.7599	0.2733	2.2930	2.6474	0.1375	16.6735	8.1454
	4	40-52						0.9790	1.0807	5.1625	5.2678	0.3116	16.5688	66.9492
	5	52-98						1.8313	0.1258	6.7648	7.1287	0.3848	17.5810	39.1320
SOB16-TEV3-3.2	1	0-5	AL	72°31'06.3'	127°53'13.3"	16.08.2016	slope	2.5183	0.1557	11.6242	12.0871	0.4442	26.1701	9.0488
	2	5-13						1.4704	0.3549	2.2827	2.5493	0.1672	13.6507	5.6711
	3	13-40						1.4274	0.1018	2.6809	2.9413	0.1981	13.5316	7.3718
	4	40-50	PF					1.3787	1.0596	1.1501	1.3915	< 0.1	11.5011	12.1861
	5	50-60						1.5490	1.0205	1.3319	1.6264	0.1023	13.0180	13.5928
	6	60-68						1.6652	0.7713	1.1475	1.4539	< 0.1	11.4749	7.0806
	7	68-80						1.7545	0.7355	1.6347	1.9205	0.1260	12.9777	14.4276
	8	80-90						1.9587	0.6057	1.7115	1.9995	0.1278	13.3948	10.3656
	9	90-100						1.6378	0.8118	1.4957	1.7686	0.1102	13.5692	12.1414
	10	100-118						1.8014	0.6997	1.9950	2.2316	0.1540	12.9520	25.1283
SOB16-TEV3-3.3	1	0-2	AL	72°31'07.1"	127°53'18.9"	16.08.2016	slope	1.7405	0.5493	5.8184	6.0203	0.2957	19.6744	6.3921
	2	2-34						1.5843	0.0585	3.3197	3.5628	0.1961	16.9245	6.2167
	3	34-41	PF					1.3073	0.4210	1.8744	2.1926	0.1313	14.2768	5.5242
	4	41-50						1.2485	1.4529	1.3741	1.6816	0.1032	13.3211	17.9678
	5	50-60						1.4312	1.1269	2.3749	2.6670	0.1772	13.4031	26.7622
	6	60-71						1.7431	0.7597	3.1893	3.3092	0.1967	16.2177	26.6525
	7	71-80						1.9749	0.6215	4.7609	4.9841	0.3268	14.5671	26.6318
	8	80-90						1.9628	0.6256	4.9795	5.0791	0.3245	15.3448	31.1519
	9	90-100						1.6962	0.8901	2.4320	2.7208	0.1570	15.4910	21.6460
	10	100-116						1.7411	0.6171	2.2016	2.3948	0.1340	16.4346	21.7391
SOB16-TEV3-3.4	1	0-6	AL	72°31'07.5"	127°53'47.8"	16.08.2016	upland	2.7281	0.1586	18.2632	19.8917	0.8768	20.8284	17.3807
	2	6-23						1.4831	0.1263	4.6391	4.9693	0.3179	14.5911	9.9591
	3	23-38	PF					1.7762	0.7302	6.0011	6.6710	0.4066	14.7604	65.7305
	4	38-51						2.3396	0.4559	5.4640	5.8172	0.3869	14.1223	32.3859
	5	51-64						1.9484	0.5853	4.9829	5.3112	0.3418	14.5804	37.9151
	6	64-75						2.5295	0.4288	3.7163	4.0032	0.2688	13.8242	17.5288
	7	75-88						2.5378	0.4954	5.5797	6.0235	0.3905	14.2899	33.1698
	8	88-103						2.3318	0.8227	2.1570	2.5919	0.1806	11.9441	17.7463

Appendix 3: Sample list of BYK with information gained during field work and results of the laboratory work

Site	Sample	Depth [cm]	AL - PF	Coordinates N	Coordinates E	Date	Geomorpho-logical unit	Water Content [%]	Bulk Density [g/m³]	TOC [wt%]	TC [wt%]	TN [wt%]	C/N-ratio	SOC [kg · m^{-2}]
BYK16-TEV5-1.1	1	0-2	AL	71°49' 15.7"	129°17' 42.0"	24.08.2016	upland	2.7131	0.1338	27.9283	30.7659	0.5965	51.5734	7.4714
	2	2-37						1.3863	0.1069	3.0966	3.5519	0.1880	18.8884	11.5843
	3	37-47	PF					1.8368	0.5763	8.9942	9.9166	0.5075	19.5397	51.8307
	4	47-57						2.5869	0.3758	16.1239	16.6769	0.9089	18.3493	60.6012
BYK16-TEV5-1.2	1	0-9	AL	71°49'13.7"	129°17'37.3"	24.08.2016	valley bed	5.2468	0.0385	25.5572	27.4067	1.2583	21.7801	8.8546
	2	9-39						2.1430	0.0849	11.7048	12.5234	0.7186	17.4280	29.7987
	3	39-51	PF					1.6911	0.6525	8.9733	10.1564	0.5334	19.0416	70.2658
	4	51-62						1.7306	0.7430	6.0041	6.9125	0.3882	17.8053	49.0691
	5	62-72						2.1535	0.5272	7.7400	8.6292	0.5234	16.4861	40.8016
	6	72-85						2.0404	0.5049	5.5408	6.2089	0.3347	18.5519	36.3648
	7	85-95						1.9593	0.4798	4.3521	5.0444	0.2697	18.7031	20.8806
	8	95-100						2.0065	0.4061	5.7815	6.4709	0.3828	16.9021	11.7396
BYK16-TEV5-1.3	1	0-5	AL	71°49'12.5"	129°17'34.5"	24.08.2016	upland	3.4465	0.0943	22.2068	24.2326	0.5952	40.7129	10.4695
	2	5-17						1.6633	0.3452	4.4638	5.0135	0.2786	17.9948	18.4900
	3	17-26	PF					1.7765	0.3053	12.5337	13.6265	0.6872	19.8299	34.4374
	4	26-34						1.9483	0.4720	10.7723	11.5598	0.5571	20.7519	40.6763
	5	34-44						3.4689	0.2114	14.1610	14.9737	0.8396	17.8342	29.9345
	6	44-54						2.9065	0.3353	11.6811	12.5626	0.7159	17.5481	39.1643
	7	54-62						1.8503	0.4432	6.7418	7.4258	0.4271	17.3875	23.9047
	8	62-72						1.8716	0.5585	7.6085	8.4472	0.4663	18.1147	42.4943
	9	72-82						2.2812	0.3002	12.7713	13.6292	0.6551	20.8051	38.3388
	10	82-93						2.2840	0.4374	11.8142	12.3117	0.5860	21.0109	56.8383

Site	Sample	Depth [cm]	AL - PF	Coordinates		Date	Geomorpho-logical unit	Water Content [%]	Bulk Density [g/m³]	TOC [wt%]	TC [wt%]	TN [wt%]	C/N-ratio	SOC [kg · m^{-2}]
				N	E									
BYK16-TEV5-2.0	1	0-7	AL	71°49' 9.084"	129°18' 35.316"	24.08.2016	upland	1.6744	0.3098	7.5615	8.8448	0.4842	18.2683	16.3984
	2	7-41						1.4831	0.0708	4.4623	5.1281	0.3236	15.8452	10.7341
	3	41-50	PF					1.6232	0.6279	5.1581	5.8386	0.3716	15.7104	29.1480
	4	50-61						2.0870	0.4033	7.1563	7.8510	0.4476	17.5392	31.7458
BYK16-TEV5-2.1	1	0-29	AL	71°49' 7.248"	129°18'3 4.344"	24.08.	slope	1.3135	0.0989	2.8856	3.3692	0.2317	14.5430	8.2765
	2	29-41						1.9542	0.1275	11.5609	12.4652	0.9059	13.7600	17.6949
	3	41-46	PF					1.4582	1.2126	4.4785	4.8656	0.3295	14.7683	27.1538
BYK16-TEV5-2.2	1	0-7	AL	71°49'7.4"	129°18'24.8"	24.08.2016	valley bed	3.9957	0.0727	12.6809	13.4355	0.6452	20.8226	6.4512
	2	7-50						1.7146	0.0752	5.1695	5.4658	0.3379	16.1754	16.7200
		50-57	PF					sample got lost						
	3	57-70						1.6115	0.8596	2.8758	3.2284	0.1942	16.6232	32.1355
	4	70-80						1.4677	0.7342	2.1177	2.5157	0.1571	16.0098	15.5469
	5	80-90						1.4643	1.1155	2.0901	2.4734	0.1631	15.1694	23.3148
BYK16-TEV5-2.3	1	0-4	AL	71°49'05.5"	129°18'23.4"	24.08.2016	slope	2.3650	0.0751	21.4401	22.2024	0.5687	39.0418	6.4409
	2	4-44						1.3250	0.0766	2.2381	2.6408	0.1950	13.5443	6.8562
	3	44-54	PF					1.4878	1.0416	3.0512	3.5056	0.2235	15.6821	31.7809
	4	54-68						1.8014	0.5419	2.9503	3.4075	0.2112	16.1354	22.3839
	5	68-80						1.5188	0.6270	2.9995	3.4254	0.2257	15.1788	22.5664
	6	80-92						1.6688	0.5489	3.1922	3.6992	0.2227	16.6098	21.0276
BYK16-TEV5-2.4	1	0-2	AL	71°49' 1.4"	129°18' 17.9"	24.08.2016	upland	2.0000	0.1820	14.5503	15.8589	0.5322	29.8011	5.2964
	2	2-36						1.3400	0.1324	2.4889	2.9323	0.2031	14.4404	11.2048
	3	36-50	PF					1.7429	0.7456	4.6887	5.2124	0.3003	17.3559	48.9394
	4	50-62						2.4702	0.4205	5.4242	6.0637	0.3744	16.1953	27.3688

Appendix 4: Results of the Shapiro-Wilk significant difference test ($p<0.05$) for the different datasets (Table 3) of KUR. Significant difference is marked with yes, no statistical difference is marked with no.

per transect

TOC per transect			
	upstream	midstream	downstream
upstream		yes	no
midstream			no
downstream			

TN per transect			
	upstream	midstream	downstream
upstream		yes	no
midstream			no
downstream			

C/N-ratio per transect			
	upstream	midstream	downstream
upstream		no	no
midstream			no
downstream			

SOC per transect			
	upstream	midstream	downstream
upstream		yes	yes
midstream			no
downstream			

per geomorphological unit

TOC per geomorphological unit			
	Yed. upland	slope	bed
Yed. upland		yes	no
slope			yes
bed			

TN per geomorphological unit			
	Yed. upland	slope	bed
Yed. upland		yes	no
slope			yes
bed			

C/N-ratio per geomorphological unit			
	Yed. upland	slope	bed
Yed. upland		no	yes
slope			yes
bed			

SOC per geomorphological unit			
	Yed. upland	slope	bed
Yed. upland		no	no
slope			no
bed			

per depth

TOC per depth			
	0-30 cm	0-50 cm	0-100 cm
0-30 cm		no	no
0-50 cm			no
0-100 cm			

TN per depth			
	0-30 cm	0-50 cm	0-100 cm
0-30 cm		no	no
0-50 cm			no
0-100 cm			

C/N-ratio per depth					SOC per depth			
	0-30 cm	0-50 cm	0-100 cm			0-30 cm	0-50 cm	0-100 cm
0-30 cm		no	no		0-30 cm		no	no
0-50 cm			no		0-50 cm			no
0-100 cm					0-100 cm			

in AL and PF

TOC in AL and PF				TN in AL and PF		
	AL	PF			AL	PF
AL		no		AL		no
PF				PF		

C/N-ratio in AL and PF				SOC in AL and PF		
	AL	PF			AL	PF
AL		yes		AL		yes
PF				PF		

Appendix 5: Results of the Shapiro-Wilk significant difference ($p<0.05$) test for the different datasets (Table 3) of SOB. Significant difference is marked with yes, no statistical difference is marked with no.

per transect

TOC per transect					TN per transect			
	upstream	midstream	downstream			upstream	midstream	downstream
upstream		no	no		upstream		no	no
midstream			no		midstream			no
downstream					downstream			

C/N-ratio per transect					SOC per transect			
	upstream	midstream	downstream			upstream	midstream	downstream
upstream		yes	no		upstream		no	no
midstream			yes		midstream			no
downstream					downstream			

per geomorphological unit

TOC per geomorphological unit			
	Yed. upland	slope	bed
Yed. upland		yes	no
slope			yes
bed			

TN per geomorphological unit			
	Yed. upland	slope	bed
Yed. upland		yes	no
slope			yes
bed			

C/N-ratio per geomorphological unit			
	Yed. upland	slope	bed
Yed. upland		yes	no
slope			yes
bed			

SOC per geomorphological unit			
	Yed. upland	slope	bed
Yed. upland		yes	yes
slope			no
bed			

per depth

TOC per depth			
	0-30 cm	0-50 cm	0-100 cm
0-30 cm		no	no
0-50 cm			no
0-100 cm			

TN per depth			
	0-30 cm	0-50 cm	0-100 cm
0-30 cm		no	no
0-50 cm			no
0-100 cm			

C/N-ratio per depth			
	0-30 cm	0-50 cm	0-100 cm
0-30 cm		no	no
0-50 cm			no
0-100 cm			

SOC per depth			
	0-30 cm	0-50 cm	0-100 cm
0-30 cm		no	yes
0-50 cm			no
0-100 cm			

in Al and PF

TOC in Al and PF		
	AL	PF
AL		no
PF		

TN in Al and PF		
	AL	PF
AL		no
PF		

C/N-ratio in Al and PF		
	AL	PF
AL		no
PF		

SOC in Al and PF		
	AL	PF
AL		yes
PF		

Appendix 6: Results of the Shapiro-Wilk significant difference test ($p<0.05$) for the different datasets (Table 3) of BYK. Significant difference is marked with yes, no statistical difference is marked with no.

per transect

TOC per transect				TN per transect		
	upstream	downstream			upstream	downstream
upstream		yes		upstream		yes
downstream				downstream		

C/N-ratio per transect				SOC per transect		
	upstream	downstream			upstream	downstream
upstream		yes		upstream		yes
downstream				downstream		

per geomorphological unit

TOC per geomorphological unit				TN per geomorphological unit			
	Yed. upland	slope	bed		Yed. upland	slope	bed
Yed. upland		yes	no	Yed. upland		yes	no
slope			yes	slope			no
bed				bed			

C/N-ratio per geomorphological unit				SOC per geomorphological unit			
	Yed. upland	slope	bed		Yed. upland	slope	bed
Yed. upland		yes	no	Yed. upland		yes	no
slope			yes	slope			no
bed				bed			

per depth

TOC per depth				TN per depth			
	0-30 cm	0-30 cm	0-100 cm		0-30 cm	0-50 cm	0-100 cm
0-30 cm		no	no	0-30 cm		no	no
0-50 cm			no	0-50 cm			no
0-100 cm				0-100 cm			

C/N-ratio per depth					SOC per depth			
0-30 cm	0-30 cm	0-30 cm	0-100 cm			0-30 cm	0-50 cm	0-100 cm
0-30 cm		no	no		0-30 cm		no	yes
0-50 cm			no		0-50 cm			yes
0-100 cm					0-100 cm			

in AL and PF

TOC in AL and PF				TN in AL and PF		
	AL	PF			AL	PF
AL		no		AL		no
PF				PF		

C/N-ratio in AL and PF				SOC in AL and PF		
	AL	PF			AL	PF
AL		no		AL		yes
PF				PF		

Appendix 7: Results of the Shapiro-Wilk significant difference test ($p<0.05$) summarized for the different datasets (Table 3) of all three investigated thermo-erosional valleys. Significant difference is marked with yes, no statistical difference is marked with no.

per transect

TOC per transect					TN per transect			
	upstream	midstream	downstream			upstream	midstream	downstream
upstream		yes	yes		upstream		yes	yes
midstream			no		midstream			no
downstream					downstream			

C/N-ratio per transect					SOC per transect			
	upstream	midstream	downstream			upstream	midstream	downstream
upstream		yes	yes		upstream		yes	yes
midstream			no		midstream			no
downstream					downstream			

per geomorphological unit

TOC per geomorphological unit					TN per geomorphological unit			
	Yed. upland	slope	bed			Yed. upland	slope	bed
Yed. upland		yes	no		Yed. upland		yes	no
slope			yes		slope			yes
bed					bed			

C/N-ratio per geomorphological unit					SOC per geomorphological unit			
	Yed. upland	slope	bed			Yed. upland	slope	bed
Yed. upland		yes	yes		Yed. upland		yes	no
slope			yes		slope			yes
bed					bed			

per depth

TOC per depth					TN per depth			
	0-30 cm	0-30 cm	0-100 cm			0-30 cm	0-50 cm	0-100 cm
0-30 cm		no	no		0-30 cm		no	no
0-50 cm			no		0-50 cm			no
0-100 cm					0-100 cm			

C/N-ratio per depth					SOC per depth			
0-30 cm	0-30 cm	0-30 cm	0-100 cm			0-30 cm	0-50 cm	0-100 cm
0-30 cm		no	yes		0-30 cm		yes	yes
0-50 cm			no		0-50 cm			yes
0-100 cm					0-100 cm			

in AL and PF

TOC in AL and PF				TN in AL and PF		
	AL	PF			AL	PF
AL		no		AL		no
PF				PF		

C/N-ratio in AL and PF				SOC in AL and PF		
	AL	PF			AL	PF
AL		yes		AL		yes
PF				PF		

Appendix 8: Distribution of TOC, TN, C/N-ratio and SOC per transect of KUR.

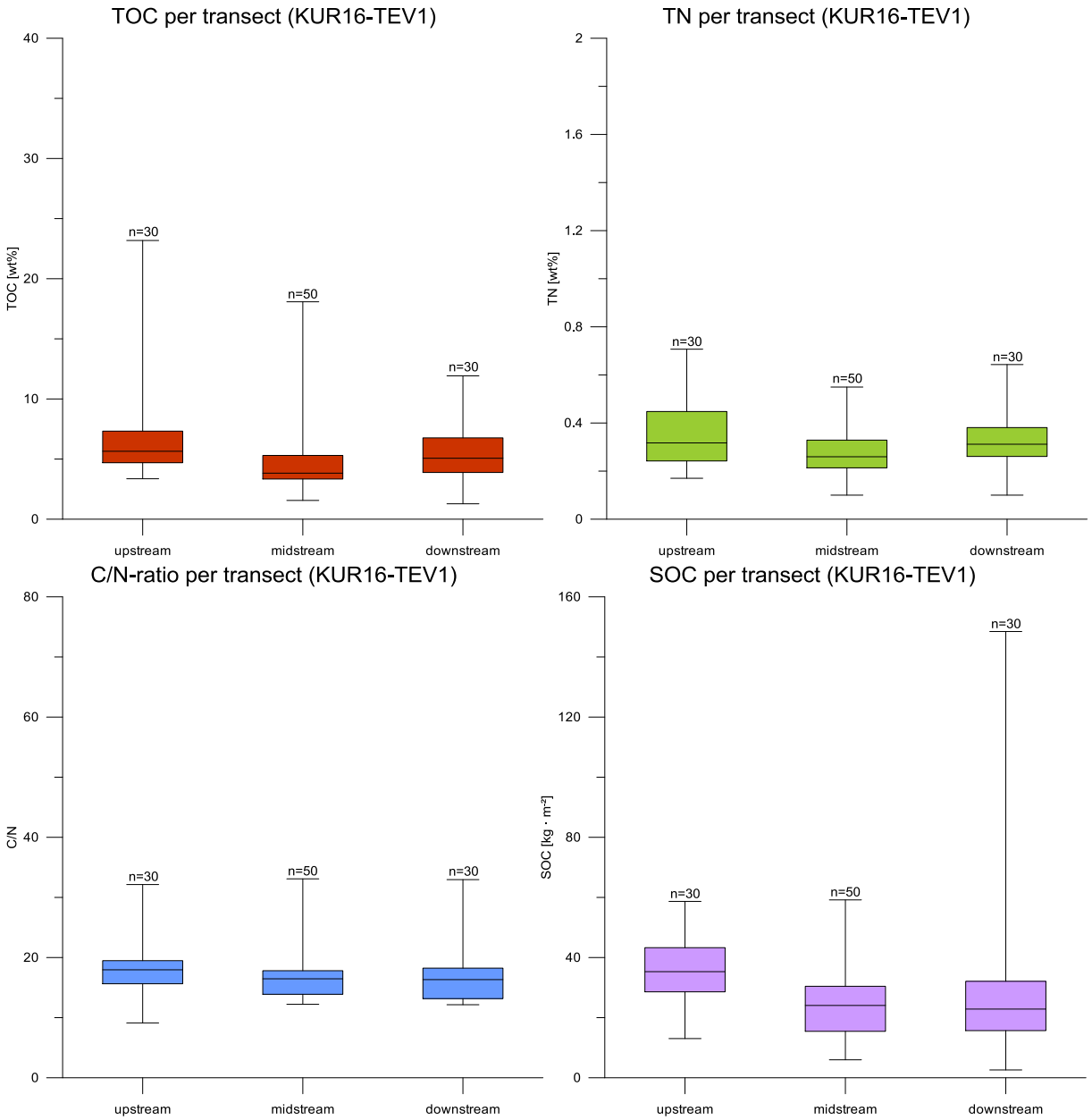

Appendix 9: Distribution of TOC, TN, C/N-ratio and SOC per geomorphological unit of KUR.

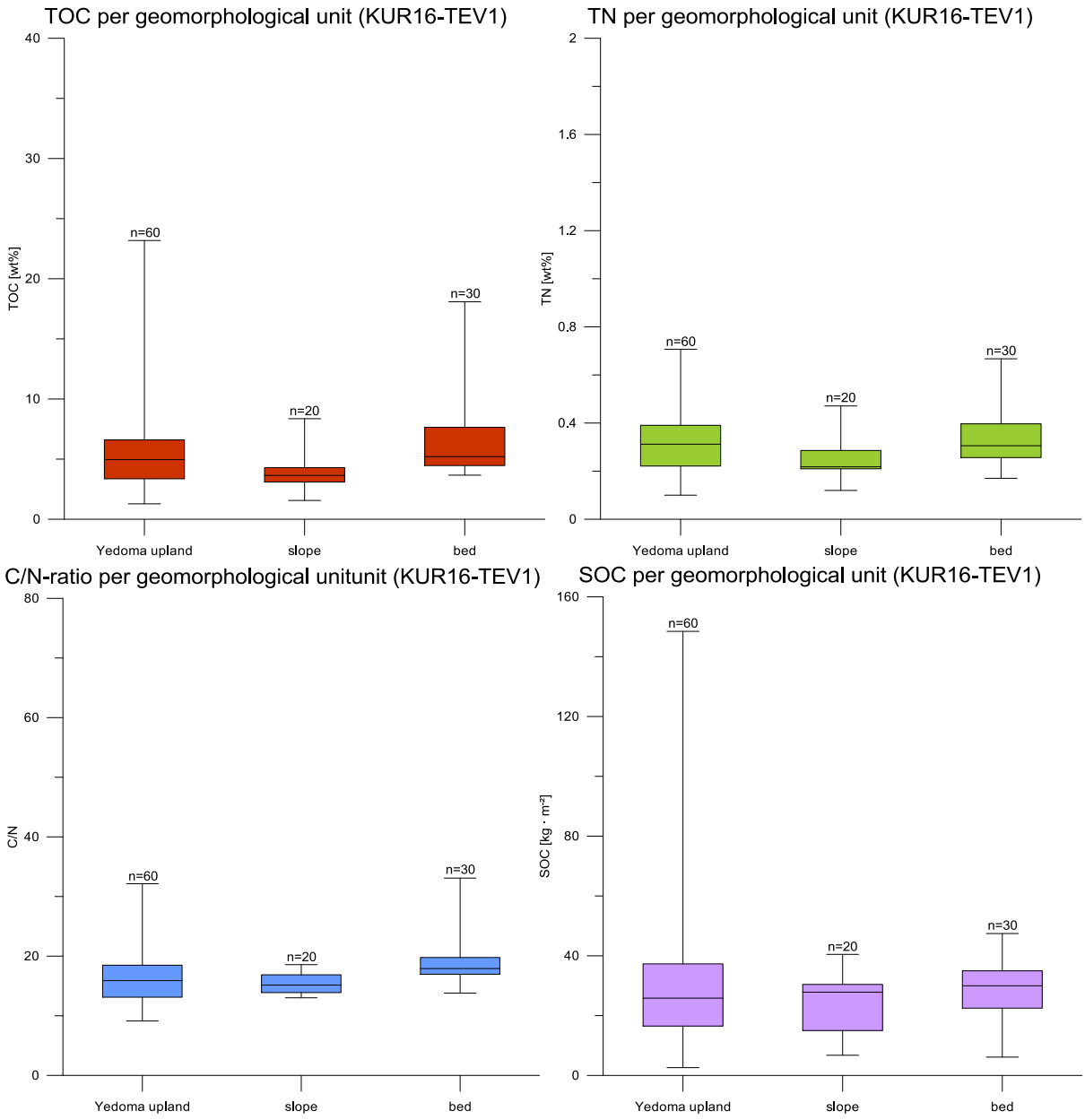

Appendix 10: Distribution of TOC, TN C/N-ratio and SOC per depth of KUR.

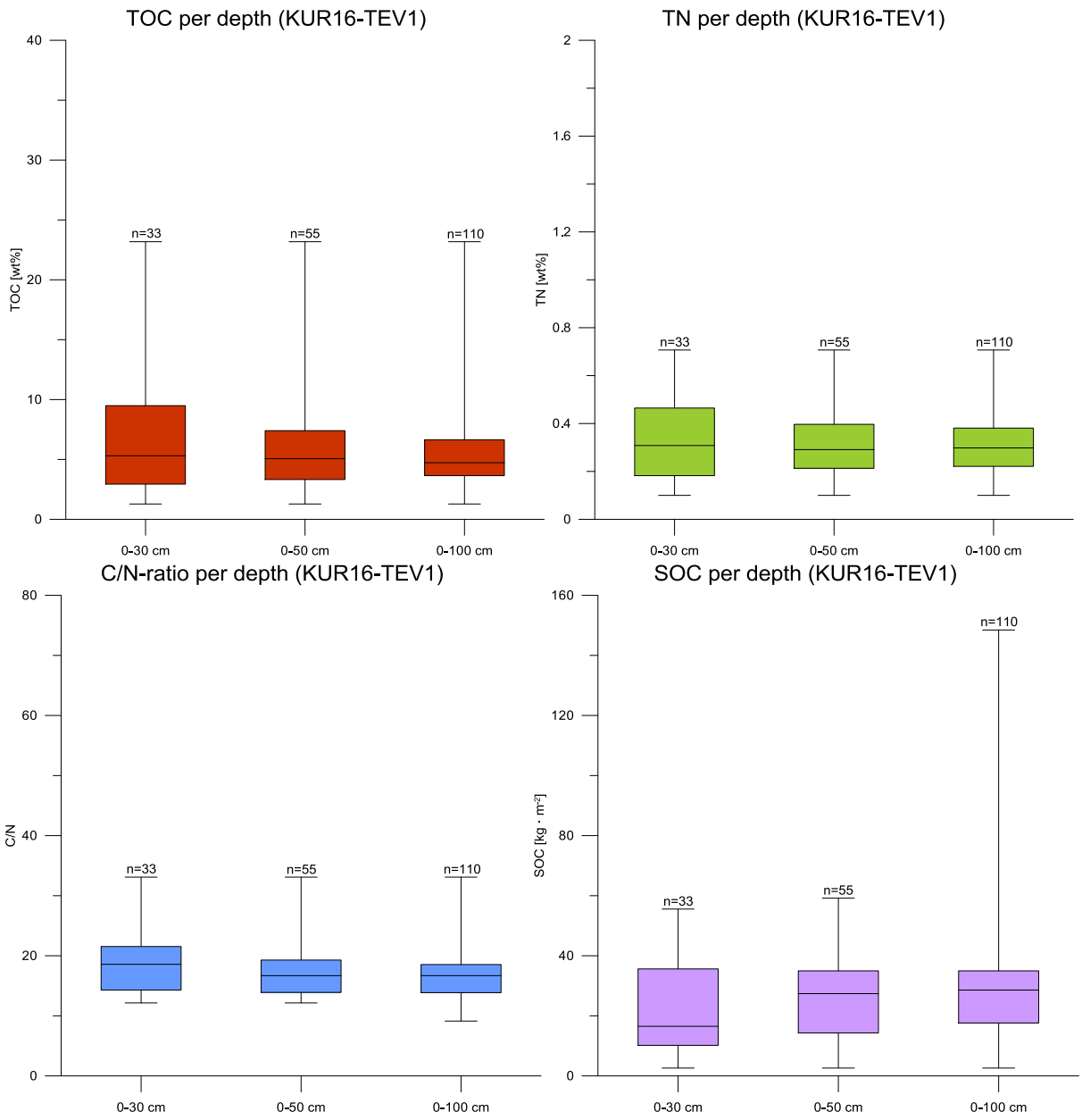

Appendix 11: Distribution of TOC, TN and the C/N-ratio in depth of the individual cores of KUR.

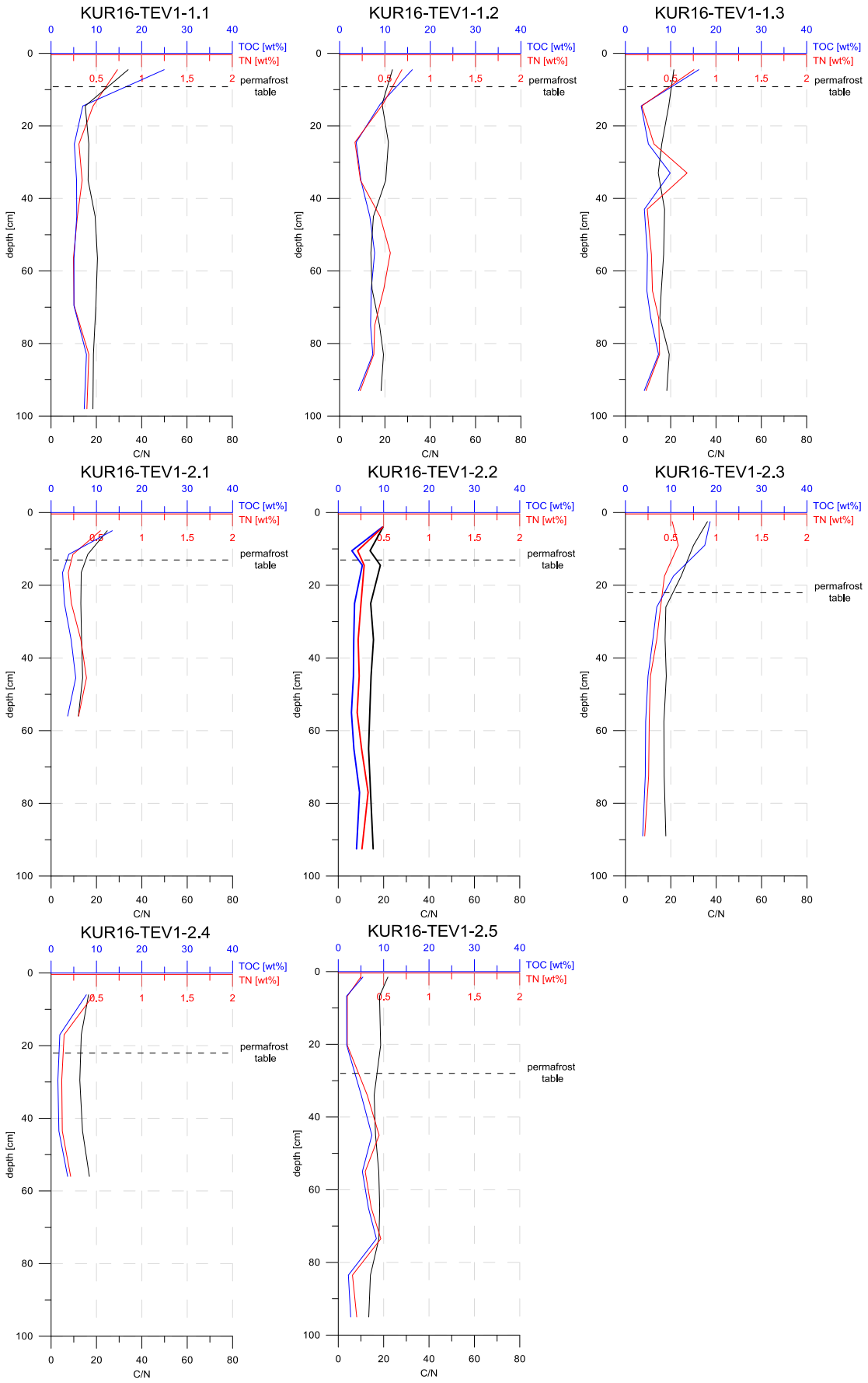

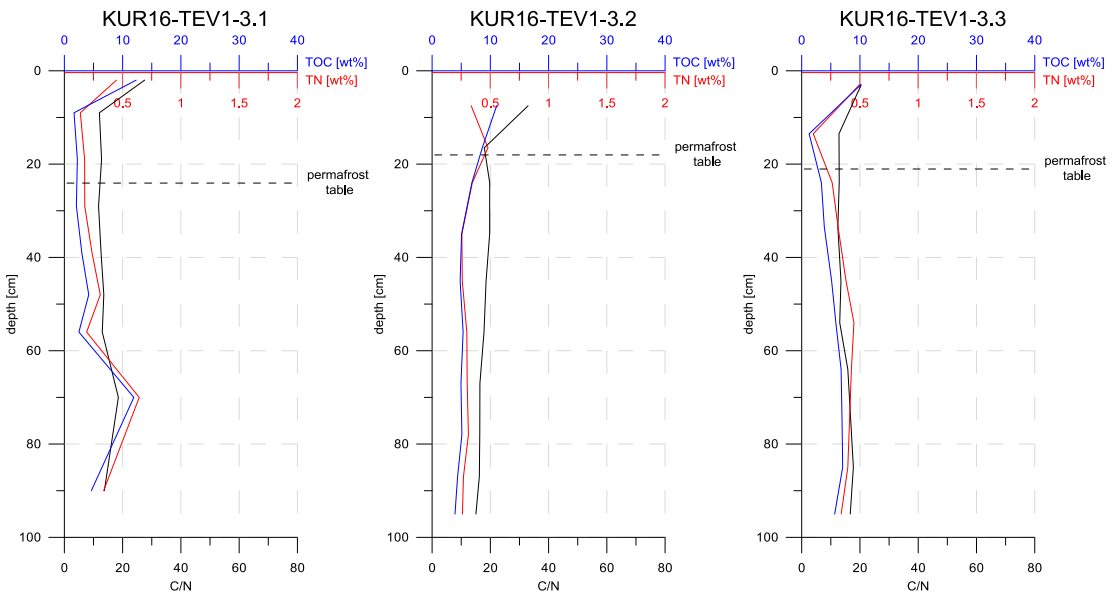

Appendix 12: Distribution of TOC, TN, C/N-ratio and SOC per transect of SOB.

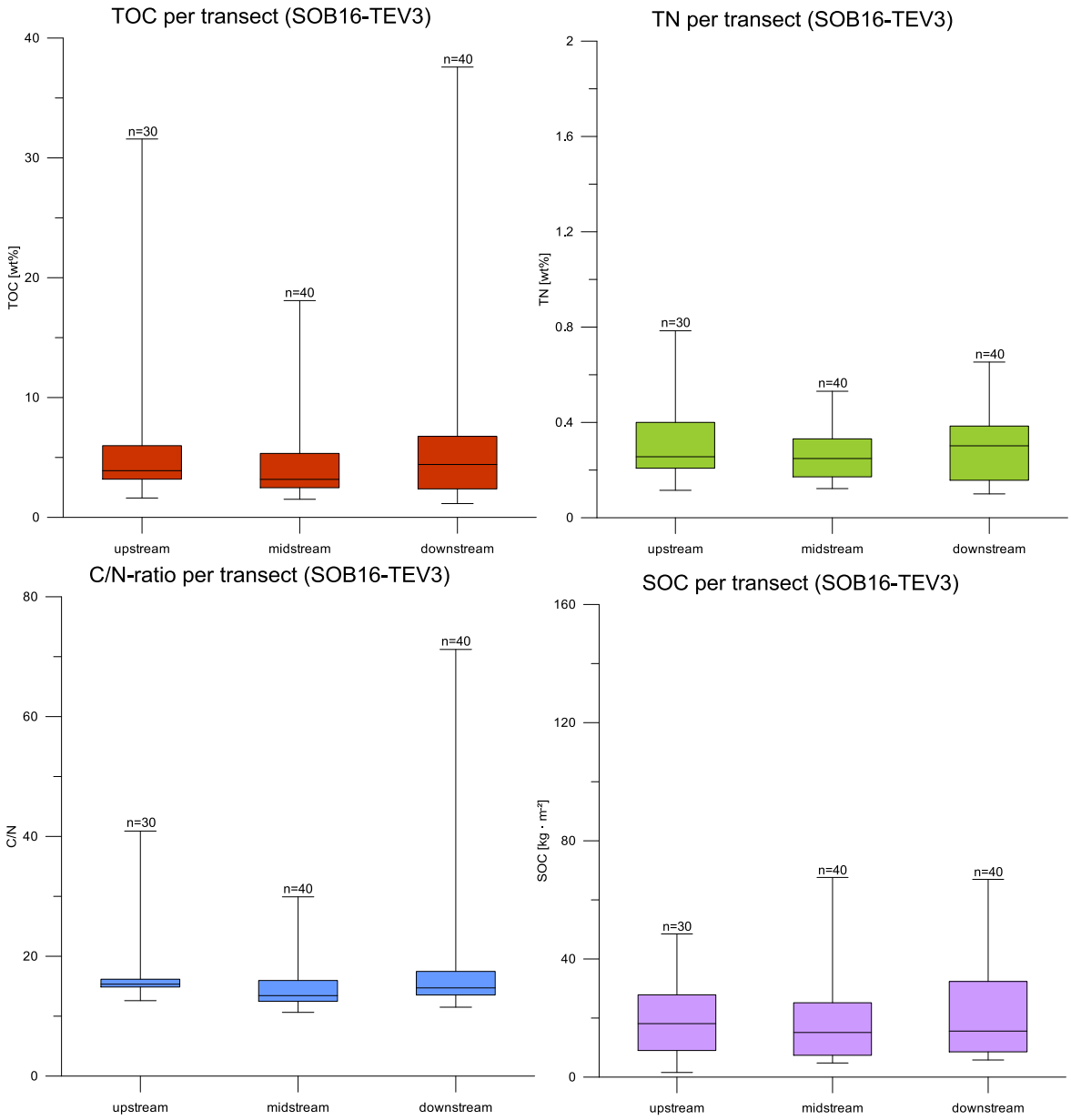

Appendix 13: Distribution of TOC, TN, C/N-ratio and SOC per geomorphological unit of SOB.

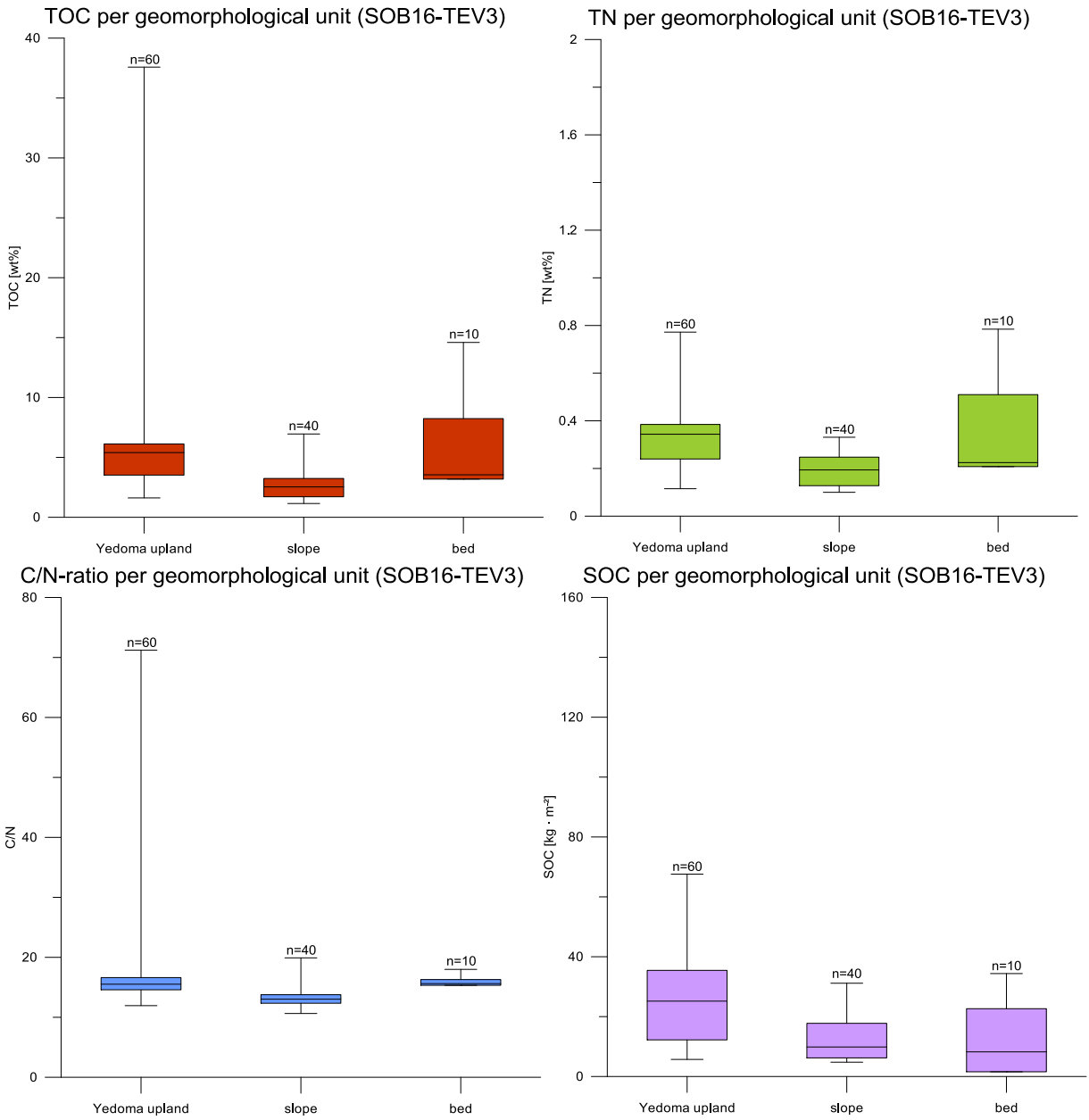

Appendix 14: Distribution of TOC, TN, C/N-ratio and SOC per depth of SOB.

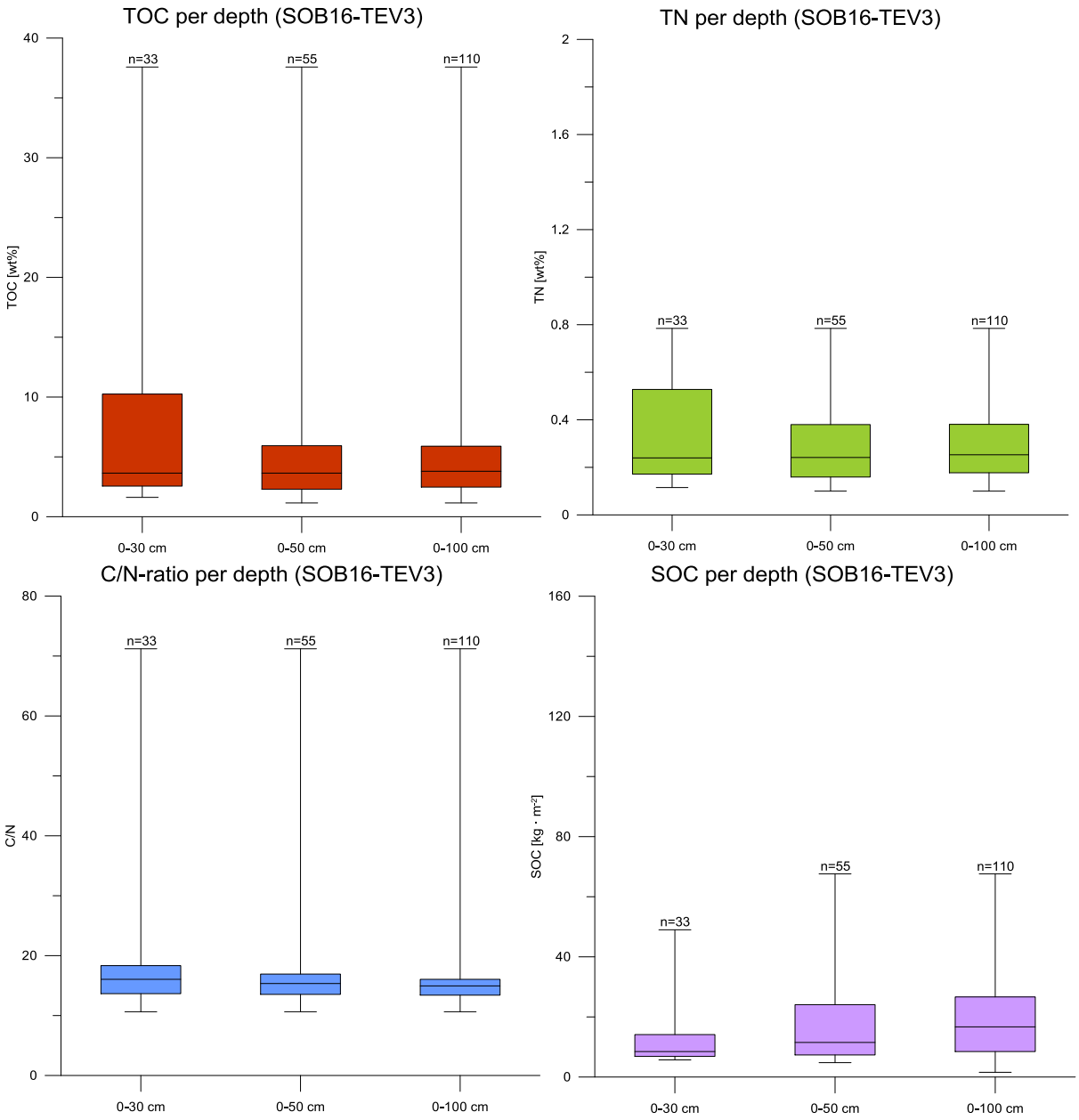

Appendix 15: Distribution of TOC, TN and the C/N-ratio in depth of the individual cores of SOB.

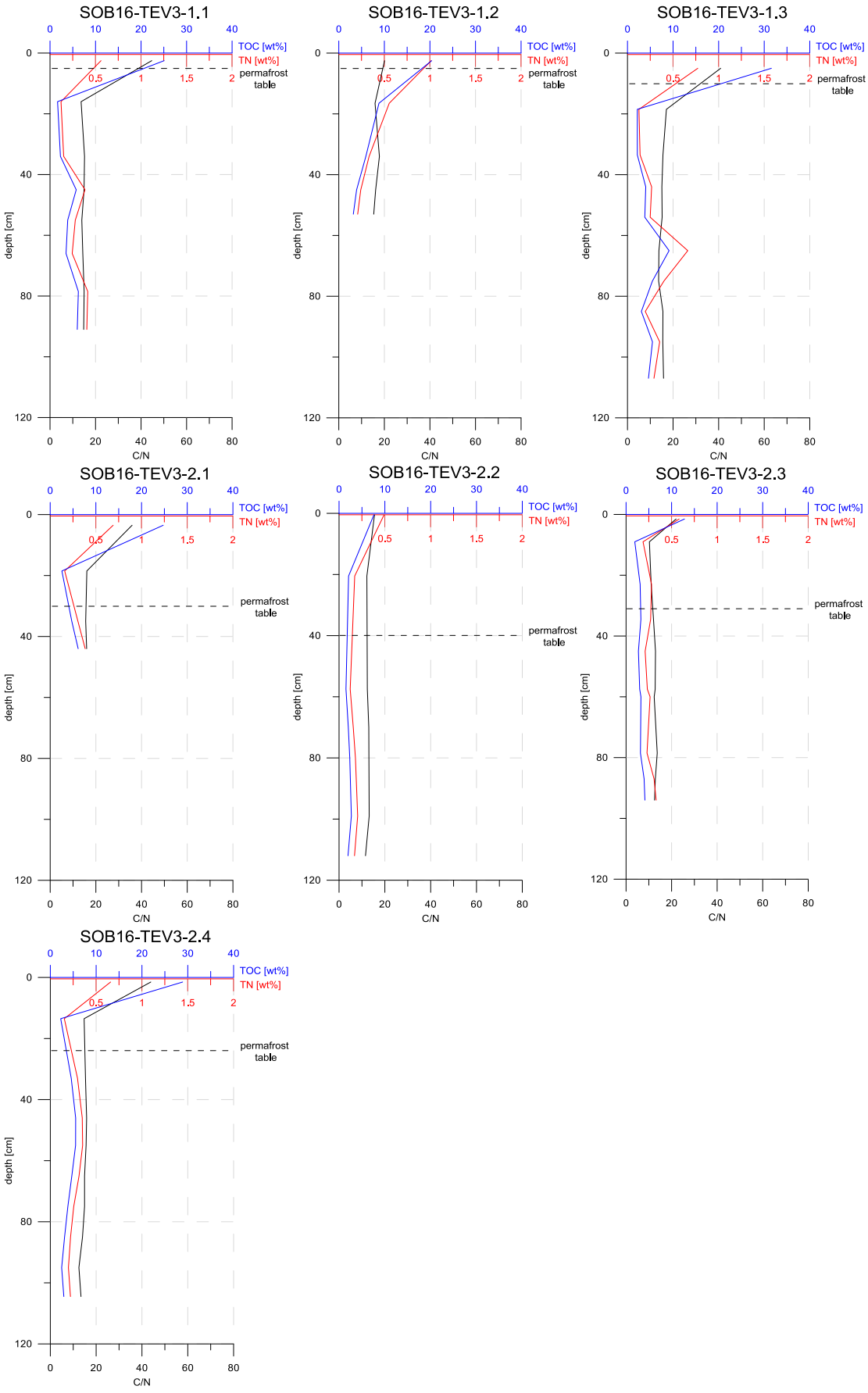

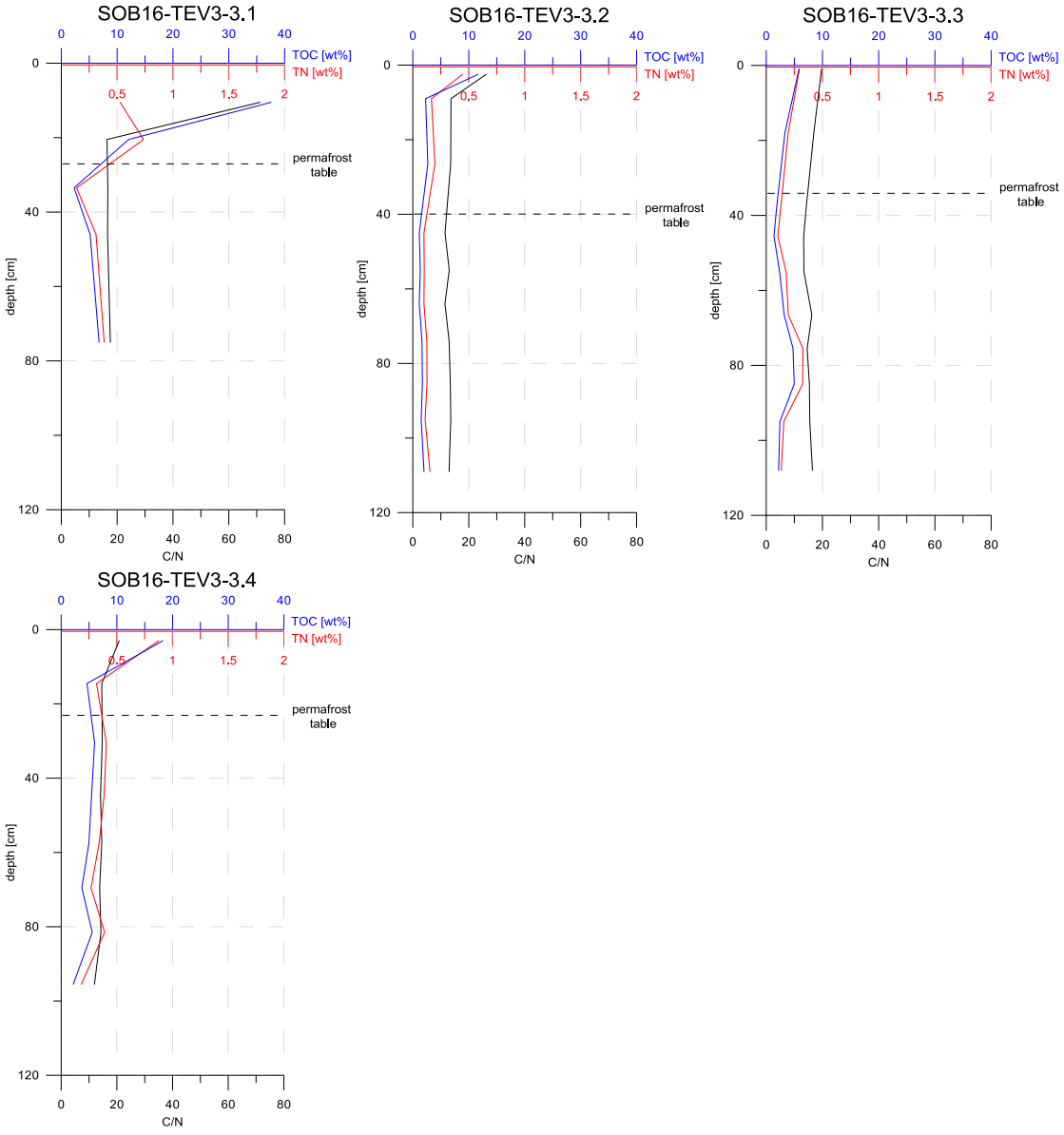
SOB16-TEV3-3.1
SOB16-TEV3-3.2
SOB16-TEV3-3.3
SOB16-TEV3-3.4
TOC [wt%]
TN [wt%]
permafrost table
depth [cm]
C/N

Appendix 16: Distribution of TOC, TN, C/N-ratio and SOC per transect of BYK.

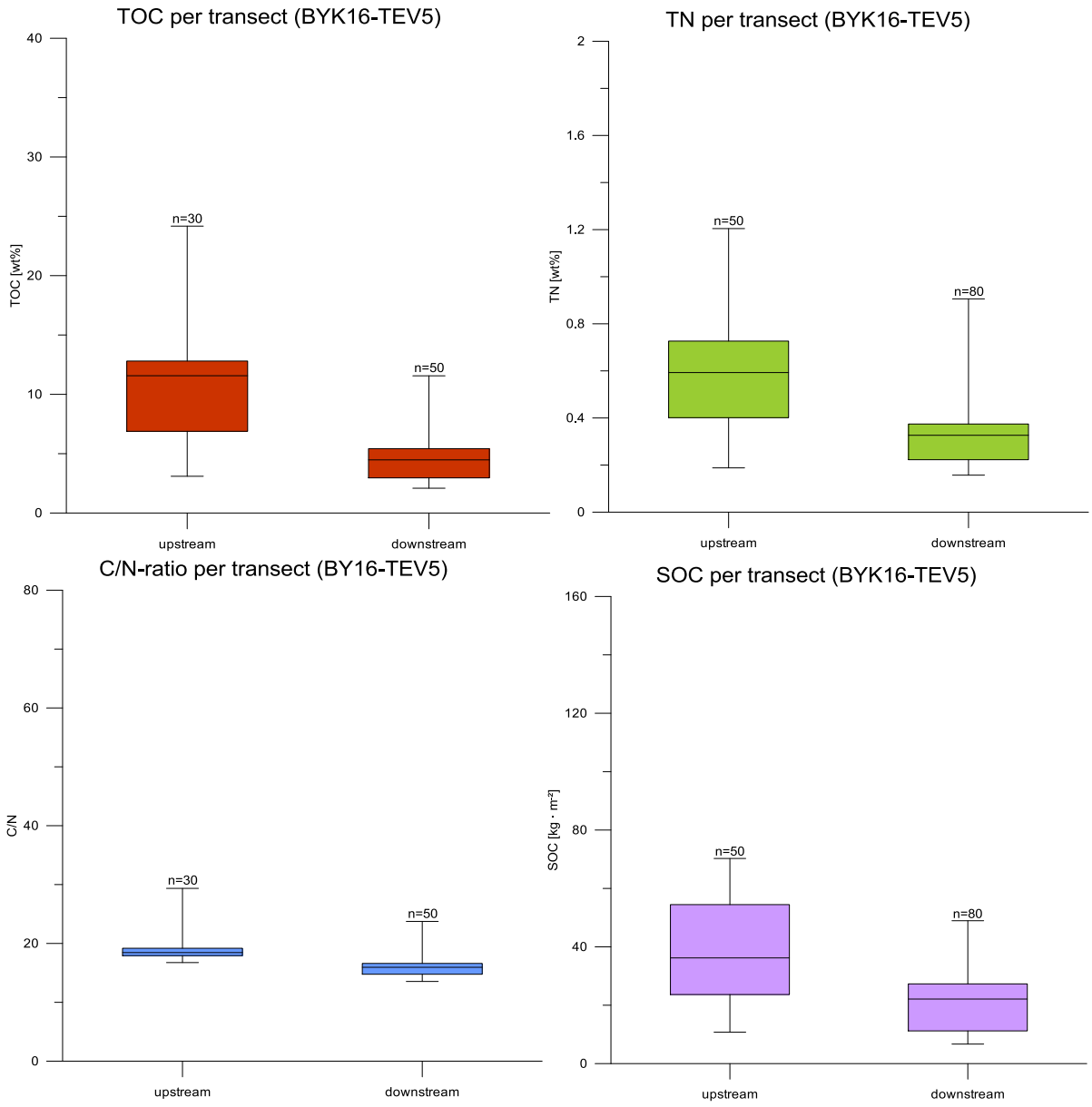

Appendix 17: Distribution of TOC, TN, C/N-ratio and SOC per geomorphological unit of BYK.

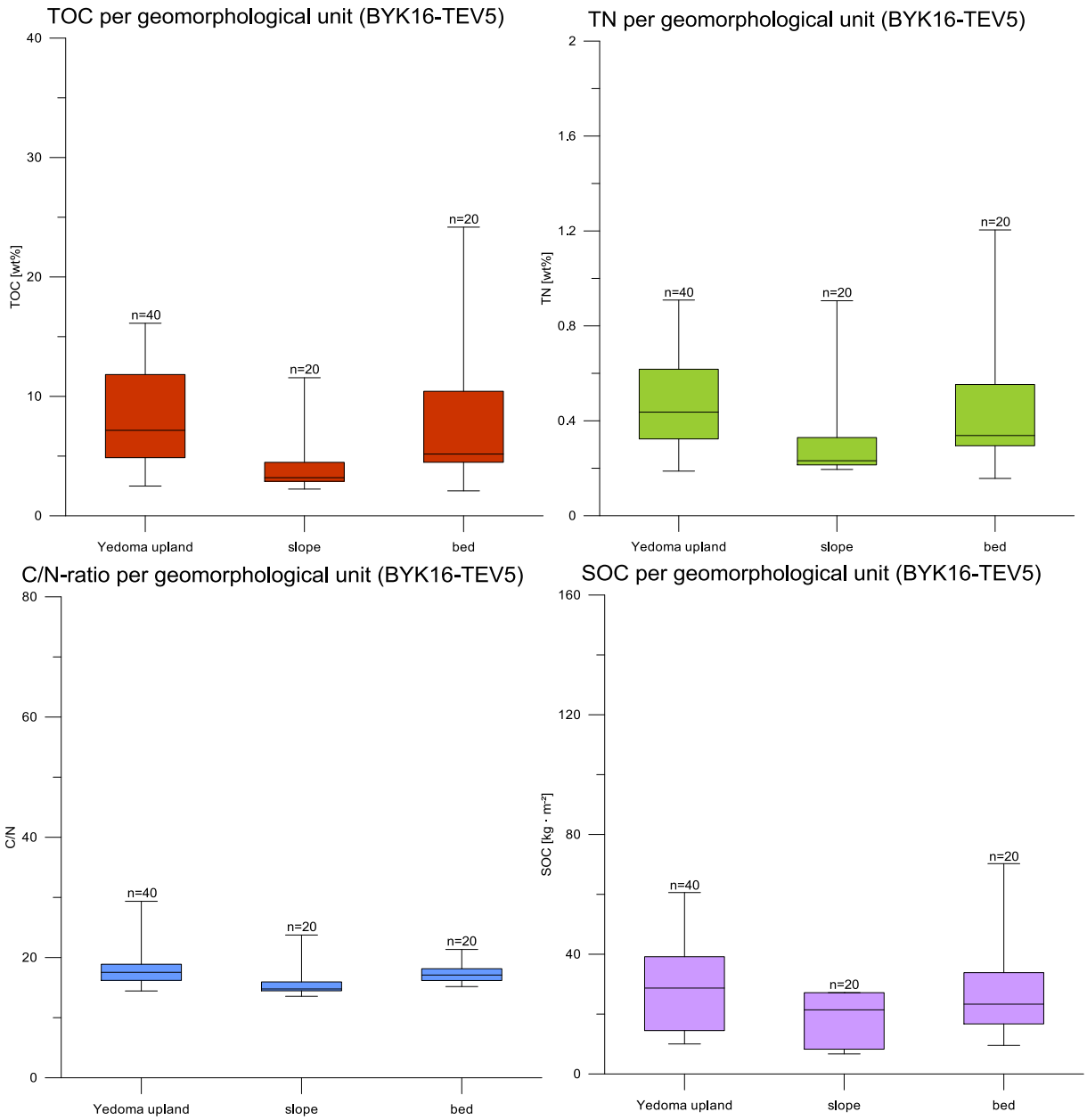

Appendix 18: Distribution of TOC, TN, C/N-ratio and SOC per depth of BYK.

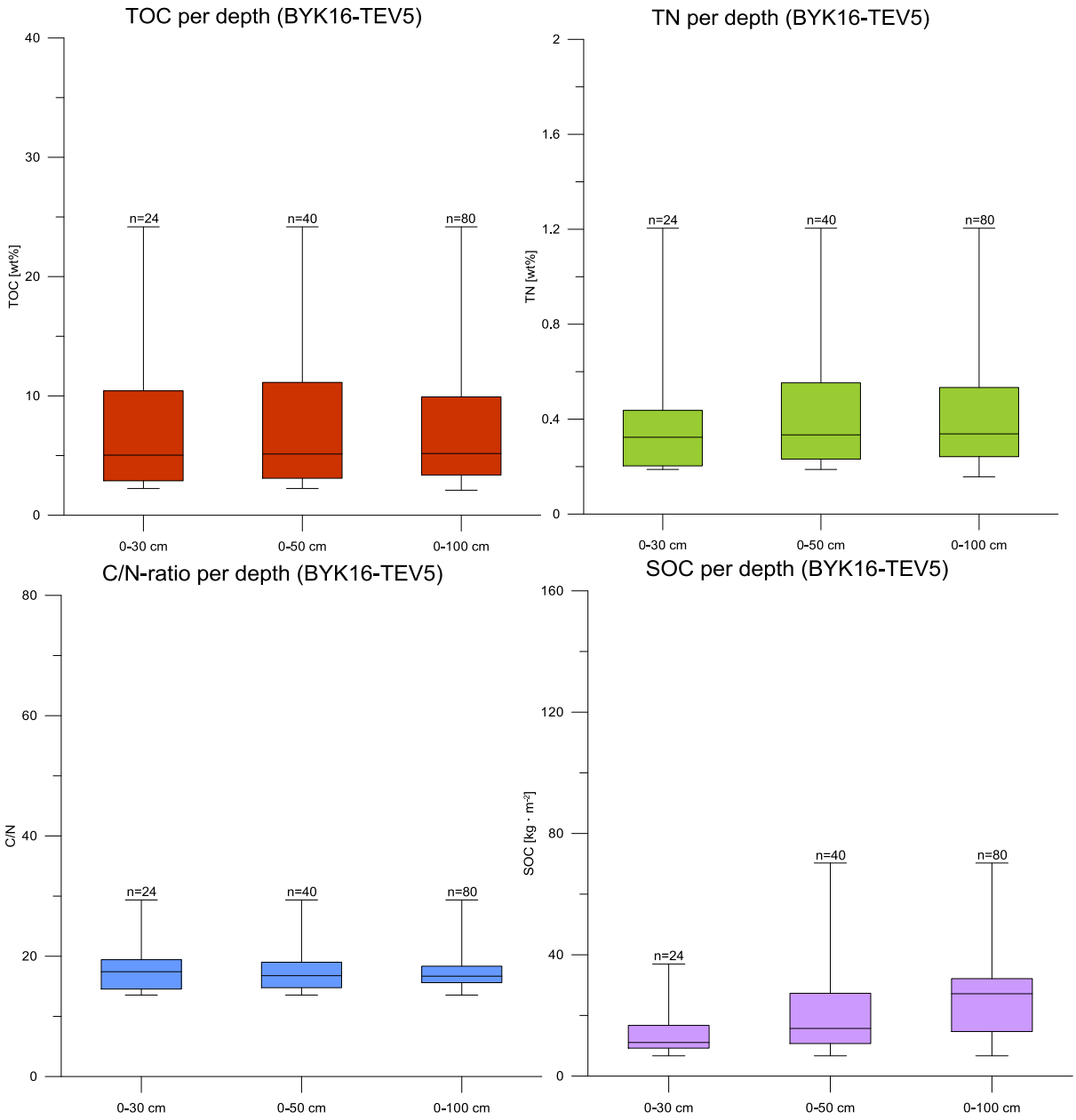

Appendix 19: Distribution of TOC, TN and the C/N-ratio in depth of the individual cores of BYK.

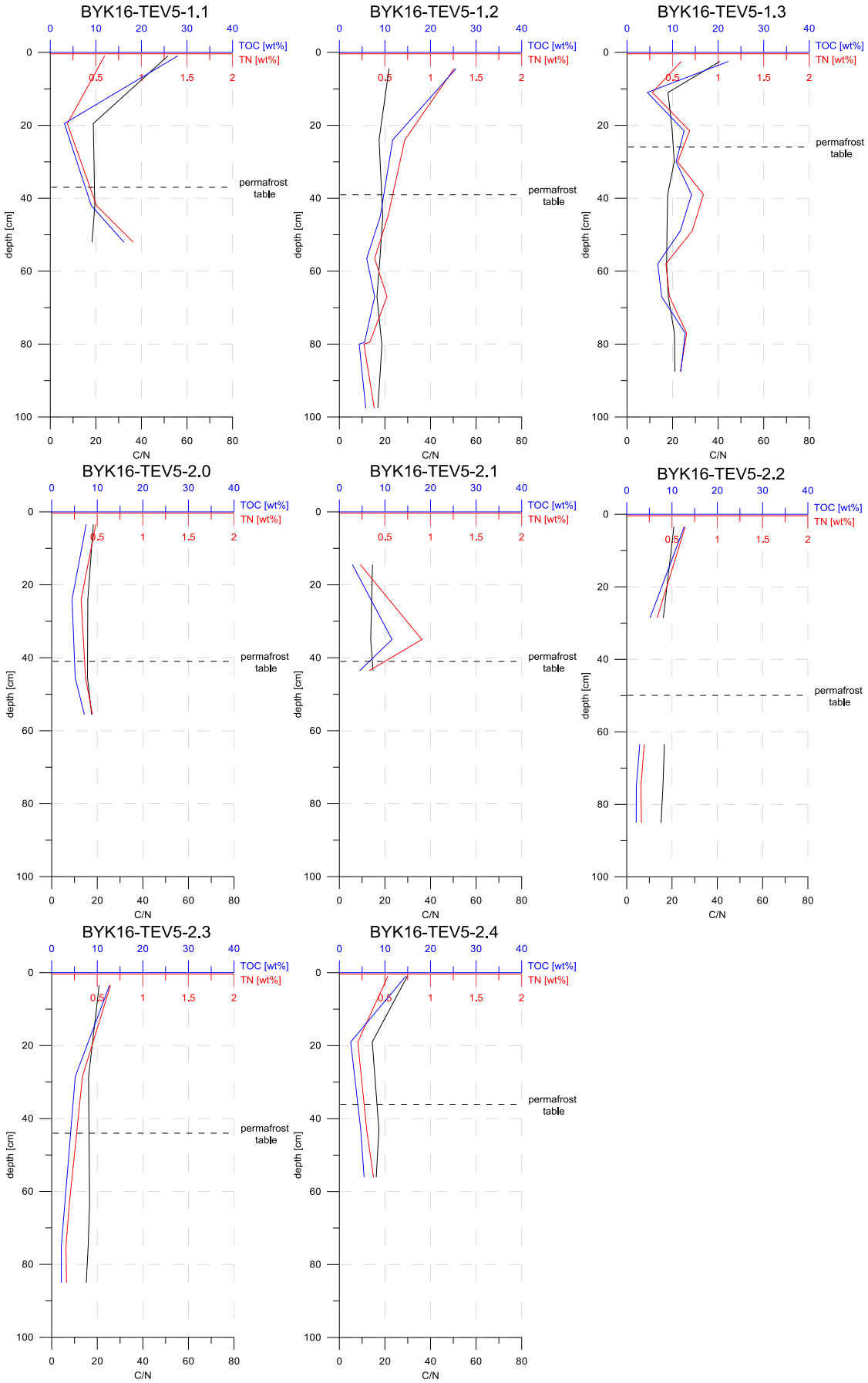

ACKNOWLEDGEMENTS

This thesis would not have been possible without the help and support of many people. At this point I would like to express my gratitude to all who accompanied me on my way to finish this thesis.

At first, I want to thank Prof. Dr. Hugues Lantuit and Dr. Anne Morgenstern for supervising this thesis in an outstanding way and for their honest and helpful feedback through all our regular and numerous meetings. Even if it was sometimes hard to hear, your comments helped a lot to improve this thesis.

I would like to give special thanks to Justine Ramage who introduced me to the thermo-erosional valleys, collected all the samples for this thesis and answered all my question even if we were in totally different time zones. Also, thank you for proof reading and commenting earlier versions of my chapters.

For supporting Justine during field work I also would like to thank Dr. Sebastian Wetterich, Georgy Maximov, Dr. Anne Morgenstern and Prof. Dr. Guido Grosse, thank you for your drilling power. I am also very grateful to Dr. Lutz Schirrmeister who helped me at the beginning of my data evaluation and gave me the right hints.

The work in the lab would not have been possible without Dyke Scheidemann. Thank you for your guidance and answering my questions sometimes twice or more. At this point I also want to thank all the people with whom I shared the lab, which made especially the many days at the balance much easier.

I would like to sincerely thank my boss Dr. Hella Wittmann-Oelze for her constant understanding and support during the whole period of my studies and especially in the last few months, which made it much easier for me to finish this thesis. Further thanks I want to give to my colleagues and friends Josi and Jutta who always found the right words and managed to rise a smile into my face even when I thought it would be impossible.

Ein besonderer Dank gilt meiner Familie, ohne deren Unterstützung mein gesamtes Studium nicht möglich gewesen wäre. Zu guter Letzt möchte ich meinem Freund danken, der immer geduldig an meiner Seite steht und mir ein unkompliziertes und angenehmes Arbeitsumfeld geschaffen hat.

SELBSTSTÄNDIGKEITSERKLÄRUNG

Hiermit versichere ich, dass ich die vorliegende Arbeit selbstständig verfasst und keine anderen als die angegebenen Quellen und Hilfsmittel verwendet habe. Alle von Autoren wörtlich übernommene Stellen, wie auch sich an die Gedanken anderer Autoren eng anlehnende Ausführungen meiner Arbeit, sind unter Angabe der Quelle kenntlich gemacht.

Weiterhin versichere ich, dass diese Arbeit in gleicher oder ähnlicher Fassung weder in einer anderen Prüfungsbehörde vorgelegt noch veröffentlicht wurde.

Berlin, den 01. Juli 2018 _____

Nadja Kuhl